AN ABSTRACT OF THE THESIS OF

Kieran O'Driscoll for the degree of Master of Science in Oceanography presented on September 9, 1999.

Title: Nonlinear Internal Waves on the Continental Shelf: Observations and KdV Solutions

Redacted for Privacy

Abstract approved: _____

Murray David Levine

Numerical solutions of the Korteweg-de Vries (KdV) and extended Korteweg-de Vries (eKdV) equations are used to model the transformation of a sinusoidal internal tide as it propagates across the continental shelf. The ocean is idealized as being a two-layer fluid, justified by the fact that most of the oceanic internal wave signal is contained in the gravest mode. The model accounts for nonlinear and dispersive effects but neglects friction, rotation, and mean shear. The KdV model is run for a variety of idealized topography and stratification to understand the role of the nonlinear and dispersive effects. In all model solutions the internal tide steepens forming a sharp front. A packet of nonlinear solitary-like waves evolve from the front. A comparison between KdV and eKdV solutions are explored.

The model results for realistic topography and stratification are compared with observations made at moorings off Massachusetts in the Mid Atlantic Bight, and close to shore off Oceanside, California. Several features observed in the data

are also found in the model results. Differences between theory and mooring observations are discussed.

Nonlinear Internal Waves on the Continental Shelf: Observations and KdV Solutions

by

Kieran O'Driscoll

A THESIS

submitted to

Oregon State University

in partial fulfillment of
the requirements for the
degree of

Master of Science

Presented September 9, 1999
Commencement June 2000

Master of Science thesis of Kieran O'Driscoll presented on September 9, 1999

APPROVED:

Redacted for Privacy

Major Professor, representing Oceanography

Redacted for Privacy

Dean of College of Oceanic and Atmospheric Sciences

Redacted for Privacy

Dean of Graduate School

I understand that my thesis will become part of the permanent collection of the Oregon State University libraries. My signature below authorizes release of thesis to any reader upon request.

Redacted for Privacy

Kieran O'Driscoll, Author

ACKNOWLEDGEMENTS

I would like to acknowledge my major professor Murray Levine for very patiently and wisely guiding me through this thesis. Murray was available at all times for all sorts of problems, and provided encouragement and security when I needed them most. I would like to thank Tim Boyd and Scott Pegau for their assistance in this work and for serving on my committee. I thank Jeff Ramsey for serving as my Graduate Council Representative. I wish to thank all of the people in oceanography and other departments who have assisted in my education here in Corvallis. Thanks to Tom Dillon for his help, support and counselling in my earlier days in Corvallis. Thanks to all who allowed me to go to sea to help in their projects.

I have made many friends and acquaintances during my stay in Corvallis, most of whom, but not all, I met either through oceanography, sports or music. Thanks to all of you for your friendship, help and support. Thanks to all my friends in Ireland, London, Boston, and New York

Last but not least, I would like to thank my family for everything. Thanks to my mother, Eleanor, my father, Derry, brothers Barry and Colm, sisters Claire, Fiona and Elaine, in-laws, nephews, niece, aunts, uncles, cousins, and my grandparents Mick Glennon, Nell O'Mahony, Tom O'Driscoll and Catie Creedon.

TABLE OF CONTENTS

LIST OF FIGURES

LIST OF FIGURES (Continued)

LIST OF FIGURES (Continued)

LIST OF FIGURES (Continued)

LIST OF FIGURES (Continued)

LIST OF FIGURES (Continued)

Nonlinear Internal Waves on the Continental Shelf : Observations and KdV Solutions

1. Introduction

Internal waves exist throughout the world's oceans wherever there is stratification from the shallowest near-shore waters to the deepest oceans. Internal waves are important to physical oceanographers because they transport momentum and energy, horizontally and vertically, through the ocean, e.g. Munk (1981), Gill (1982). They provide shear to turbulence which results in energy dissipation and vertical mixing, e.g. Holloway (1991), Sandstrom & Elliott (1984). Biological oceanographers are interested because the internal waves carry nutrients onto the continental shelf and into the euphotic zone, e.g. Shea & Broenkow (1988), Sandstrom & Elliott (1984), and Holloway et al. (1985). They are of interest to geological oceanographers because the waves cause sediment transport on the shelf, e.g. Cacchione & Drake (1986). Civil, hydraulic and ocean engineers are interested because the internal waves generate local tidal and residual currents, e.g. Willmott & Edwards (1987), which can cause scour on nearshore as well as offshore structures, e.g. Osborne et al. (1978). They are also of interest to the navy because of the ability of the waves to affect propagation of optic and acoustic signals.

This study is focused on the internal tide and subsequent evolution of nonlinear waves. Internal waves in the ocean span the frequency spectrum from the

buoyancy frequency, N, to the inertial frequency, f. However, the internal, or baroclinic, tide accounts for a large fraction of the energy contained in these waves. The internal tide is generated by the interaction of barotropic tidal current with topography and not directly by the gravitational attraction of sun and moon. The properties and propagation of linear internal tide and waves have been treated in detail by many investigators, see, for example, Garrett & Munk (1979), or the monographs by Gill (1982), Lighthill (1978), or Apel (1987).

As the internal tide shoals, the nonlinear terms in the Navier-Stokes equations become important. These tidal waves of finite amplitude may evolve into packets of high frequency nonlinear waves. The equations describing these waves are much more complex than the linear equations and few mathematical solutions exist.

We are interested in nonlinear internal waves because they are a very energetic part of the signal in time series that we have observed on continental shelves and in the shallow ocean. We are guided by numerical solutions of Korteweg-de Vries (KdV) type equations that incorporate both weak nonlinear and weak dispersive effects.

The derivation of the Korteweg-de Vries (KdV) equation, and an extended form of it, the eKdV, are reviewed and discussed in Chapter 2. The numerical scheme used to run the model is discussed, as is the transformation of the equations. Model runs and results are presented in Chapter 3 to explain the transformation of the internal tide and the evolution of solitary-like waves on the

continental shelf. These results are compared with data and observations collected at two sites: in the Mid Atlantic Bight, to the south of Massachusetts, during the Coastal Mixing and Optics experiment (CMO), and near shore at Oceanside, California, during the Littoral Optics Experiment (LOE) (Chapter 4). The CMO data was collected at a mooring in July and August 1996, and the LOE experiment conducted in October 1995. The location sites are further discussed in Chapter 4. Chapter 5 contains a summary and conclusions of the work.

We conclude the introduction with a brief historical review of internal waves, particularly nonlinear waves, and the work and events leading to the present understanding of these waves.

Historical review Internal wave research has been an area of interest within the physical oceanography community for decades. Gill (1982) gives several historical examples of observations of internal gravity waves. The phenomenon of 'dead water' experienced by Norwegian ships in certain coastal waters led V. Bjerknes to give perhaps the first explanation of an ocean phenomenon in terms of internal waves. A preface to Ekman's 1904 paper by V. Bjerknes reads:

> The present investigation of "Dead-Water" was occasioned by a letter in 1898 from Prof. Nansen asking my opinion on the subject. In my reply to Prof. Nansen I remarked that in the case of a layer of fresh water resting on the top of salt water, a ship will not only produce the ordinary visible waves at the boundary between the water and the air, but will also generate invisible waves in the salt-water fresh-water boundary below; I suggested that the great resistance

> experienced by the ship was due to the work done in generating these invisible waves.

Internal waves were subsequently observed during all the major oceanographic expeditions of the early 20th century. Defant (1960), for example, gives details of the observation of long internal waves while on anchor station 254 (31st of January to 2nd of February 1927) during the "Meteor" expedition. The series of papers by Ufford (1947a, 1947b, 1947c) gives details of the observation of high frequency large amplitude internal waves in shallow water off the coast of San Diego collected aboard the U.S.S. Beaumont, the E.W. Scripps and the U.S.S. Democracy in 1942 and 1944.

Most of the work on internal waves in the 20th century has been focused on linear internal waves but observations in coastal and near-shore waters regularly contain nonlinear internal waves. That is not to say that nonlinear internal waves are confined to the continental shelf and coastal seas, see for example Pinkel (1979), Osborn & Burch (1980), and Fu & Holt (1984), but the vast majority of observations of internal nonlinear and solitary-like waves in the oceans have been in shallow regions and adjacent to the continental shelf and slope.

Surface solitary waves appear to have been first documented following their chance observation by Russell in 1834 :

> I was observing the motion of a boat which was rapidly drawn along a narrow channel by a pair of horses, when the boat suddenly stopped - not so the mass of water in the channel which it had put in motion; it accumulated around

> the prow of the vessel in a state of violent agitation, then suddenly leaving it behind, rolled forward with great velocity, assuming the form of a large solitary elevation, a rounded, smooth and well-defined heap of water, which continued its course along the channel apparently without change of form or diminution of speed. I followed it on horseback, and overtook it still rolling on at a rate of some eight or nine miles an hour, preserving its figure some thirty feet long and a foot to a foot and a half in height. Its height gradually diminished and after a chase of one or two miles I lost it in the windings of the channel. Such in the month of August, 1834, was my first chance interview with that singular and beautiful phenomenon.

Russell was fascinated by the fact and the idea that a wave so steep did not break but propagated away in one direction without becoming deformed. Thus the great investigation of solitary and nonlinear waves was born. Russell made some rather precise observations of solitary waves with the aid of experiments. Several notable scientists of the latter part of the 19^{th} century published papers describing their work concerning solitary waves among whom are included Boussinesq (1872), Kelvin (1887), and Rayleigh (1876). Korteweg and de Vries (1895) were the first to develop a mathematical model for solitary waves when they approximated the Navier-Stokes equations for small finite-amplitude waves. Though nonlinear waves received lots of attention throughout the 20^{th} century, the Korteweg-de Vries (KdV) equation was put aside shortly after the work of Korteweg & de Vries since solitary waves were just considered to be a relatively unimportant curiosity within the field. Zabusky & Kruskal (1965) showed, using a computer simulation, that upon collision two solitary waves which satisfied the KdV equation retained their

shapes and propagation velocity after the collision. Zabusky & Kruskal coined the term 'soliton' to describe these waves since they behaved in a somewhat particle-like fashion.

An early documentation of the emission of internal waves of finite amplitude from the baroclinic tide was made by Halpern (1971) when temperature measurements were made at station T, 9 km west of Stellwagen Bank in Massachusetts Bay. In this case, the internal tide steepens upon propagation over Stellwagen Bank, which separates Massachusetts Bay from the broader continental shelf. In the lee of the bank, an internal hydraulic jump is followed by several high frequency, large amplitude oscillations. The process repeats itself at the M_2 period. These observations led to an experimental investigation by Lee & Beardsley (1974) in which the propagation of the internal tide past Stellwagen Bank was imitated in a laboratory tank with movable bottom topography. They also made a theoretical investigation, following on the work of Benney (1966), wherein a Korteweg-de Vries type equation for the stream function was derived for the wave and fluid motion in the tank by a perturbation expansion using three small parameters corresponding to nonlinear, dispersive and non-Boussinesq effects. The theoretical investigation was carried out for the case of both weakly stratified shear flow and also for the case of a two layer fluid. Their theoretical results led to a numerical investigation which ultimately resulted in the conclusion that nonlinearity and dispersion are important factors to explain the observations of Halpern. Haury, Briscoe & Orr (1979) following up on the observations of Halpern, studied the

passage of the same high frequency internal wave packets past Stellwagen Bank and concluded that these waves seriously impact plankton distributions to an extent that may effect primary production in Massachusetts Bay.

Sandstrom & Elliott (1984) investigated the links between horizontal and vertical nutrient transport and mixing at the shelf break strip on the Scotian shelf. They made observations with the 'sawtoothing' Batfish during two cruises in November 1980 and November 1981, respectively. Based on their observations and theory, they found that the barotropic tide interacts with the continental shelf and slope to generate a baroclinic response in the form of an interfacial wave. As the fundamental internal mode crosses the shelf, the isopycnals are depressed and steepening occurs due to nonlinear effects. Dispersive effects become important during the process, and solitary waves can be formed once the dispersive effects become comparable to the nonlinear effects. Microsructure activity occurred at the base of the mixed layer due to the baroclinic shear which ultimately acts to maintain the vertical nutrient fluxes necessary to sustain the observed primary production on the shelf.

In a series of papers Holloway (1983, 1984, 1985, 1987) has reported on and investigated the existence of large amplitude internal tidal waves at the shelf break region of the Australian North West Shelf. As in the Scotian Shelf case, he found that the internal tide is predominantly a first mode internal wave of large amplitude. He also found that the wave steepens on its leading face as it crosses the shelf break strip leading to the formation of an undular bore, or internal hydraulic

jump, on the forward face. A reverse internal hydraulic jump forms later in the cycle, that is after the wave has propagated onto the shelf. These internal hydraulic jumps are often followed by a packet of internal solitons. Holloway (1987) has shown that a significant fraction of the baroclinic tidal energy is associated with these internal hydraulic jumps and solitons, and that most of the baroclinic tidal flux has been dissipated upon propagation past the shelf break onto the shelf. Holloway et al. (1985) examined the transport and mixing of nutrients in this continental shelf region and concluded that these internal tidal waves may cause a significant flux of nutrients onto the continental shelf.

Winant (1974) discusses very high frequency large amplitude internal wave oscillations observed in very shallow water off the Scripps Pier in San Diego, California. These wave packets have super tidal frequency and are very complex.

Other examples of strongly nonlinear soliton formation include the packets formed as a result of tidal flow over the Sill of Gibraltar and these solitons can be seen to propagate into the Mediterranean Sea, see for example the photograph in Figure 5.32 of the monograph by Apel (1987) or the paper by Farmer & Armi (1988). Ivanov & Konyaev (1976) have investigated soliton formation over a sill in the Caspian Sea.

Internal wave packets can also be observed by SAR (synthetic aperture radar) where the internal wave packets appear as distinct linear wave packets of varying intensity in SAR imagery. Packets of internal waves of tidal frequency have been observed on continental shelves by this method. Perhaps the most

visible of these regions is the area of the SARSEX experiment, that is a 50 km box to the east of the Hudson Canyon, inshore of the shelf break and the packets are discussed by Gasparovic et al. (1988). Subsequent remote observations, for instance from satellite, have made a strong case for the existence of these packets of solitary waves throughout the world ocean, see Apel & Gonzalez (1983), Apel & Lin (1991).

2. Theoretical Background

The Korteweg de Vries (KdV) equation is well known to be a suitable physical model for describing weakly nonlinear advective effects and linear dispersion in internal waves. It was originally developed by Benney (1966) and extended to second order by Lee & Beardsley (1974). We begin this study by briefly reviewing the derivation of the KdV equation following the procedure of Lee & Beardsley (1974) and the discussion by Lamb & Yan (1996) but without mean current. The KdV equation is derived from classical nonlinear long wave theory using a two-parameter perturbation expansion in ε and δ which scale the nonlinear and dispersive effects, respectively.

The two dimensional equations for an incompressible, inviscid Boussinesq fluid are

$$\rho_0(u_t + uu_x + wu_z) = -p_x \qquad 2.1$$

$$\rho_0(w_t + uw_x + ww_z) = -p_z - g\rho \qquad 2.2$$

$$u_x + w_z = 0 \qquad 2.3$$

$$\rho_t + u\rho_x + w\rho_z = 0 \qquad 2.4$$

where equations 2.1 and 2.2 are the momentum equations, equation 2.3 is the continuity equation and equation 2.4 is the conservation of density. u is the

horizontal velocity, w is the vertical velocity, p is the pressure deviation from hydrostatic $\rho_0 gz$, g is the acceleration of gravity, and the subscripts represent derivatives with respect to x, z, and t. In the Boussinesq approximation the density, ρ_0, is a constant and $\rho = \bar{\rho}(z) + \rho'(x, z, t)$. Cross differentiation between equations 2.1 and 2.2 leads to elimination of the pressure term resulting in the vorticity equation

$$[\rho_0(u_t + uu_x + wu_z)]_z - g\rho_x - [\rho_0(w_t + uw_x + ww_z)]_x = 0. \qquad 2.5$$

Next, all variables are scaled as follows

$$x = Lx^* \qquad z = Dz^* \qquad t = \frac{L}{U}t^*$$

$$u = \varepsilon U u^* \qquad w = \varepsilon U \delta^{1/2} w^*$$

$$\rho = \rho_0[\overline{\rho}^*(z) + \varepsilon\rho^{*\prime}(x, z, t)]$$

where D is the water depth, L is the horizontal scale, U is the horizontal velocity scale, and asterisks indicate dimensionless quantities. The non-dimensional wave amplitude is given by ε, and $\delta = D^2/L^2$. The continuity equation (2.3) permits us to define a stream function ψ by

$$u = \psi_z \qquad\qquad w = -\psi_x. \qquad\qquad 2.6$$

Introducing the dimensionless variables into the conservation equations for density and vorticity (equations 2.4, 2.5) we have

$$\rho_t - \bar{\rho}_z \psi_x + \varepsilon \psi_z \rho_x - \varepsilon \psi_x \rho_z = 0 \qquad\qquad 2.7$$

$$\begin{aligned} &\left(\psi_{xt} + \varepsilon \psi_z \psi_{zx} - \varepsilon \psi_x \psi_{zz}\right)_z - \rho_x \\ &+ \delta\left(\psi_{xt} + \varepsilon \psi_z \psi_{xx} - \varepsilon \psi_x \psi_{xz}\right)_x = 0 \end{aligned} \qquad\qquad 2.8$$

where the asterisks have been dropped for convenience. The boundary conditions for a rigid level surface and bottom are

$$\psi_x = 0 \qquad @ \qquad z = 0 \qquad\qquad 2.9$$

$$\psi_x = 0 \qquad @ \qquad z = 1. \qquad\qquad 2.10$$

The stream function ψ and the perturbation density ρ' are expanded by the two parameters ε and δ, which are assumed small but not necessarily of the same magnitude, as follows:

$$\psi(x,z,t) = \sum_{i=0}^{\infty} \sum_{j=0}^{\infty} \varepsilon^i \delta^j \psi^{(i,j)}(x,z,t) \qquad\qquad 2.11$$

$$\rho'(x,z,t)=\sum_{i=0}^{\infty}\sum_{j=0}^{\infty}\varepsilon^i\delta^j\rho'^{(i,j)}(x,z,t). \qquad 2.12$$

Substituting equations 2.11 and 2.12 into equations 2.7 - 2.10, and searching for a separable solution, the 0^{th} order solution in ε and δ is assumed to have the form

$$\psi^{(0,0)}(x,z,t)=A(x,t)\phi^{(0,0)}(z) \qquad 2.13$$

with the evolution of the amplitude A given by

$$A_t=-CA_x \qquad 2.14$$

and $\phi^{(0,0)}(z)$ and C are eigenfunctions and eigenvalues of the vertical boundary value problem

$$\phi_{zz}^{(0,0)}+\frac{\overline{\rho}_z}{C^2}\phi^{(0,0)}=0$$
$$\phi^{(0,0)}(0)=\phi^{(0,0)}(1)=0 \qquad 2.15$$

There are an infinite set of solutions ($\phi_n^{(0,0)}$, C_n); however we will consider only mode one solutions and for notational convenience set $\phi=\phi_1^{(0,0)}$ and $C=C_1$. Without loss of generality the eigenfunction is normalized such that $max\ \phi(z)=1$.

Assuming a separable solution (product of a function of x, t and a function of z) at 1st order in ε and δ, the amplitude evolution equation becomes

$$A_t = -CA_x + \varepsilon rAA_x + \delta sA_{xxx} \qquad 2.16$$

with the 1st order stream functions given by

$$\psi^{(1,0)}(x,z,t) = A^2\phi^{(1,0)}(z) \qquad 2.17$$

$$\psi^{(0,1)}(x,z,t) = A_{xx}\phi^{(0,1)}(z). \qquad 2.18$$

The constants r and s are found by satisfying the integrability conditions applied to the boundary value problems that define the functions $\phi^{(1,0)}(z)$ and $\phi^{(0,1)}(z)$. The function A is now replaced by B since the parameter of principal interest is the vertical displacement of a streamline, rather than the amplitude of the stream function. The relationship between B and A to lowest order, for given depth z_0, is

$$B(x,t,z_0) = \frac{A(x,t)\phi(z_0)^{(0,0)}}{C}. \qquad 2.19$$

The evolution equation 2.16 is now redimensionalized and becomes the KdV equation:

$$\eta_t + c\eta_x + \alpha\eta\eta_x + \beta\eta_{xxx} = 0 \qquad 2.20$$

where η is the vertical displacement amplitude, dimensional c replaces C, D is the dimensional depth, and α and β are defined as follows:

$$\alpha = \left(\frac{3}{2}\right)\frac{\int_0^D c^2(\phi_z)^3 dz}{\int_0^D c(\phi_z)^2 dz} \qquad 2.21$$

$$\beta = \left(\frac{1}{2}\right)\frac{\int_0^D c^2\phi^2 dz}{\int_0^D c(\phi_z)^2 dz}. \qquad 2.22$$

Progressing to 2nd order in ε and δ yields four additional terms to 2.20 and is known as the fully extended KdV equation (feKdV). Often only the second-order nonlinear term ('cubic nonlinearity') is added resulting in the dimensional extended KdV (eKdV) equation

$$\eta_t + c\eta_x + (\alpha + \alpha_1\eta)\eta\eta_x + \beta\eta_{xxx} = 0 \qquad 2.23$$

where α_1 is a complicated function of α, c, ϕ, and N, where N is the buoyancy frequency.

Continuous stratification can support an infinite number of modes. For simplicity we will consider wave propagation in a two-layer stratification which can only support one mode. The justification for making this approximation is that most of the energy in the ocean appears to be contained in the first mode anyway. Also the shelf often has the appearance of a two-layer stratification: an upper mixed layer separated from a weakly stratified bottom layer by a thin pycnocline. The coefficients of the KdV and eKdV equations are greatly simplified for a two-layer fluid and are written (e.g. Ostrovsky & Stepanyants, 1989)

$$c = \sqrt{\frac{g\Delta\rho}{\rho}\frac{h_1 h_2}{h_1 + h_2}} \qquad 2.24$$

$$\alpha = \frac{3}{2} c \frac{h_1 - h_2}{h_1 h_2} \qquad 2.25$$

$$\beta = c\frac{h_1 h_2}{6} \qquad 2.26$$

$$\alpha_1 = -\frac{3c}{8h_1^{\,2}h_2^{\,2}}\left(h_1^{\,2} + h_2^{\,2} + 6h_1 h_2\right) \qquad 2.27$$

where $\Delta\rho$ is the density difference between the upper and lower layers, and h_1 and h_2 are the thickness of the upper and lower layers, respectively.

We are interested in applying the KdV and eKdV equations to situations where the coefficients vary spatially. This problem has been investigated for slowly varying topography and stratification by Grimshaw (1979) and Pelinovsky et al. (1977). The eKdV equation then has variable coefficients and an additional term:

$$\eta_t + c\eta_x + (\alpha + \alpha_1\eta)\eta\eta_x + \beta\eta_{xxx} + \frac{c}{2Q}Q_x\eta = 0 \qquad 2.28$$

where the term in Q accounts for the horizontal variability of the ocean and is given by

$$Q = \frac{Mc^3}{M_0 c_0{}^3} \qquad 2.29$$

with

$$M = \frac{h_1 + h_2}{h_1 h_2} \,. \qquad 2.30$$

The zero subscript indicates a constant value at a predetermined position. The variable coefficient KdV equation is the same as the variable coefficient eKdV equation but with $\alpha_1 = 0$.

For convenience in solving the equation, we use a transformation used by Pelinovsky & Shavratsky (1976) of the space and time variables x and t to variables l and s given by

$$s = \int_0^x \frac{dx}{c(x)} - t, \qquad l = x. \tag{2.31}$$

The transformed eKdV is

$$\zeta_l + \frac{1}{c^2\sqrt{Q}}(\alpha + \alpha_1\zeta)\zeta\zeta_s + \frac{\beta}{c^4}\zeta_{sss} = 0 \tag{2.32}$$

where

$$\zeta = \eta\sqrt{Q(l)}. \tag{2.33}$$

The transformation scales time so that disturbances traveling at the linear speed, c, remain at constant s. The system is often referred to as a slowness coordinate system. Because ζ varies relatively slowly in l/c compared to s, terms such as $c\zeta_l$ are neglected relative to ζ_s. The transformed KdV equation is the same as the transformed eKdV equation with $\alpha_1 = 0$ such that

$$\zeta_l + \frac{\alpha}{c^2\sqrt{Q}}\zeta\zeta_s + \frac{\beta}{c^4}\zeta_{sss} = 0. \tag{2.34}$$

Important solutions of the KdV and eKdV equations are waves of permanent form. One family of these waves are the solitary waves. There is a strong tendency for a long but otherwise arbitrary initial condition to evolve into a

train of solitary waves (e.g. Lee & Beardsley, 1974; Drazin & Johnson, 1989). The solitary wave solution for the KdV equation in (l, s) space for constant parameters is given by (Zhou & Grimshaw, 1989)

$$\eta = \eta_0 \operatorname{sech}^2\left(\frac{\frac{c-V}{c}l + cs}{\Delta}\right) \qquad 2.35$$

where

$$V = c + \frac{\alpha\eta_0}{3} \qquad 2.36(a)$$

and

$$\Delta^2 = \frac{12\beta}{\alpha\eta_0}. \qquad 2.36(b)$$

The solitary wave is a single 'bump' propagating at speed V without change in form - nonlinearity being balanced by dispersion (Figure 2.1). The amplitude, η_0, is inversely proportional to the square root of the width, Δ - higher amplitudes imply narrower widths. The solitary waves can be either waves of elevation ($\eta_0 > 0$, $\alpha > 0$) or waves of depression ($\eta_0 < 0$, $\alpha < 0$). Since the product $\alpha\eta_0$ is always greater than zero, KdV solitary-like waves always travel with wave speed greater than c. For future use, it is useful to consider the difference between the magnitude of the nonlinear and dispersive terms:

$$\chi = \left|\frac{\alpha}{c^2}\eta\eta_s\right| - \left|\frac{\beta}{c^4}\eta_{sss}\right| \qquad 2.37\ (a)$$

and the analytical values of these terms for $\eta=\eta_0\mathrm{sech}^2(\xi)$, where ξ is the argument given in equation 2.35, are:

$$\frac{\alpha}{c^2}\eta\eta_s = -\frac{2\alpha}{c\Delta}\eta\eta_0\,\mathrm{sech}^2(\xi) \qquad 2.37\ (b)$$

$$\frac{\beta}{c^4}\eta_{sss} = 8\frac{\beta}{c\Delta^3}\eta_0\left(\mathrm{sech}^2(\xi)\tanh(\xi)\right)\left(2\mathrm{sech}^2(\xi) - \tanh(\xi)\right). \qquad 2.37\ (c)$$

Note that for $\mathrm{sech}^2(\xi)$ the nonlinear term is for the most part larger than the dispersive (Figure 2.1).

The solitary wave solution to the eKdV equation has a more complicated analytical form (Stanton & Ostrovsky, 1998):

$$\eta = -\frac{\alpha v}{2\alpha_1}\left\{\tanh\left(\frac{\frac{c-V}{c}l + cs}{\Delta} + \sigma\right) - \tanh\left(\frac{\frac{c-V}{c}l + cs}{\Delta} - \sigma\right)\right\} \qquad 2.38$$

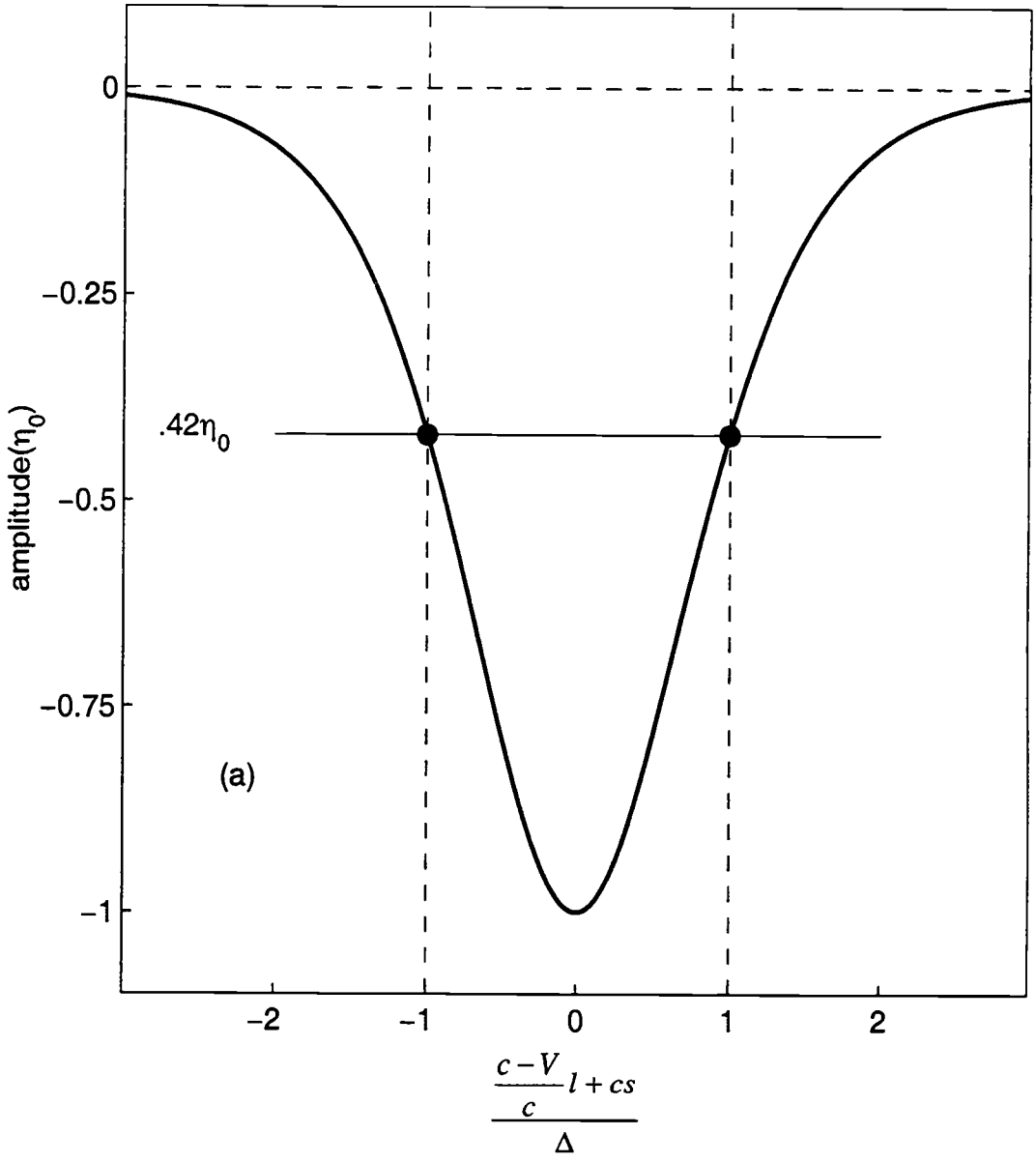

Figure 2.1. (a) KdV 'sech^2' wave with amplitude of -1 m, where the wave argument value is shown on the abscissa and parameter values are calculated from Case 1 model runs (h_1 = 50 m, h_2 = 150 m, $g\Delta\rho/\rho$ = .014 m/s^2, see Chapter 3). The amplitude of these waves is reduced to 42% of its maximum value when the argument is 1 (continued).

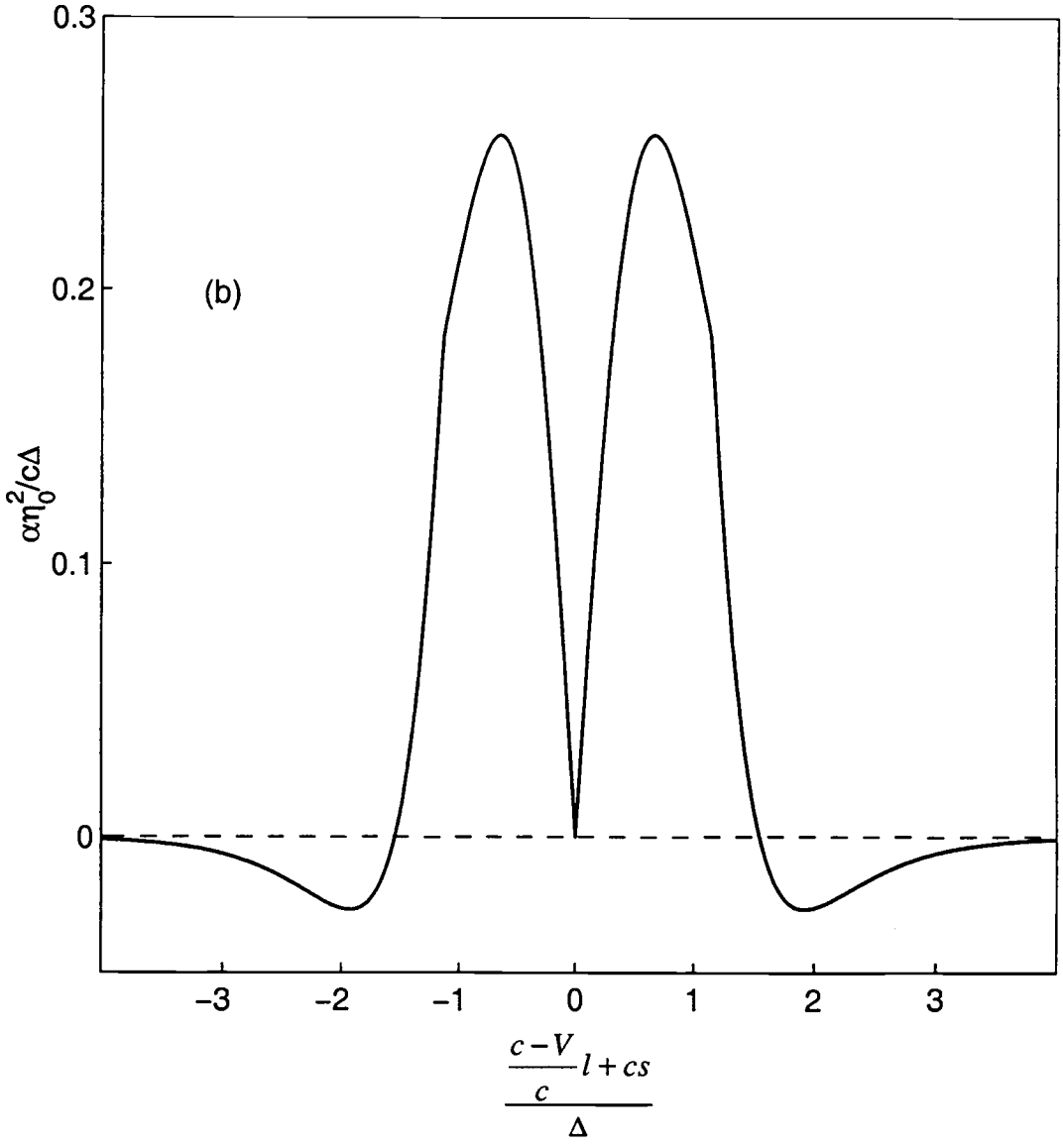

Figure 2.1 (b). The difference of the absolute values of the nonlinear and dispersive terms, χ, in the KdV equation for the 'sech^2' wave shown in (a).

where ν is a nonlinearity parameter between zero and one, and the other parameters are

$$V = c - \frac{\alpha^2 \nu^2}{6\alpha_1} \qquad 2.39\ (a)$$

$$\Delta^2 = -\frac{24\alpha_1 \beta}{\alpha^2 \nu^2} \qquad 2.39\ (b)$$

$$\sigma(\nu) = \frac{1}{4} \ln\left[\frac{1+\nu}{1-\nu}\right]. \qquad 2.39\ (c)$$

The shape of the "tanh" eKdV solitary wave is similar to the "sech^2" KdV solitary waves for small amplitude (Figure 2.2). As amplitude increases the eKdV solitary waves become thicker than the KdV solutions. Unlike the sech^2 solitary wave, the tanh wave has a maximum amplitude, which is given by α/α_1 (e.g. Stanton & Ostrovsky, 1998).

For our application we assume sinusoidal tidal forcing at the boundary $l = 0$

$$\zeta(s, l=0) = a_0 \sin(\omega s) \qquad 2.40$$

where a_0 is the tidal amplitude and ω is the frequency of the internal tide, with periodic conditions

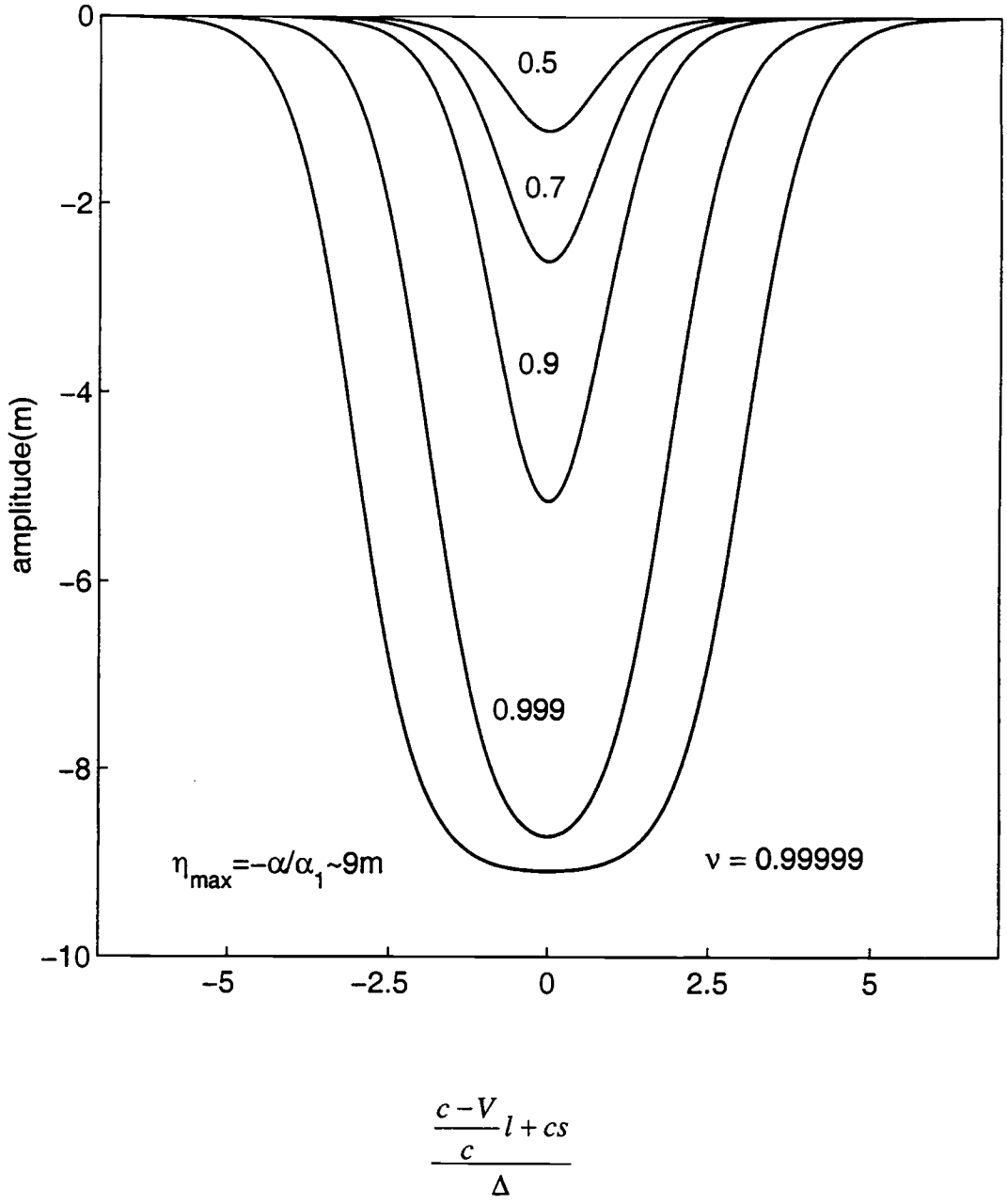

Figure 2.2. eKdV 'tanh' wave for several values of the nonlinear parameter, ν. The parameter values are calculated from Case 1 model runs (h_1 = 50 m, h_2 = 150 m, $g\Delta\rho/\rho$ = .014 m/s^2, see Chapter 3). The limit of the wave amplitude, α/α_1 is approached as $\nu \rightarrow 1$ and the waves become more square-like.

$$\zeta\left(s+\frac{2\pi}{\omega},l\right)=\zeta(s,l). \qquad 2.41$$

We employ the same finite difference scheme as Holloway et al. (1997) to solve the eKdV equation (2.34) numerically. The eKdV equation in this form is written as:

$$\frac{\zeta_j^{n+1}-\zeta_j^{n-1}}{2\Delta l}+\frac{1}{c_j^{\,2}\sqrt{Q}}\left(\alpha_j+\alpha_{1j}\zeta_j^n\right)\zeta_j^n\frac{\zeta_{j+1}^n-\zeta_{j-1}^n}{2\Delta s}$$

$$+\frac{\beta_j}{c_j^{\,4}}\frac{\zeta_{j+2}^n-2\zeta_{j+1}^n+2\zeta_{j-1}^n-\zeta_{j-2}^n}{2(\Delta s)^3}=0 \qquad 2.42$$

where Δl and Δs are the grid resolution spacing values in space and time, respectively. For the first step the temporal difference $(\zeta_j^{n+1}-\zeta_j^{n-1})/2\Delta l$ is replaced by $(\zeta_j^{1}-\zeta_j^{0})/\Delta l$, where ζ_j^0 is the value of the initial wave form. The finite difference scheme is a central difference method, (e.g. Lapidus & Pinder, 1982), which was first developed for the KdV equation by Berezin (1987), and for the variable coefficients KdV equation by Pelinovsky et al. (1994). The difference scheme for the generalized KdV equation remains numerically stable provided

$$\frac{\Delta s}{\Delta l}\left(|\alpha\zeta|+\frac{3\sqrt{3}\beta}{2(\Delta l)^2}\right)<1 \qquad 2.43$$

(e.g. Holloway et al., 1997). Note that we use values of Δs = 55s and Δl = 10 m throughout this work.

3. Two-Layer Model

We are interested in modeling the evolution of the internal tide as it propagates shoreward from the shelf break. Since the greatest oceanic signal is the first internal mode, the stratification of the continental shelf / slope region is modeled as a two-layer fluid. This approximation greatly simplifies the problem; the numerical scheme is much less complex for the two-layer case than the continuously stratified case, and the results are easier to interpret. Using the two-layer model, we will explore the propagation of the internal tide over various types of topography. These include the simplest case of flat bottom with level interface, progressing to realistic topography with sloping interface. All of these cases will be run within the quadratic nonlinear framework of the KdV equation. The results will then be compared with the eKdV model results.

For the KdV equation (2.20) and the eKdV equation (2.23) to be valid, the leading two terms must constitute the primary balance. The nonlinear and dispersive terms can become important, but the assumptions leading to the KdV and eKdV equations are violated if either of the nonlinearity or dispersion terms approach the magnitude of the leading terms. Nonlinear transformation of the internal tide leads to the generation of nonlinear waves which tend to become solitary-like in form as the dispersive term becomes important.

We begin by discussing the coefficients of the KdV and eKdV equations for a two-layer fluid. Throughout this chapter the density difference between the layers is

chosen to be a constant: $g\Delta\rho/\rho = .014$ m/s^2, a representative value for the Coastal Mixing and Optics (CMO) experiment. The linear phase speed, c, is then a function of h_1 and h_2 only (equation 2.24, Figure 3.1). The values of c are symmetric about the line $h_1 = h_2$, this is immediately obvious from the parameter for the effective or harmonic depth contained within the phase speed (Apel, 1987)

$$h' = \frac{h_1 h_2}{h_1 + h_2} . \qquad 3.1$$

Lines of constant total water depth are perpendicular to the line $h_1 = h_2$. For a given total water depth, the speed is greatest when $h_1 = h_2$ and the speed decreases as the difference in layer thickness increases. Starting at a point on the line $h_1 = h_2$ and keeping the thickness of one of the layers constant, the speed of the wave decreases exponentially as the thickness of the other layer decreases.

The coefficient α is also a function of h_1 and h_2 only (equation 2.25, Figure 3.2). The values of α/c are anti-symmetric about the line $h_1 = h_2$, where $\alpha/c = 0$. Starting at a point on the line $h_1 = h_2$ and keeping the thickness of one layer constant, the value of $\alpha \rightarrow \infty$ exponentially as the thickness of the other layer decreases. The absolute value of α/c changes least rapidly when $h_1 \approx h_2$. When the thick layer is larger than the thin layer by at least a factor of 2 to 3, then α/c is relatively insensitive to the thickness of the thick layer, that is when $h_2 >> h_1$, then $|\alpha/c| \approx 3/2h_1$ and is not a function of h_2. The parameter α/c is also important

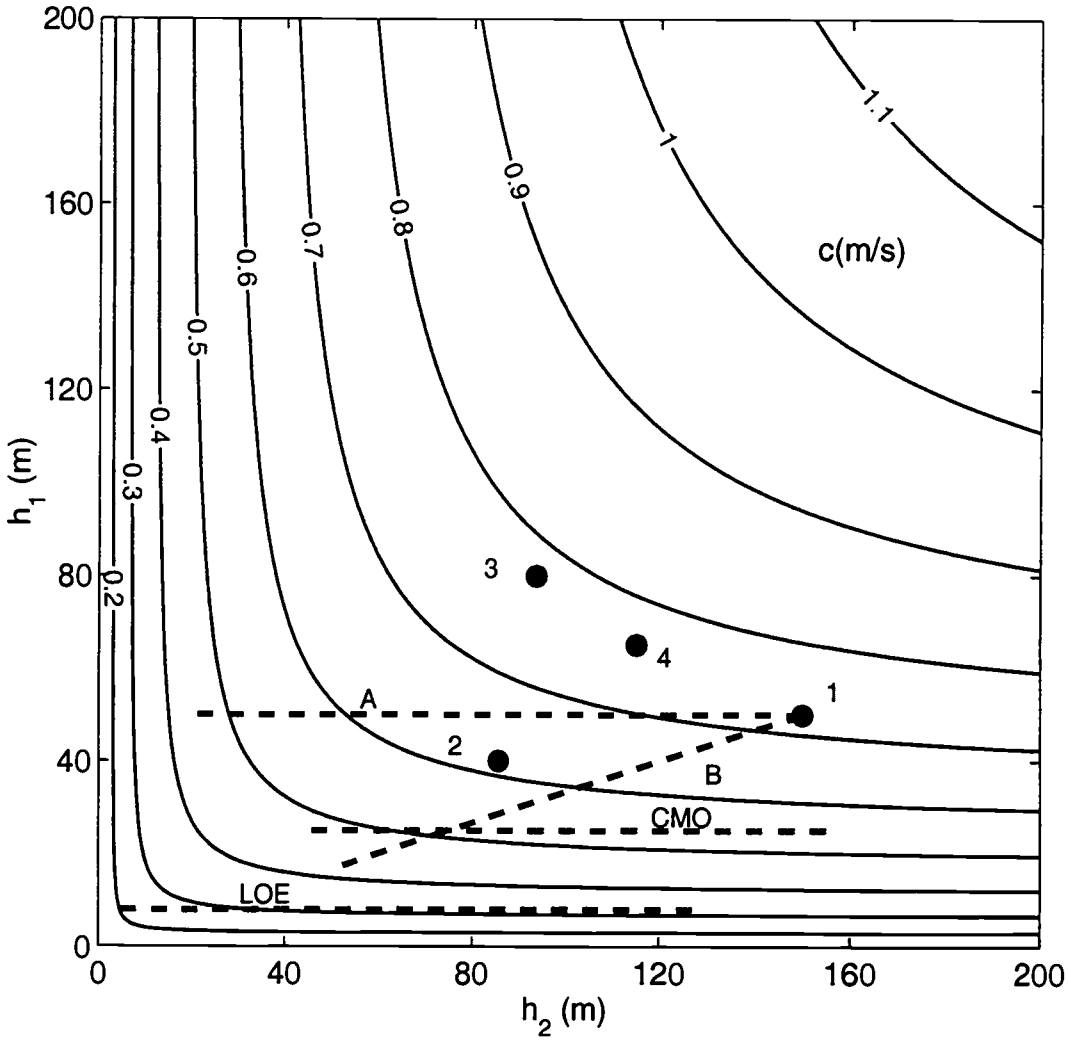

Figure 3.1. Linear wave speed, c, as a function of the depth of the upper layer, h_1, and lower layer, h_2. Also shown are the values for level bottom (Cases 1 - 4), sloping bottom (Cases A and B) and realistic slope and stratification (LOE and CMO).

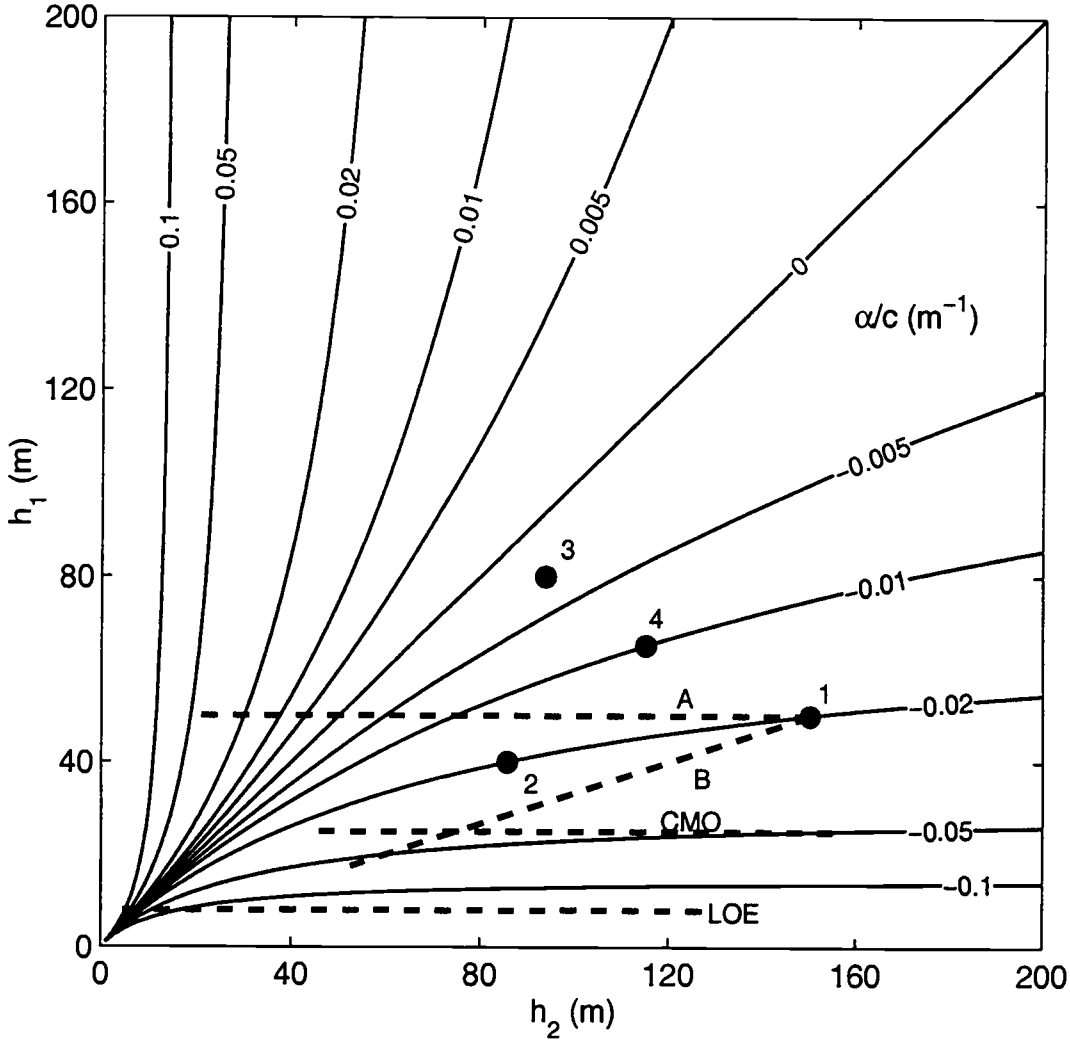

Figure 3.2. KdV quadratic nonlinear parameter, α, divided by the linear wave speed, c, as a function of the depth of the upper layer, h_1, and lower layer, h_2. Also shown are the values for level bottom (Cases 1 - 4), sloping bottom (Cases A and B) and realistic slope and stratification (LOE and CMO).

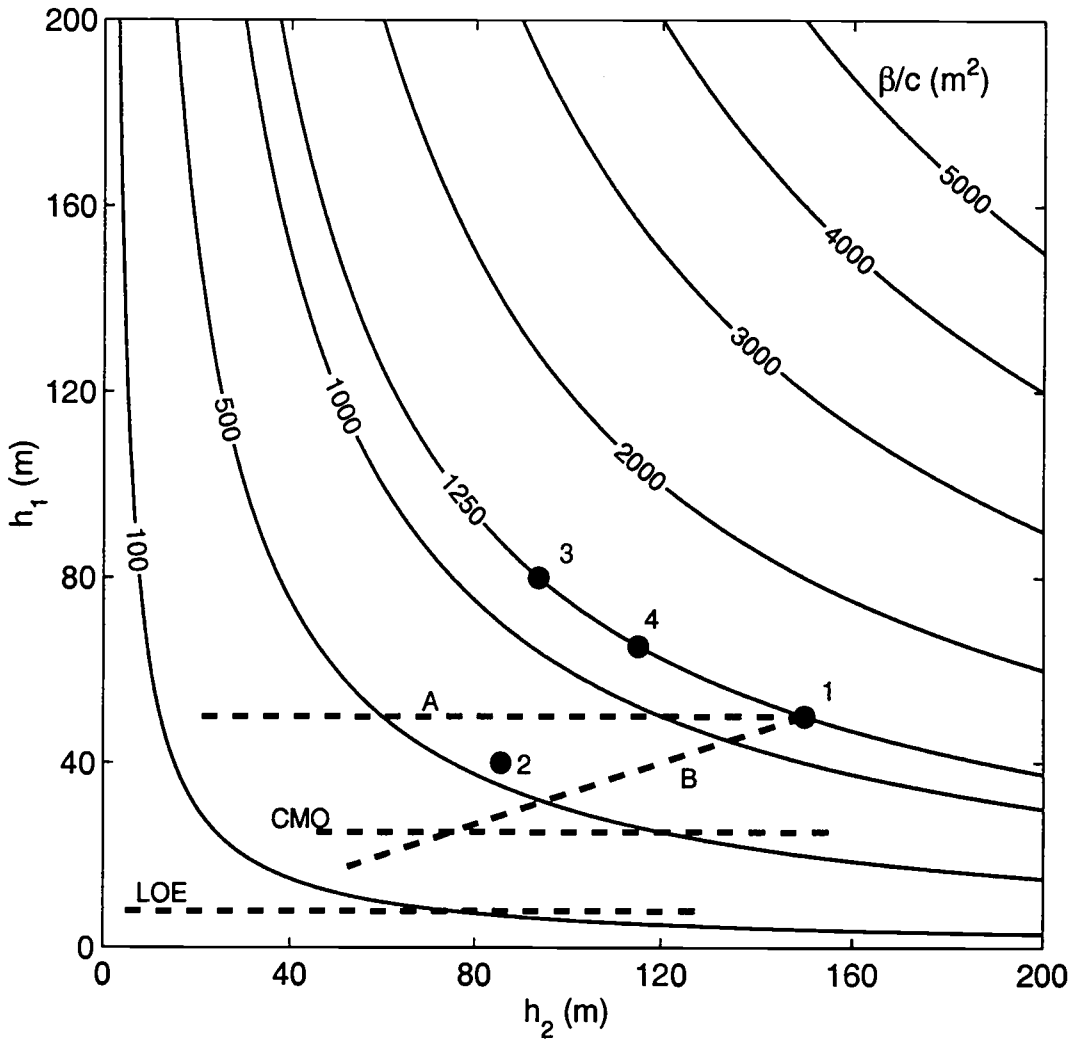

Figure 3.3. KdV dispersion parameter, β, divided by the linear wave speed, c, as a function of the depth of the upper layer, h_1, and lower layer, h_2. Also shown are the values for level bottom (Cases 1 - 4), sloping bottom (Cases A and B) and realistic slope and stratification (LOE and CMO).

because when multiplied by the amplitude, η, it represents the ratio of the nonlinear to the linear terms in the KdV equation (equation 2.20).

The coefficient of the dispersive term, β, divided by c is also a function of h_1 and h_2 only (equation 2.27, Figure 3.3). The values are symmetric about the line $h_1 = h_2$. The value of β/c for any given water depth is a maximum when the individual layer depths are equal, $h_1 = h_2$. The parameter value decreases as either one of the layers becomes small. The interpretation of Figure 3.3 as a ratio of terms is complicated. Unlike Figure 3.2 the derivatives do not cancel and the ratio cannot be simplified.

The coefficient of the cubic nonlinear term, α_1, when divided by c is also a function of h_1 and h_2 only (equation 2.27, Figure 3.4). The value of α_1 is always negative and is symmetric about the line $h_1 = h_2$. For a given water depth, the magnitude of α_1 is least when $h_1 = h_2$. The value of $\alpha_1 \rightarrow -\infty$ as either one of h_1 or $h_2 \rightarrow 0$.

It is also useful to calculate the ratio α/α_1 (Figure 3.5). The relative importance of the quadratic to cubic nonlinearity is given by $\alpha/\alpha_1\eta$. For a given water depth cubic nonlinearity is most important when $h_1 \approx h_2$, i.e. when the magnitude of α is small. The magnitude of the quadratic nonlinear term is much greater than that of the cubic nonlinear term when the water depth of one layer is much greater than the other and in this case the eKdV model is very similar to the KdV model.

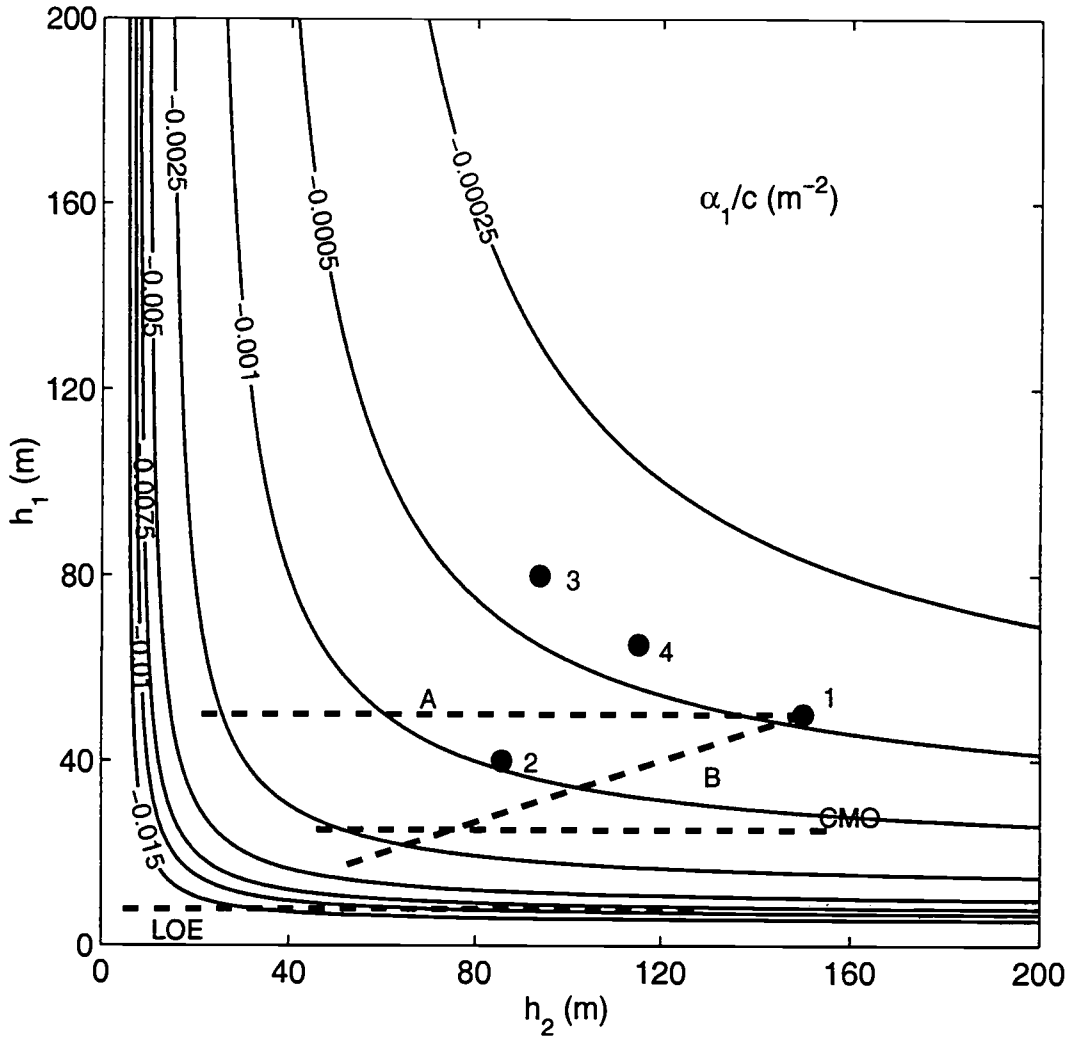

Figure 3.4. eKdV cubic nonlinear parameter, α_1, divided by the linear wave speed, c, as a function of the depth of the upper layer, h_1, and lower layer, h_2. Also shown are the values for level bottom (Cases 1 - 4), sloping bottom (Cases A and B) and realistic slope and stratification (LOE and CMO).

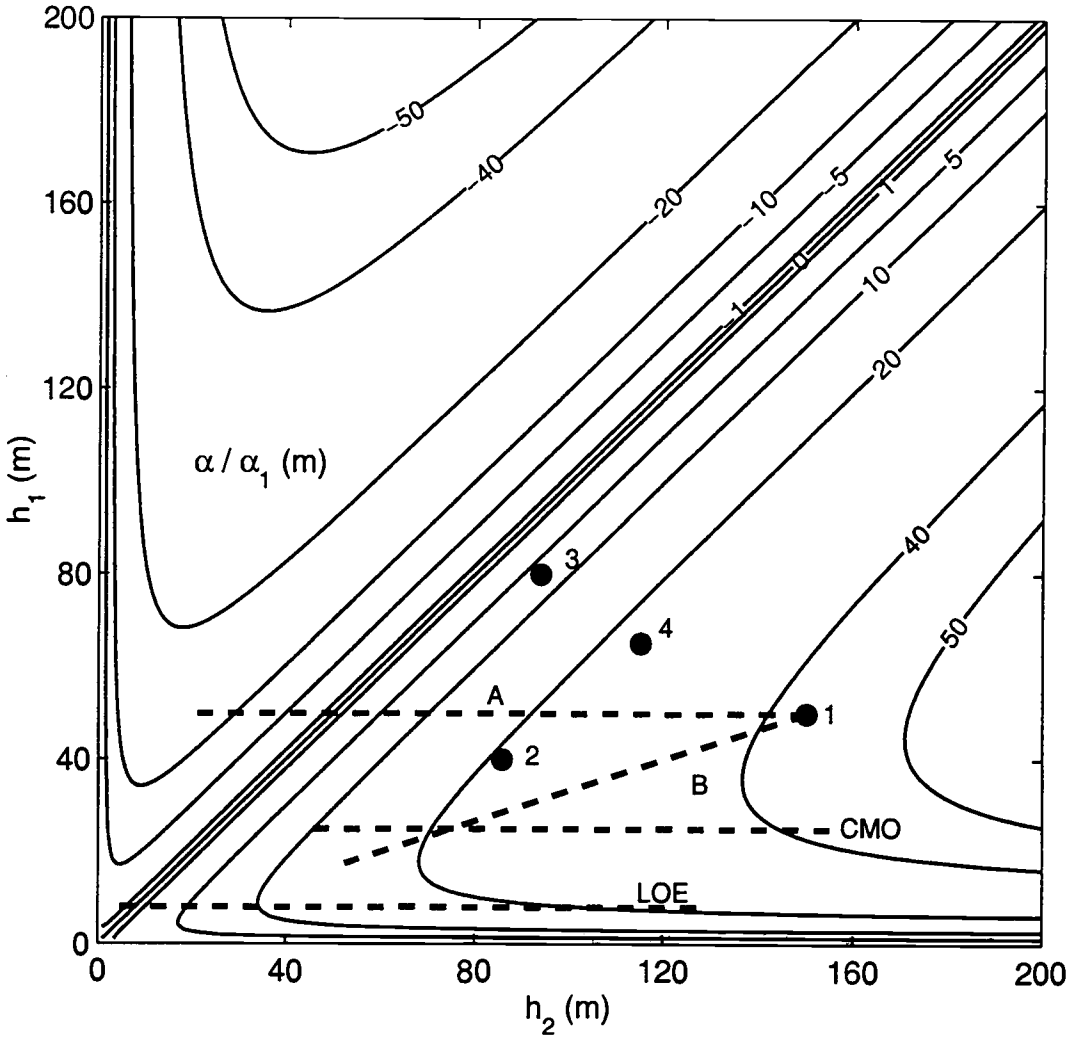

Figure 3.5 Quadratic nonlinear parameter, α, divided by the cubic nonlinear parameter, α_1, as a function of the depth of the upper layer, h_1, and lower layer, h_2. Also shown are the values for level bottom (Cases 1 - 4), sloping bottom (Cases A and B) and realistic slope and stratification (LOE and CMO).

We note that the effective depth, h', is the inverse of the parameter M (equation 2.30) contained in Q. For level bottom with horizontal interface the values of h_1 and h_2 are constant and $Q = 1$ everywhere which means that the horizontal variability term vanishes, and the canonical KdV is the valid model.

We begin with the solutions of the KdV equation. The eKdV model solutions are discussed in section 3.2.

3.1 The Korteweg de Vries (KdV) Model

Using the KdV equation, we first investigate 4 cases with level bottom for different combinations of h_1 and h_2. We then progress to constant sloping bottom, first with a horizontal interface and then with a sloping interface. Finally, we make model runs with realistic topography at the sites of the Coastal Mixing and Optics experiment (CMO) and the Littoral Optics Experiment (LOE).

3.1.1 Level Bottom

We begin by examining the evolution of the internal tide over a level bottom. We also choose a level interface (h_1 and h_2 constant). This simple fluid arrangement is instructive when developing an intuitive feel for the generation and propagation of internal wave packets. A level bottom is also a good approximation for the continental shelf where the total water depth changes slowly in the

horizontal. Four cases with different upper and lower layer thickness were selected to look at the effects of different relative magnitudes of α and β (Table 1). The first case, with h_1 = 50 m and h_2 = 150 m, was chosen because these are reasonable values of upper and lower layer depth on outer continental shelves.

Case	h_1	h_2	α/c	β/c	α	β	c	$(12\beta/\alpha)^{1/2}$
1	50	150	- .02	1250	- .0145	906	0.725	628
2	40	85.7	- .02	571	- .0124	353	0.618	362
3	80	93.8	- .0021	1250	- .0016	972	0.777	2041
4	65.1	115.1	- .01	1250	- .0076	954	0.763	1227

Table 1. KdV parameter values for Cases 1 - 4.

The results of Case 1 are shown in Figures 3.6 and 3.7. A sinusoidal internal tidal amplitude of 5 m was used as the forcing at $l = 0$ (equation 2.40). As it propagates, the internal tide steepens on the trailing edge or "back face" of the sine wave and a shock-like front forms at about $l \approx 50$ km. At this stage we also see the beginnings of undulations developing behind the shock-like front. By 75 km a pack of nonlinear solitary-like waves has begun to form. It is evident at 100 km that the solitary-like waves of depression are rank ordered with the largest amplitude first.

The first three waves at 100 km are compared with the sech^2 solitary wave-form in Figure 3.8. Using the values of α, β and c, the shape of the solitary wave (equation 2.36) is determined by a single parameter, the amplitude, which is subjectively adjusted for best fit. The subjectively chosen sech^2 fits with offset are exact solutions of the KdV equation albeit with modified velocity given by:

$$V = c + \alpha\left(\frac{\eta_0}{3} + \frac{2}{3}\eta_\infty\right) \qquad 3.2$$

where η_0 - η_∞ is the wave amplitude and η_∞ is the low frequency interface offset (Zabusky & Kruskal, 1965). The smaller amplitude trailing waves appear more symmetric and sinusoidal in shape compared to solitary waves. Figure 3.7 is a contour plot of displacement showing propagation of the internal tide in (l,s) space. The transformation to s and l space results in a wave of speed c following a line of constant s. A solitary wave with phase speed $V > c$ will appear at smaller value of s for increasing l along the propagation path, i.e. will curve to the left as the tide progresses vertically up the plot along a maximum / minimum. The maxima and minima of the nonlinear waves travel at different speeds with the leading one (at smallest s) traveling fastest. Since a given solitary-like wave may vary in amplitude and offset as it propagates in l, we also expect the track of the wave to curve in s and l space. The trailing sinusoidal-like waves travel with wave speed less than c, indicating that dispersion is important. An interesting observation is that some of

the minima of the nonlinear waves initially travel with wave speed less than c and eventually travel with speeds greater than c (for example see the 7th minimum in Figure 3.7).

Figure 3.9 shows the difference between the magnitudes of the nonlinear and dispersive terms, χ (Figure 2.1 (b)), for Case 1 at various distances in l. At 100 km we see the balance changing over the tidal period. The leading waves at the left have the shape expected for a sech^2 solitary wave (Figure 3.8). The trailing waves to the right appear more sinusoidal in shape, and are relatively more dispersive than a sech^2 wave. Upwards of twenty waves have formed when the internal tide has traveled 160 km. The leading six to seven waves travel with speed greater than c and have a nearly sech^2 form. The trailing waves travel slower than c as expected for waves that are more dispersive.

For Case 2 we choose h_1 and h_2 such that $\alpha/c = -.02$ as in Case 1, but the value of β/c is less than half that of Case 1. Since the ratio of the dispersive coefficient to the nonlinear coefficient has been reduced by more than half, we expect Case 2 to be more nonlinear, that is we expect the internal tide to steepen sooner, and nonlinear internal waves to form at smaller l. Figures 3.10 and 3.11 show that the internal tide evolves similarly to that for Case 1. However, as expected, the shock-like front and subsequent undulations appear at smaller values of l than for Case 1. Comparing Figures 3.6 and 3.10, the internal tide is more nonlinear at $l = 50$ km for Case 2 than it is for Case 1. Also, a greater number of

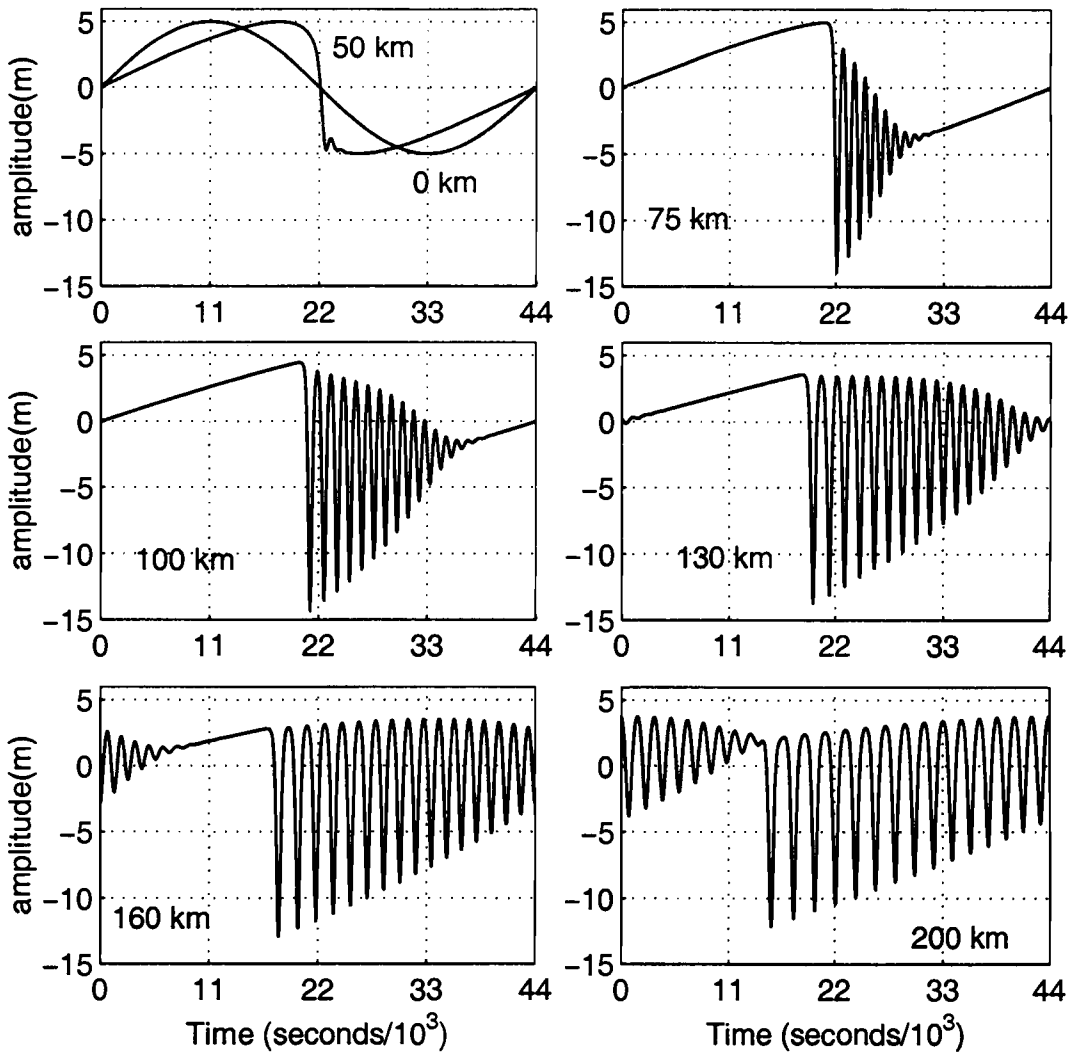

Figure 3.6. Case 1 (h_1 = 50 m, h_2 = 150 m, level bottom) amplitude of the internal mode for two layer fluid at various distances from the boundary within KdV model framework.

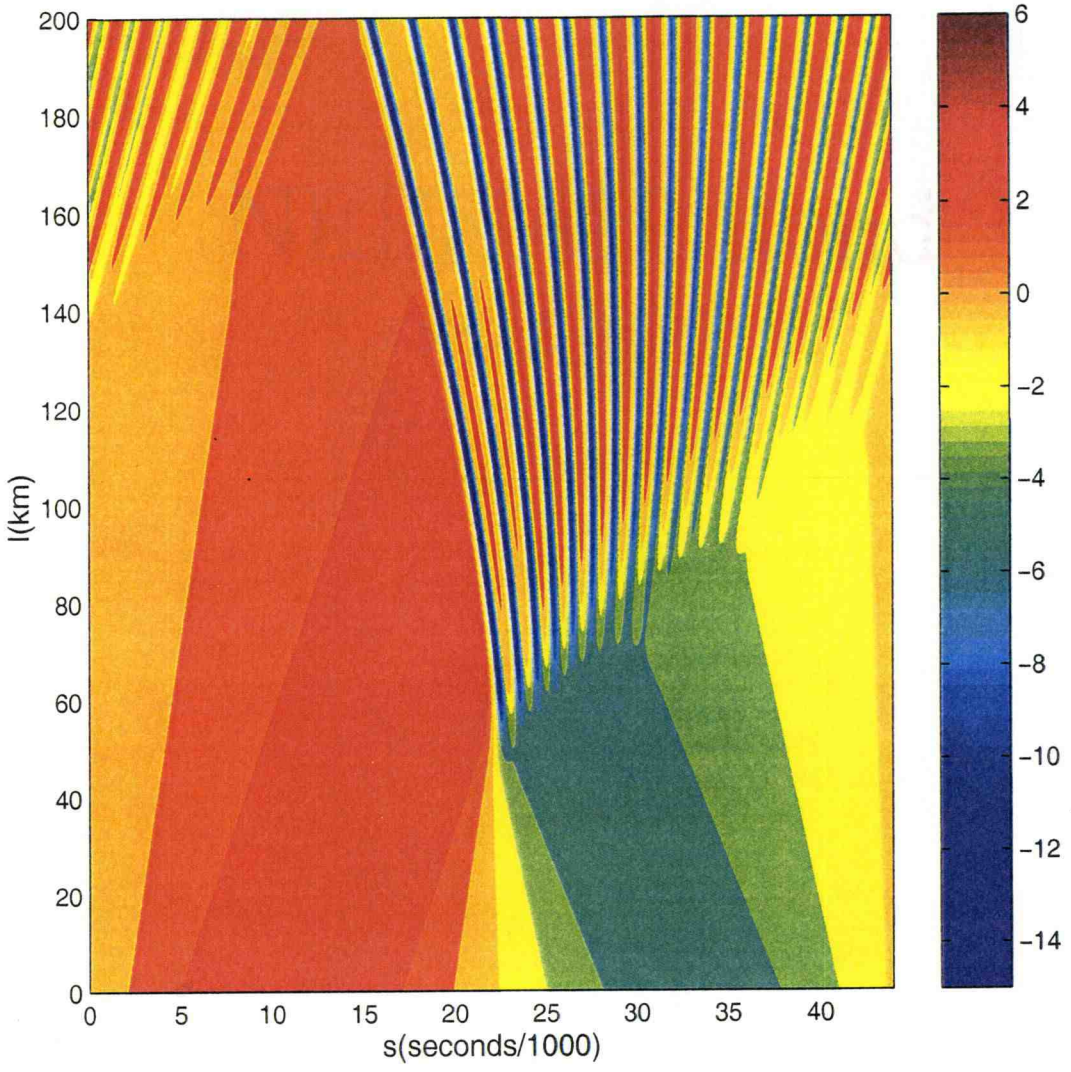

Figure 3.7. Case 1 (h_1 = 50 m, h_2 = 150 m, level bottom) amplitude of the internal mode for two layer fluid as a function of distance l and time s within KdV model framework. The panel on the right corresponds to the amplitude of the waves in meters.

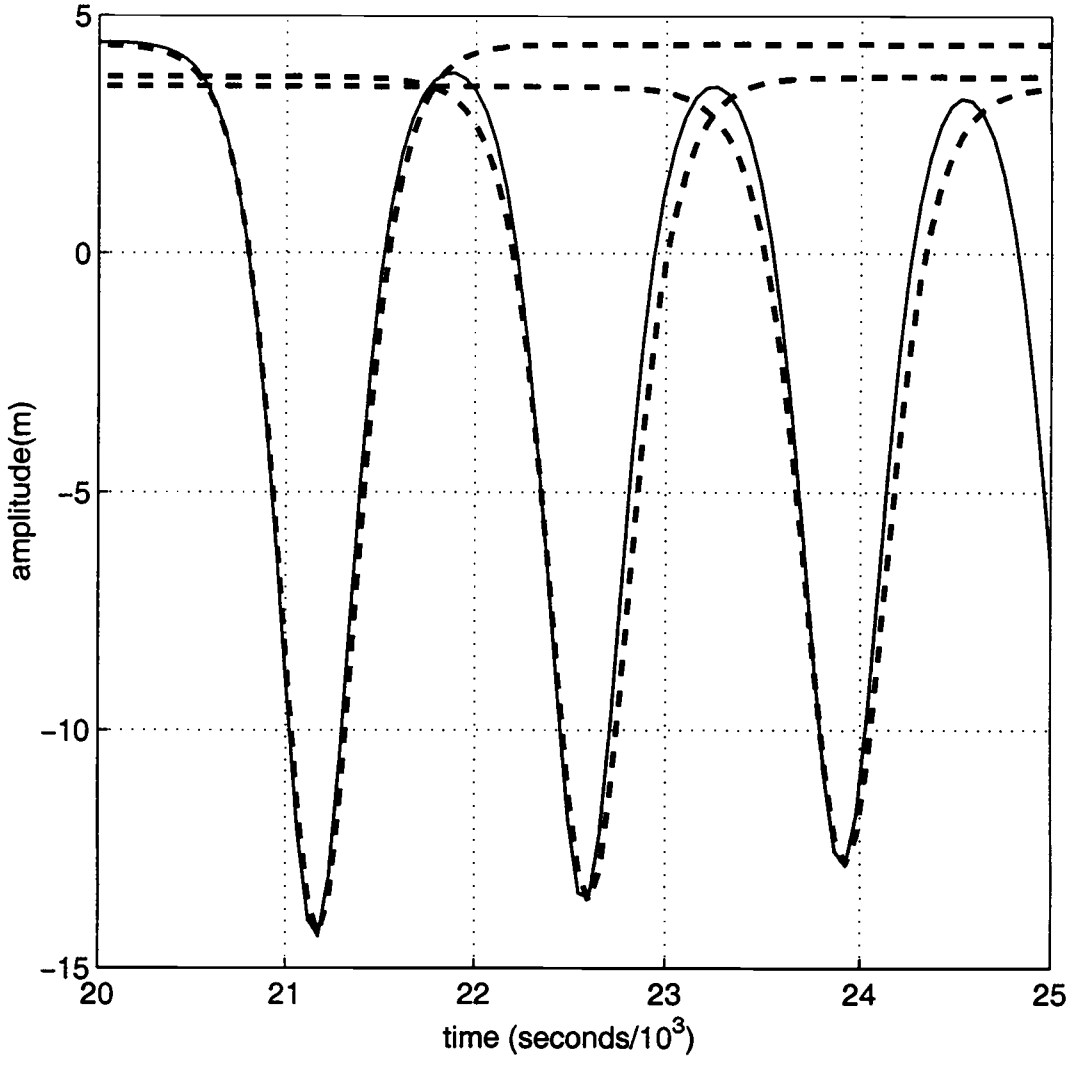

Figure 3.8 (a). Case 1 (h_1 = 50 m, h_2 = 150 m, level bottom). The three leading waves of depression (solid line) at a distance of 100 km from the boundary shown in Figure 3.6 are plotted with three individual sech^2 waves (broken lines). (continued)

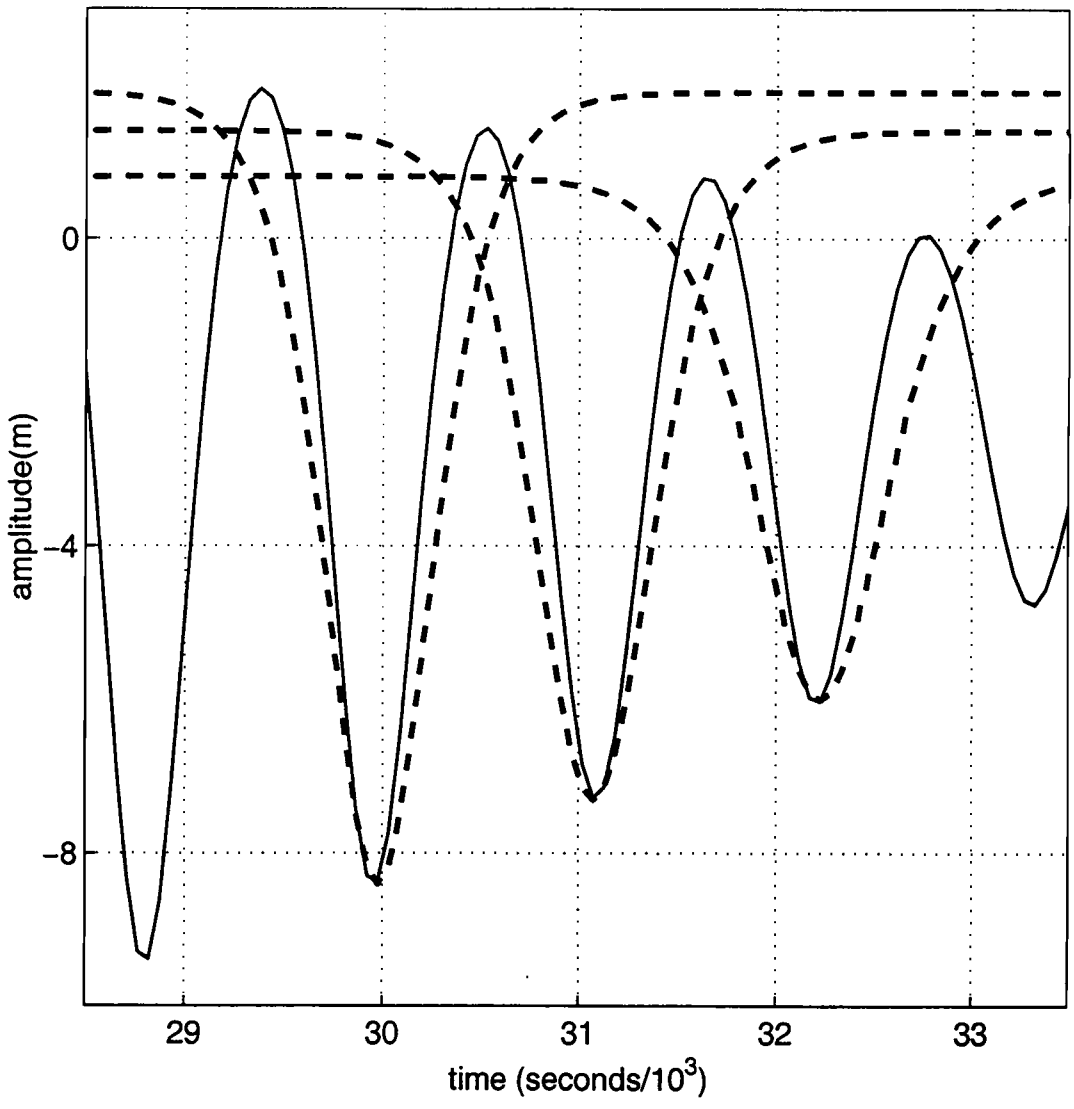

Figure 3.8 (b). Same as Figure 3.8 (a) but for trailing waves in the packet.

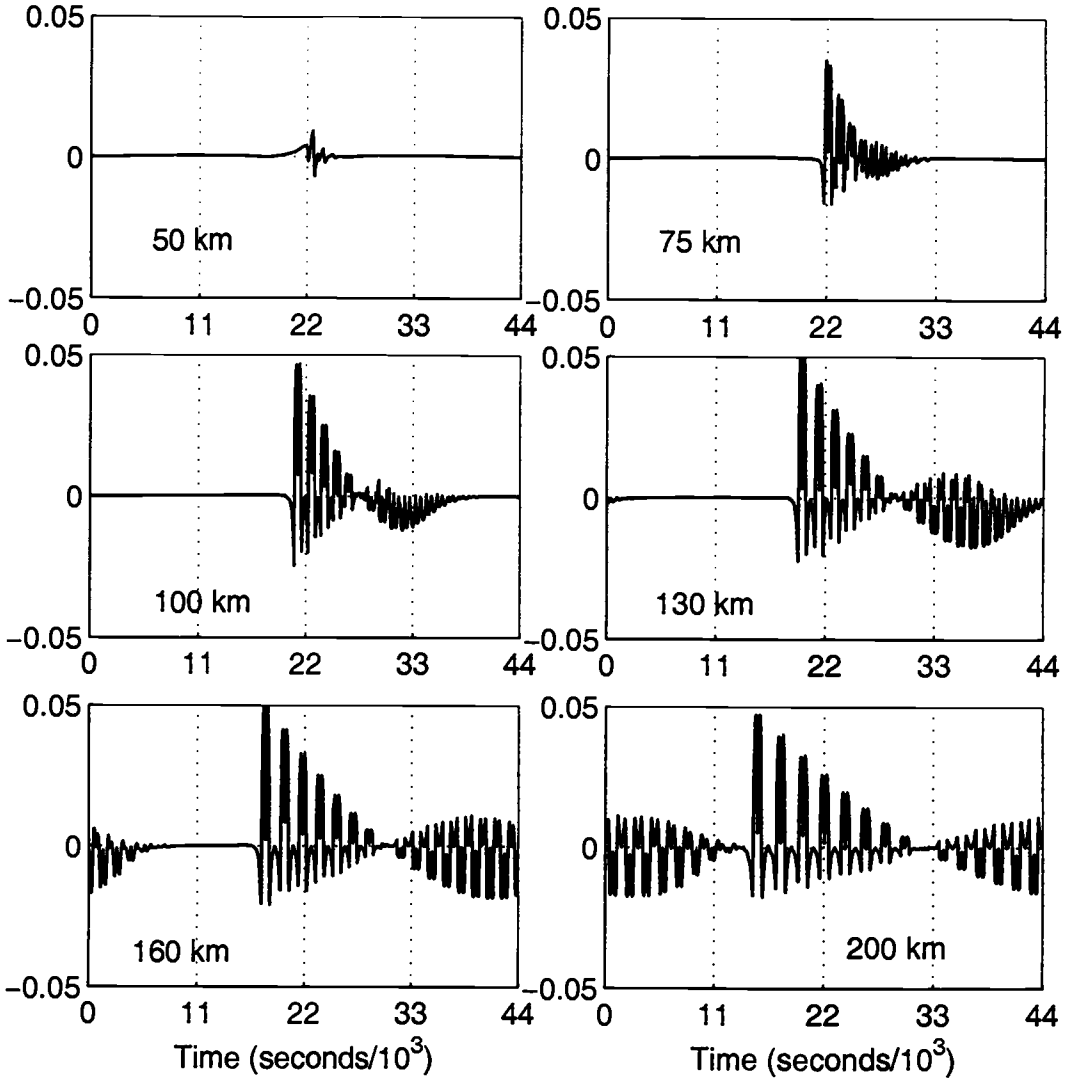

Figure 3.9. Case 1 (h_1 = 50 m, h_2 = 150 m, level bottom) difference between the magnitudes of the nonlinear and dispersive terms, χ (non-dimensional), at various distances from the boundary within KdV model framework.

solitary waves have formed in Case 2 by l = 100 km, and they are more closely spaced.

Figure 3.12 is a plot of the difference between the magnitudes of the nonlinear and dispersive terms, χ, for Case 2. It appears that more of the leading waves have sech^2 form at 165 km in Case 2 when compared to Case 1. For Case 2, a few more of the leading waves travel with speed greater than c compared with Case 1; the remaining waves have speed less than c, and disperse from the leading waves as l increases.

For Case 3 we choose β/c = 1250, as in Case 1, but with α/c = −.0021, a factor of ten less than the value used in both Case 1 and Case 2. As a result, we expect the internal tide to be much less nonlinear. Indeed the internal tide steepens slowly and even by l = 200 km solitary-type waves have not been generated (Figure 3.13). We expect the internal tide would continue to steepen as it propagates, and eventually form a nonlinear wave packet.

For Case 4 the nonlinearity parameter is half that used in Case 1, α/c = −.01and β/c is the same value (Table 1). We expect the resultant internal tide to be more nonlinear than Case 3 but less so than either of Cases 1 or 2. The internal tide steepens slowly and the first wave of depression begins to form when $l \approx 100$ km (Figures 3.14, 3.15). Fewer nonlinear waves have formed at this point than in either Case 1 or Case 2. By l = 200 km only two or three solitary-like waves have formed. The rest of the oscillations travel with speeds less than c. This is

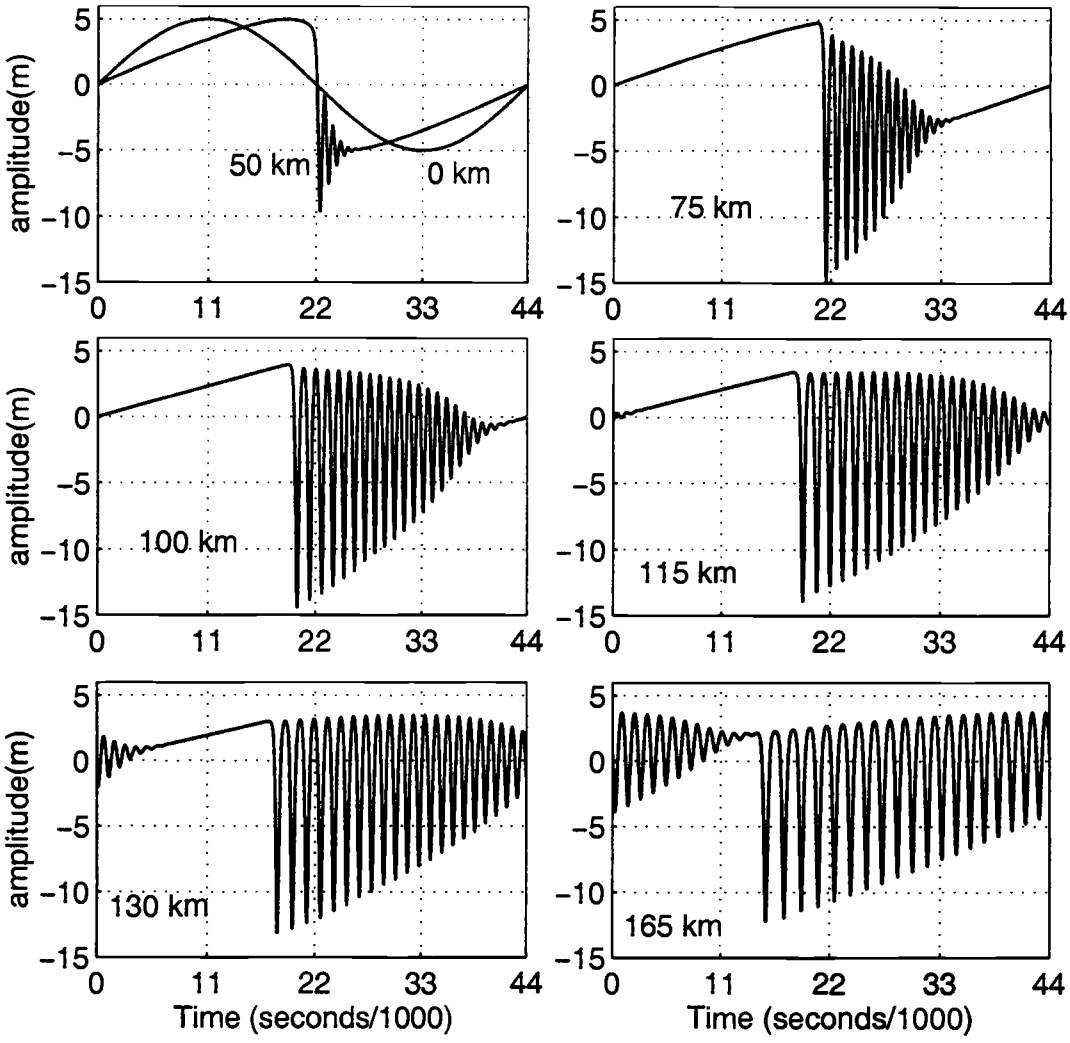

Figure 3.10. Case 2 (h_1 = 40 m, h_2 = 85.7 m, level bottom) amplitude of the internal mode for two layer fluid at various distances from the boundary within KdV model framework.

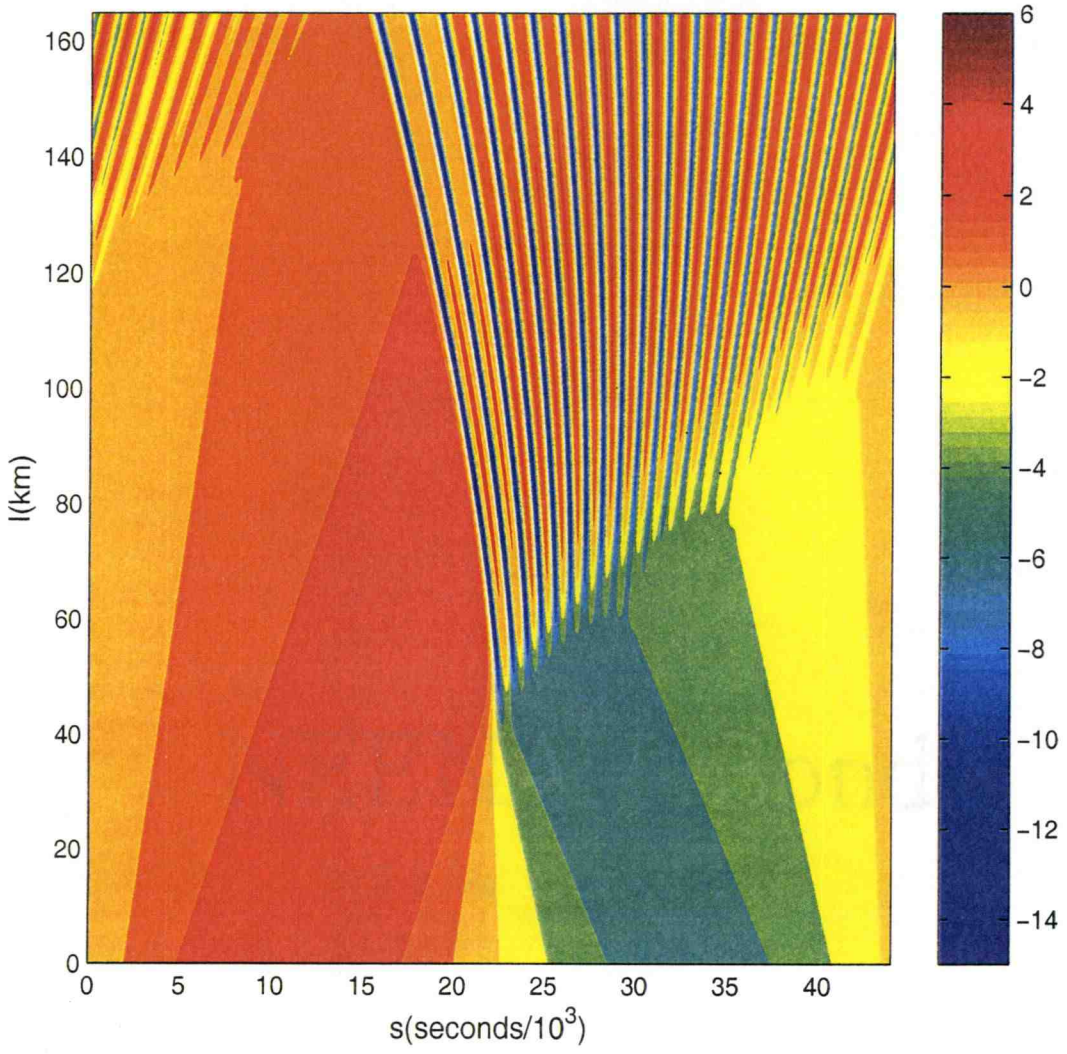

Figure 3.11. Case 2 (h_1 = 40 m, h_2 = 85.7 m, level bottom) amplitude of the internal mode for two layer fluid as a function of distance l and time s within KdV model framework. The panel on the right corresponds to the amplitude of the waves in meters.

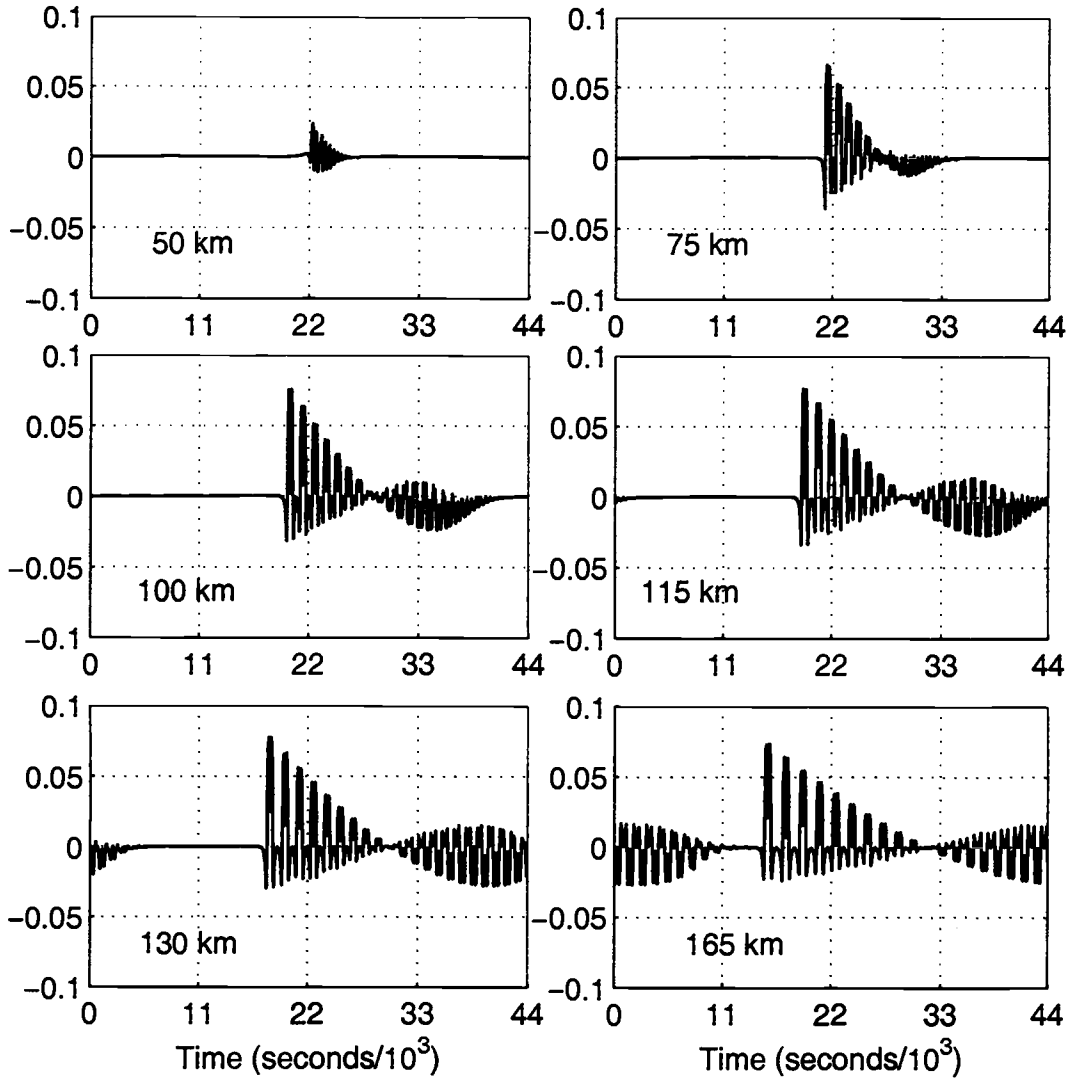

Figure 3.12. Case 2 (h_1 = 40 m, h_2 = 85.7 m, level bottom) difference between the magnitudes of the nonlinear and dispersive terms, χ (non-dimensional), at various distances from the boundary within KdV model framework.

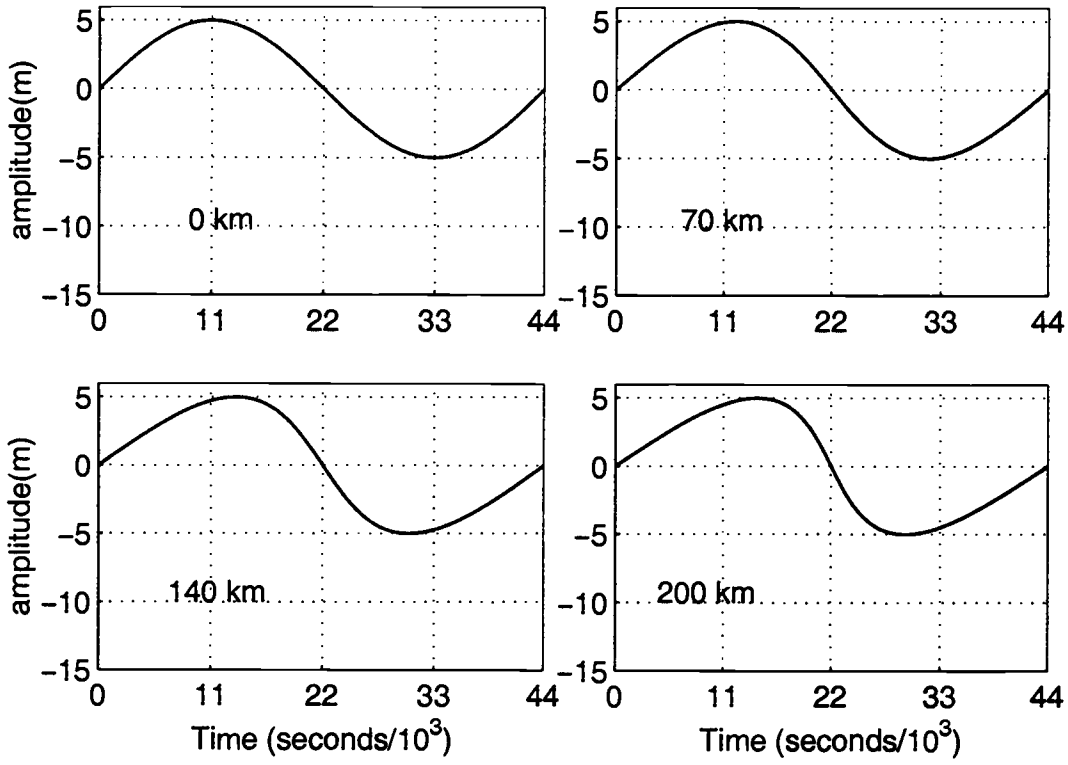

Figure 3.13. Case 3 (h_1 = 80 m, h_2 = 93.8 m, level bottom) amplitude of the internal mode for two layer fluid at various distances from the boundary within KdV model framework.

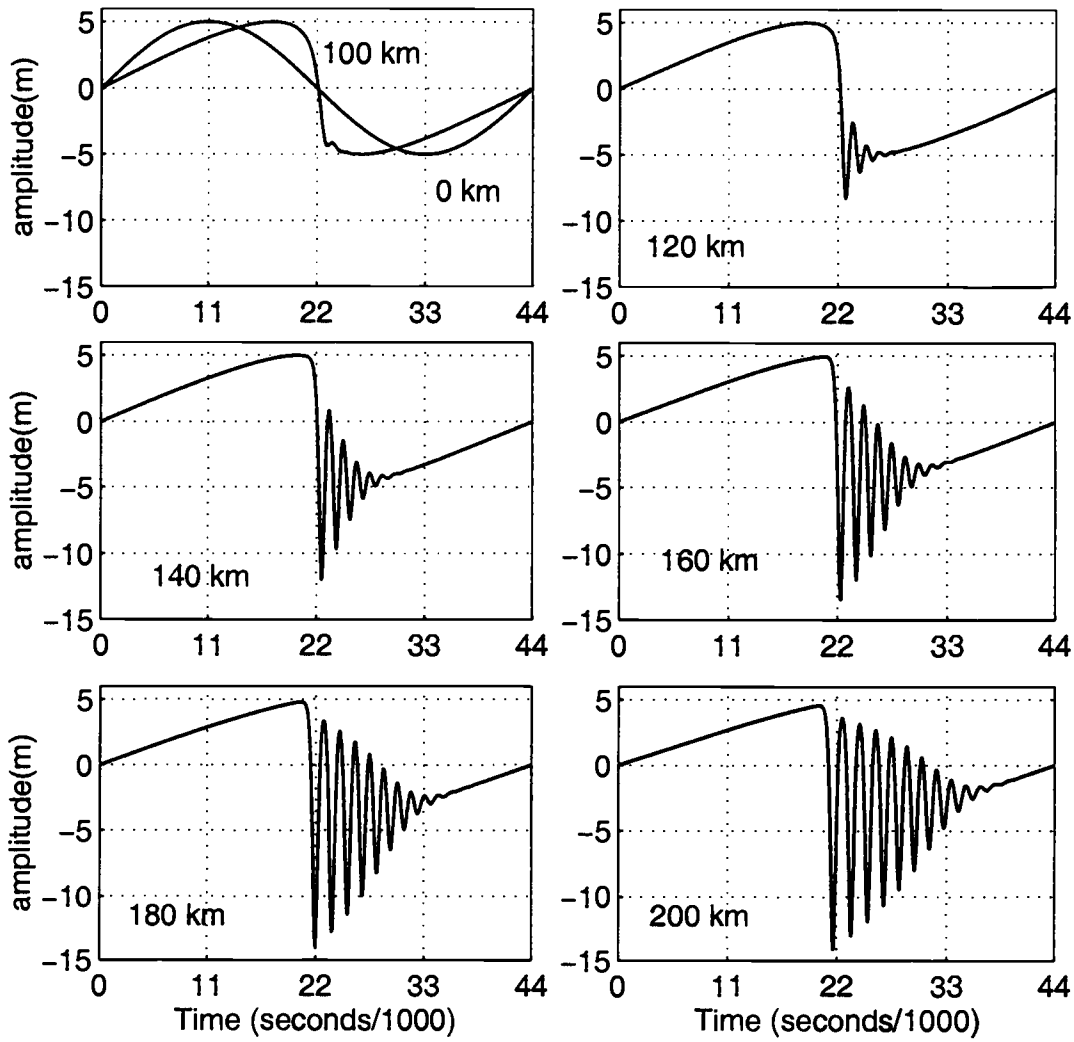

Figure 3.14. Case 4 (h_1 = 65.1 m, h_2 = 115.1 m, level bottom) amplitude of the internal mode for two layer fluid at various distances from the boundary within KdV model framework.

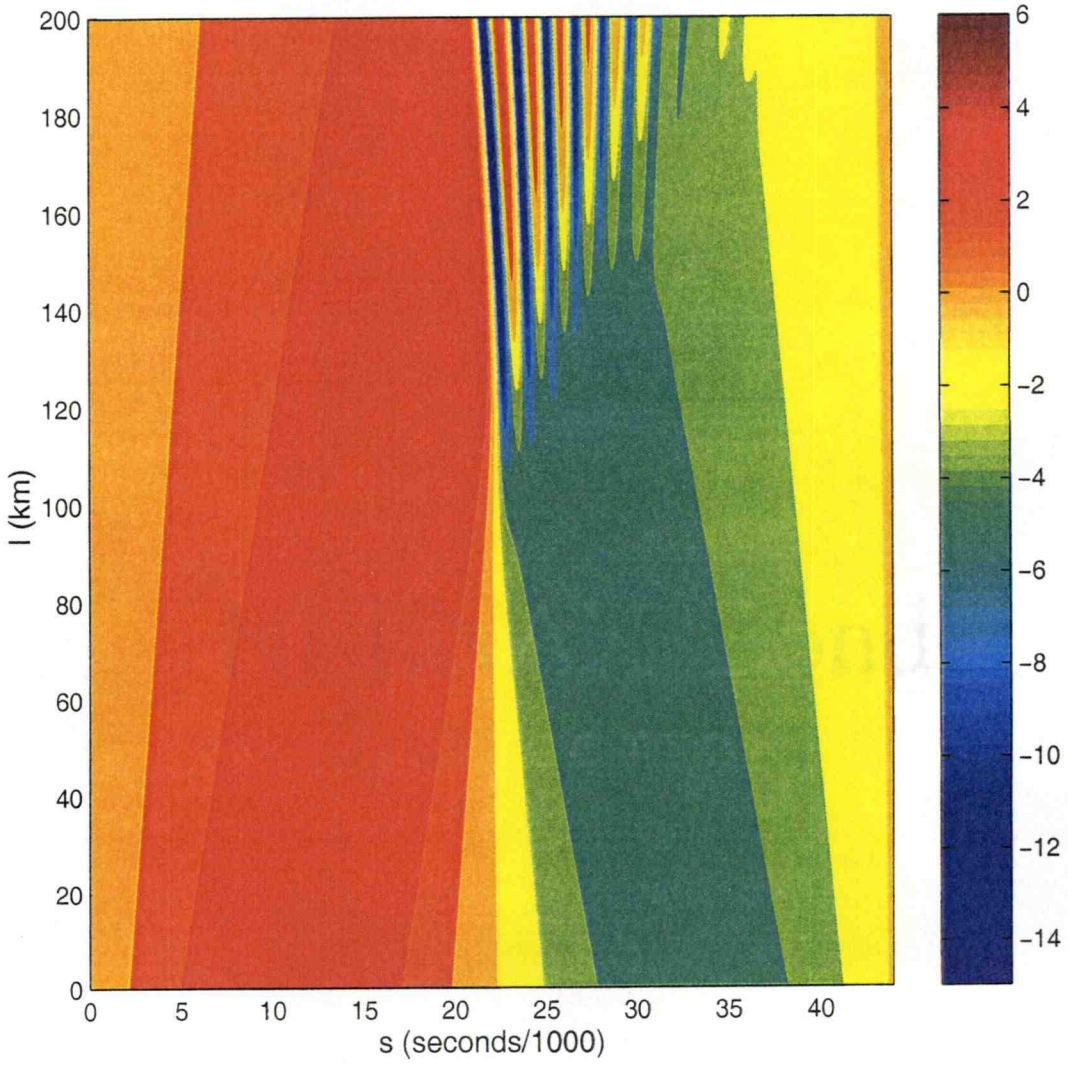

Figure 3.15. Case 4 (h_1 = 65.1 m, h_2 = 115.1 m, level bottom) amplitude of the internal mode for two layer fluid as a function of distance l and time s within KdV model framework. The panel on the right corresponds to the amplitude of the waves in meters.

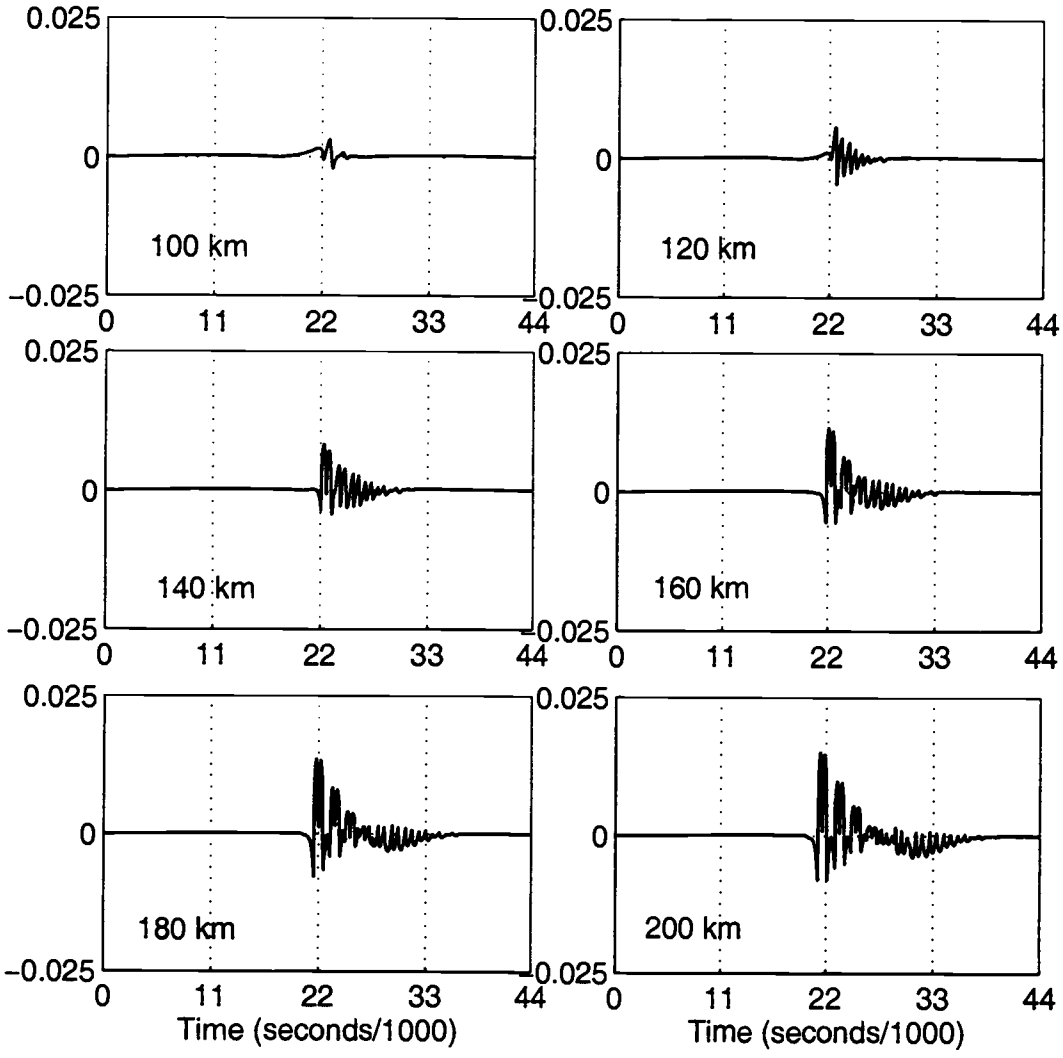

Figure 3.16. Case 4 (h_1 = 65.1 m, h_2 = 115.1 m, level bottom) difference between the magnitudes of the nonlinear and dispersive terms, χ (non-dimensional), at various distances from the boundary within KdV model framework.

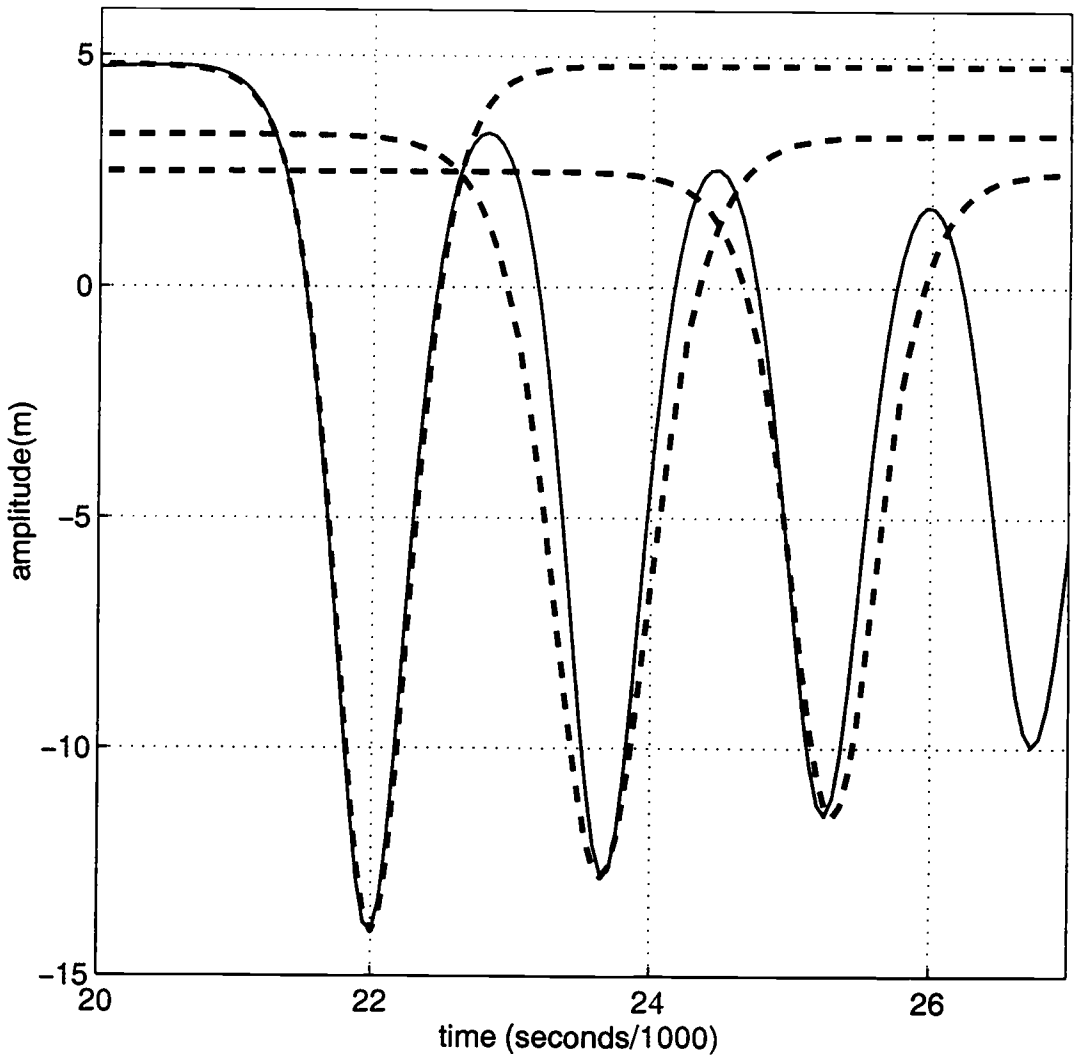

Figure 3.17. Case 4 (h_1 = 65.1 m, h_2 = 115.1 m, level bottom). The three leading waves of depression (solid line) at a distance of 100 km from the boundary shown in Figure 3.14 are plotted with three individual sech^2 waves (broken lines).

demonstrated in Figures 3.16, and 3.17 where comparisons with $sech^2$ solitary waves are made.

In summary, in Cases 1, 2 and 4, we have employed a relatively large factor of α/c with the result that internal solitary waves are formed as the internal tide propagates and steepens along a flat bottom. For Case 2 the nonlinearity parameter is the same as Case 1 with a reduced dispersive parameter. This results in the internal tide becoming nonlinear sooner and forming more solitary waves at the same l. In Case 4 the nonlinearity parameter has been reduced by a factor of two compared to Case 1 with the same dispersive parameter. This results in the internal tide being less nonlinear and solitary-like waves forming at greater l. In Case 3 the nonlinearity parameter is reduced by a factor of 10 from Case 1 with the result that the internal tide steepens very slowly. No internal solitary waves have formed by 200 km. The leading solitary-type waves have evolved from the transforming internal tide with wave speed which appears to be always greater than the linear speed, c. All of the waves which are formed after the leading solitary-type waves are more symmetric and sinusoidal and travel with speed less than the linear wave speed thereby dispersing from the leading waves. Some of these waves later change form becoming more nonlinear and solitary-like and ultimately traveling at wave speed greater than the linear wave speed.

3.1.2 Constant Bottom Slope

We next investigate the propagation of the internal tide onto a constant bottom slope. We present two cases of stratification: a constant upper layer thickness (Case A) and a sloping interface (Case B). Both cases are possible on continental shelves. The starting layer thickness we have used at $l = 0$ is the same as Case 1 for a flat bottom, i.e. $h_1 = 50$ m and $h_2 = 150$ m. We have chosen a bottom slope of 1/1000, that is the total depth changes from 200 to 0 m over a distance of 200 km.

We first investigate the case of constant sloping bottom with constant upper layer thickness (Case A). The value of c decreases in shallow water (Figures 3.1 and 3.18). The nonlinear parameter $\alpha \rightarrow 0$ as $h_2 \rightarrow h_1$ at water depth of 100 m. Seaward of this depth, where $h_2 > h_1$, $\alpha < 0$ and solitary waves are waves of depression; shoreward of this depth, where $h_2 < h_1$, $\alpha > 0$ and solitary waves only exist as waves of elevation. The value of $\beta \rightarrow 0$ as the product $h_1 h_2 \rightarrow 0$. Since the magnitude of α is initially relatively large we expect the sinusoidal internal tide to transform rapidly resulting in the formation of several nonlinear waves (as previously seen for the flat bottom cases). Since $\alpha \rightarrow 0$, these waves may not be so nonlinear as to violate the weakly nonlinear constraint on the KdV model. However, since the value of α rapidly increases for $l > 100$ km, we expect the

waves of elevation to become highly nonlinear thereby possibly violating the weakly nonlinear condition.

Figures 3.19 and 3.20 show the internal tide signal for Case A at different values of l, i.e. at different water depths. The internal tide steepens and rapidly becomes nonlinear, resulting in the generation of a shock-like front and subsequent undulations by $l \approx 50$ km. Shoaling further, the internal tide becomes more nonlinear with the oscillations starting to resemble solitary waves by $l = 70$ km. However, unlike Cases 1, 2, and 4, the waves never develop into mature internal solitary waves as the magnitude of α continually decreases. By $l = 90$ km the waves resemble a symmetric, dispersive packet, as further evidenced by Figure 3.21. Initially the relatively large magnitude of α resulted in the rapid steepening of the internal tide, so much so that the Case A tidal signal at $l = 50$ km resembles those of both Case 1 and Case 2 for flat bottom. However, as the value of α approaches zero the nonlinear waves are prevented from developing into solitary waves, since higher order terms (neglected in KdV) become of order α or larger and thus cannot be ignored thereby rendering the KdV model invalid in this neighborhood. At $l = 100$ km the packet certainly looks symmetrical about a horizontal axis, that is to say the waves are neither polarized as waves of depression nor elevation. This is due to the fact that KdV solitary waves cannot exist when $\alpha = 0$. At 115 km the waves have switched polarity; they have become waves of elevation, a result of α having become positive. This transition can be seen in Figure 3.22 where the leading waves are compared with sech^2 solitary form.

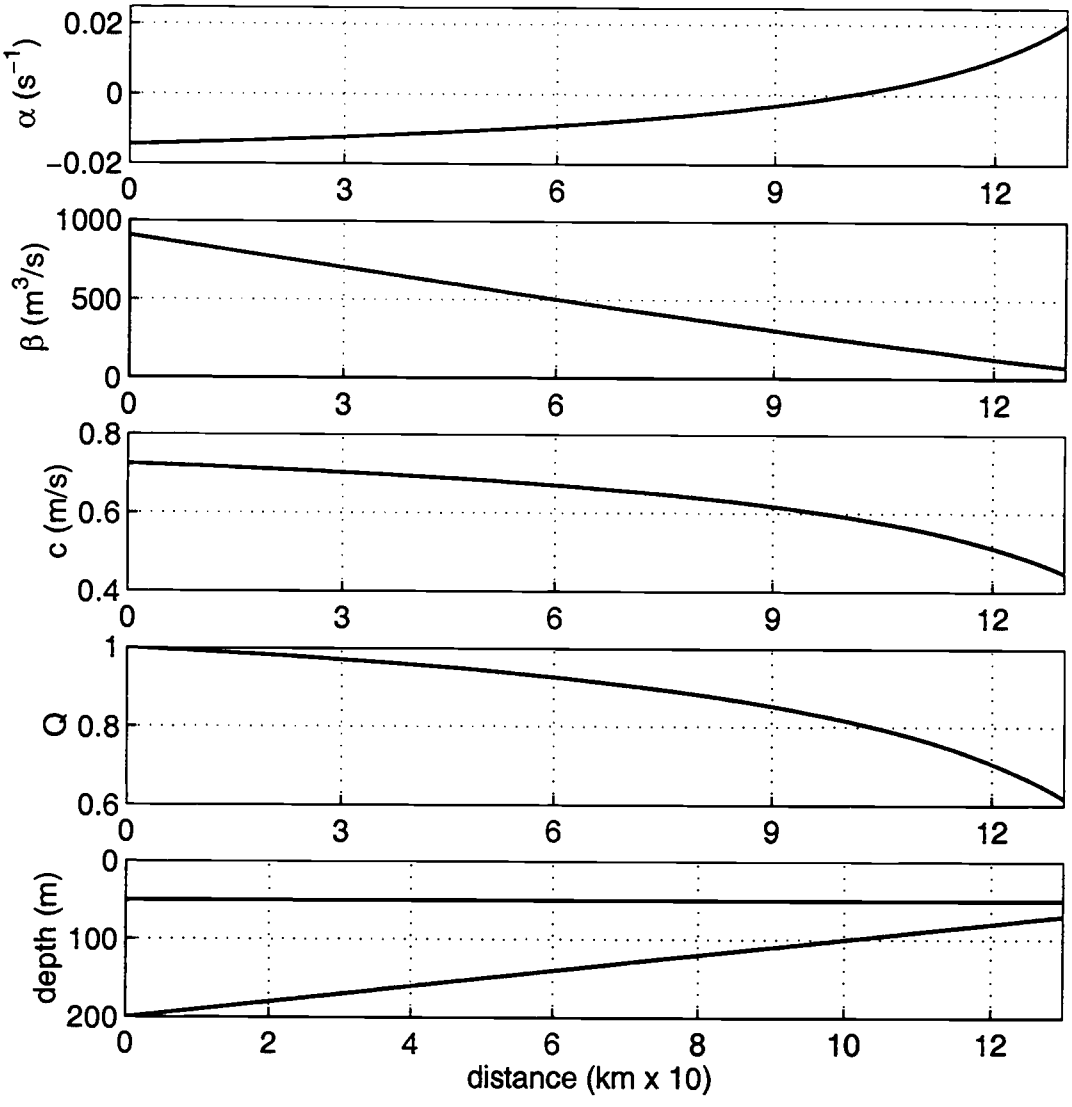

Figure 3.18. Case A (constant sloping bottom with level interface, h_1 = 50 m) KdV parameter values for quadratic nonlinear parameter, α, dispersion parameter, β, linear phase speed, c, horizontal variability factor, Q, and depth.

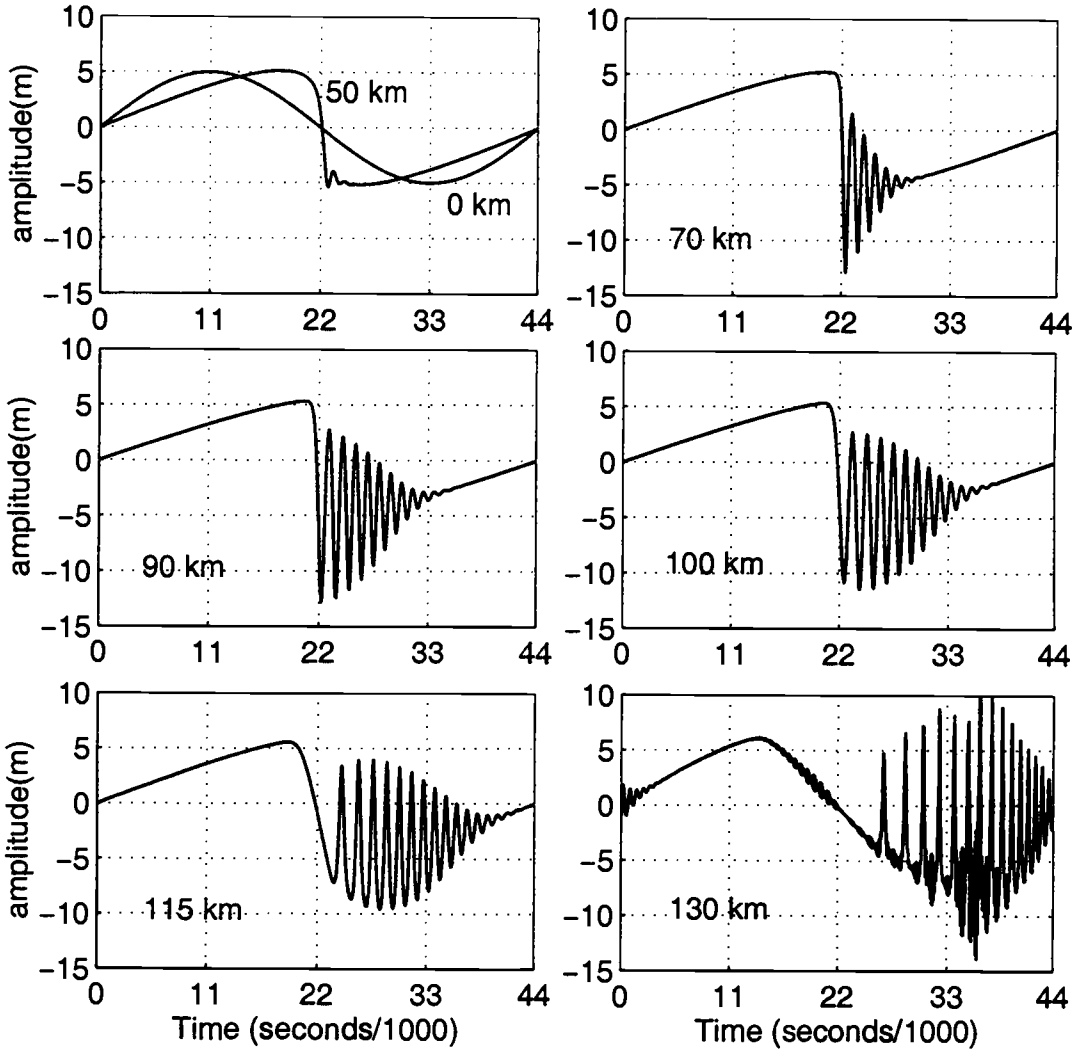

Figure 3.19. Case A (constant sloping bottom with flat interface, h_1 = 50 m) amplitude of the internal mode for two layer fluid at various distances from the boundary within KdV model framework.

Beyond 100 km the waves rapidly approach solitary waves of elevation since the value of α becomes large quickly.

As the tide propagates into shallow water the leading face of the internal tide steepens but, unlike cases 1 – 4, the decreasing magnitude of the nonlinear parameter, α, causes this steepening to slow down and there is virtually no change in the wave slope steepness between 70 and 90 km. The rate of change of the slope of the leading face changes sign when α becomes positive and the slope steepens rapidly. The back face of the internal tide slackens at the same time. The steepening of the leading wave will lead to the formation of a second shock-like front (or a "reverse hydraulic jump" as has been described by Holloway et al., 1997).

Figure 3.20 gives a clear picture of the wave speed. The leading solitary-type wave initially travels with speed very slightly greater than c but becomes slower than c at $l \sim 90$ km. The second solitary-type wave also has initial speed greater than c but becomes slower than c when $l \sim 80$ km. All of the other waves travel with phase speed less than c. For values of $l > 100$ km all waves travel with speed less than c, a result of the large negative offset for solitary waves of elevation (Zabusky & Kruskal, 1965).

Figure 3.21 is a plot of the difference between the magnitudes of the nonlinear and dispersive terms, χ (non-dimensional), for Case A. The leading waves are slightly more nonlinear than dispersive when $l \approx 70$ km but become less

so as l approaches 100 km. When $\alpha = 0$ (l = 100 km) the value of the nonlinear term is zero and the waves look like a dispersive packet. Since $\alpha > 0$ for $l > 100$ km, the nonlinear term is again a factor and the waves become a hybrid by l = 115 km interchanging back and forth across the length of the wave between being more nonlinear and dispersive.

For Case B with constant sloping bottom and sloping upper layer, we also begin in 200 m water with h_1 = 50 m and h_2 = 150 m. For this case the bottom slope is again 1/1000 and the interface slope is chosen to be 1/4000 with the result that both layers will disappear simultaneously at 200 km. The values of the KdV parameters are shown in Figure 3.23 and Figures 3.1 to 3.5. The magnitude of α increases from l = 0 all the way to the shallowest water, unlike Case A where α passes through zero. As a result, we expect the internal tide to become nonlinear sooner than for Case A, and any solitary waves to remain as waves of depression. We do, however, expect the waves to become unstable, a result of the increasing magnitude of the nonlinear parameter combined with the decreasing value of the dispersive parameter. This combination of events will result in the weakly nonlinear, weakly dispersive KdV becoming invalid at l = 95 km. Figure 3.24 is a plot of the internal tide for Case B at several values of l. The internal tide steepens rapidly and a shock-like wave, followed by undulations, has evolved from the transforming tide by l = 40 km. The internal tide continues to steepen and several nonlinear waves have formed by l = 55 km. These leading nonlinear waves mature

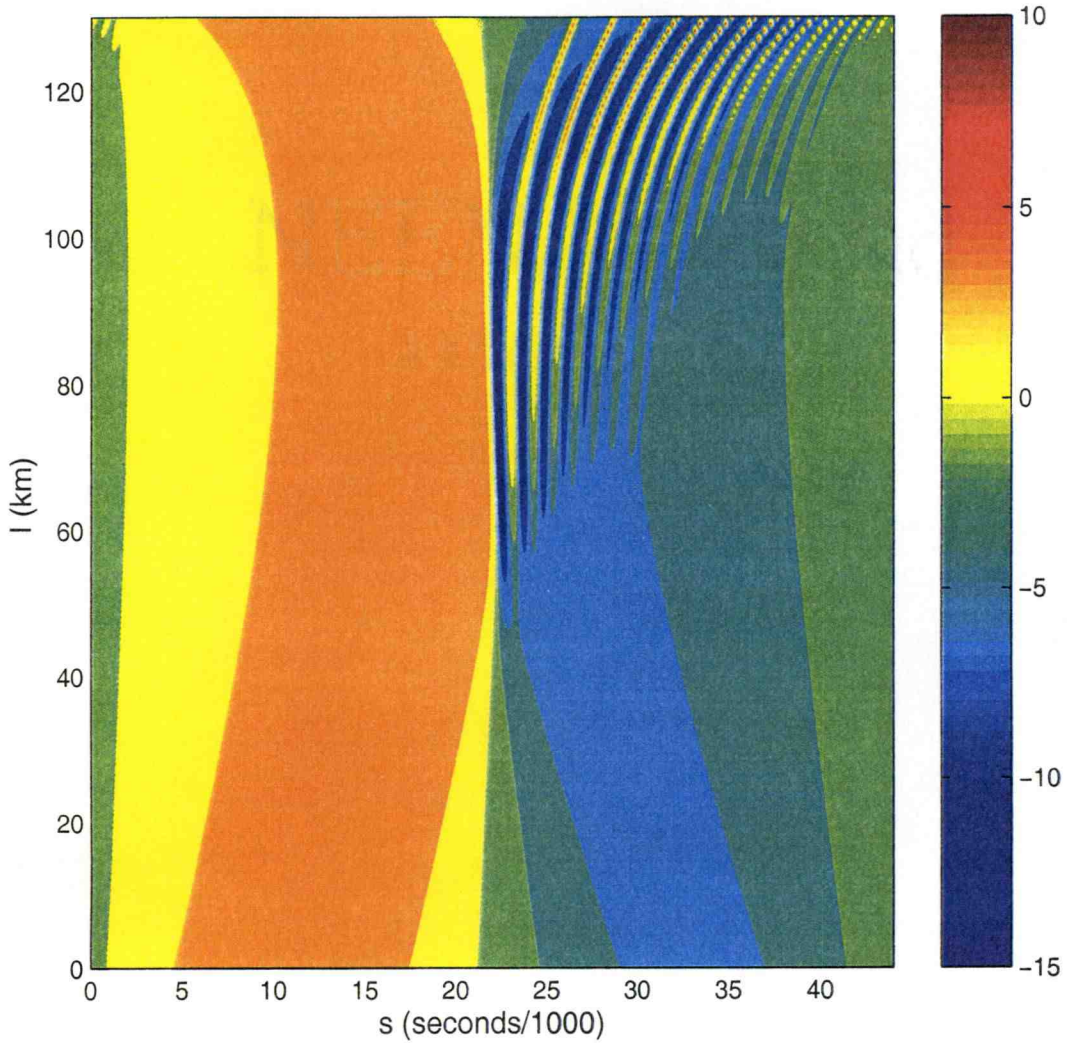

Figure 3.20. Case A (constant sloping bottom with flat interface, h_1 = 50 m) amplitude of the internal mode for two layer fluid as a function of distance l and time s within KdV model framework. The panel on the right corresponds to the amplitude of the waves in meters.

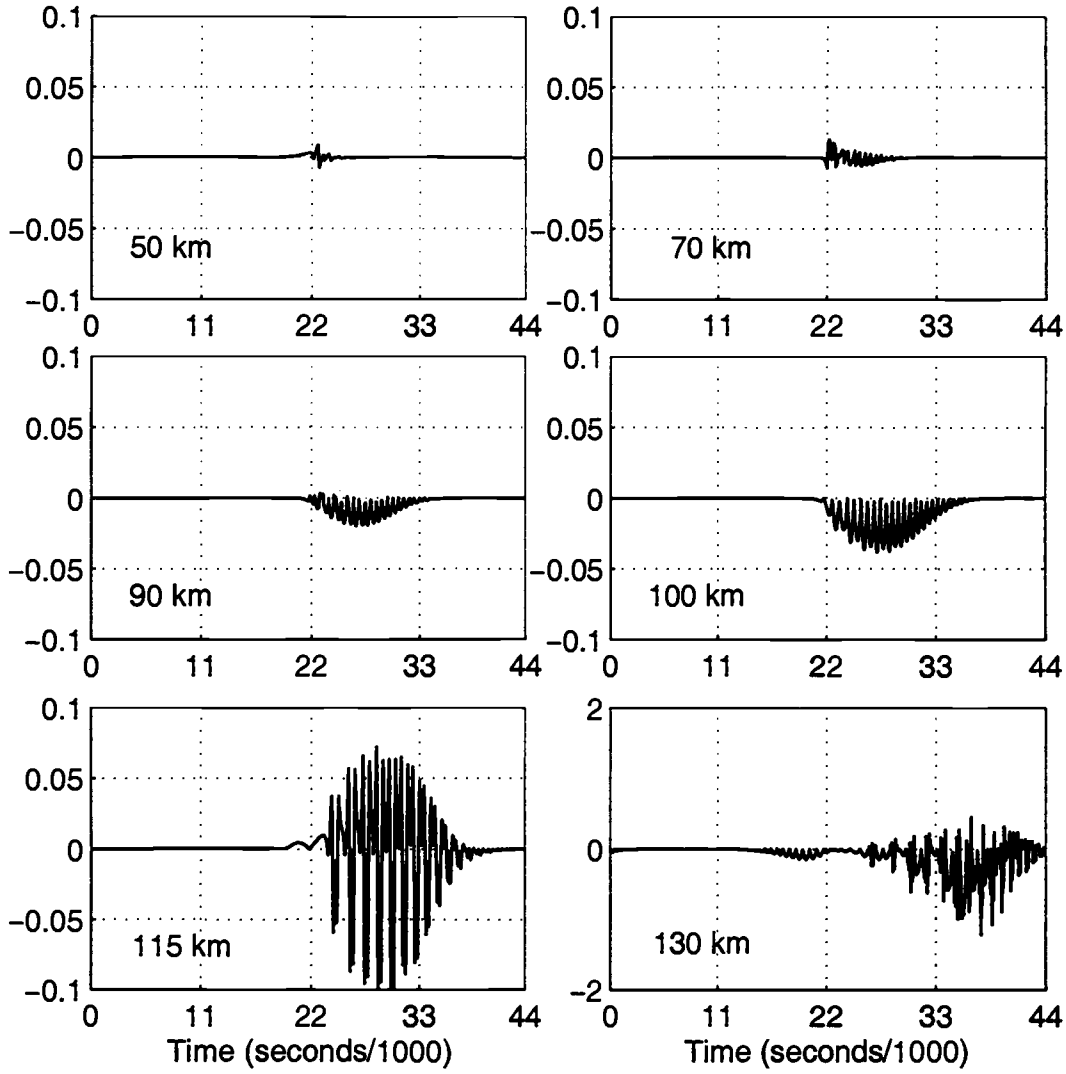

Figure 3.21. Case A (constant sloping bottom with flat interface, h_1 = 50 m) difference between the magnitudes of the nonlinear and dispersive terms, χ (non-dimensional), at various distances from the boundary.

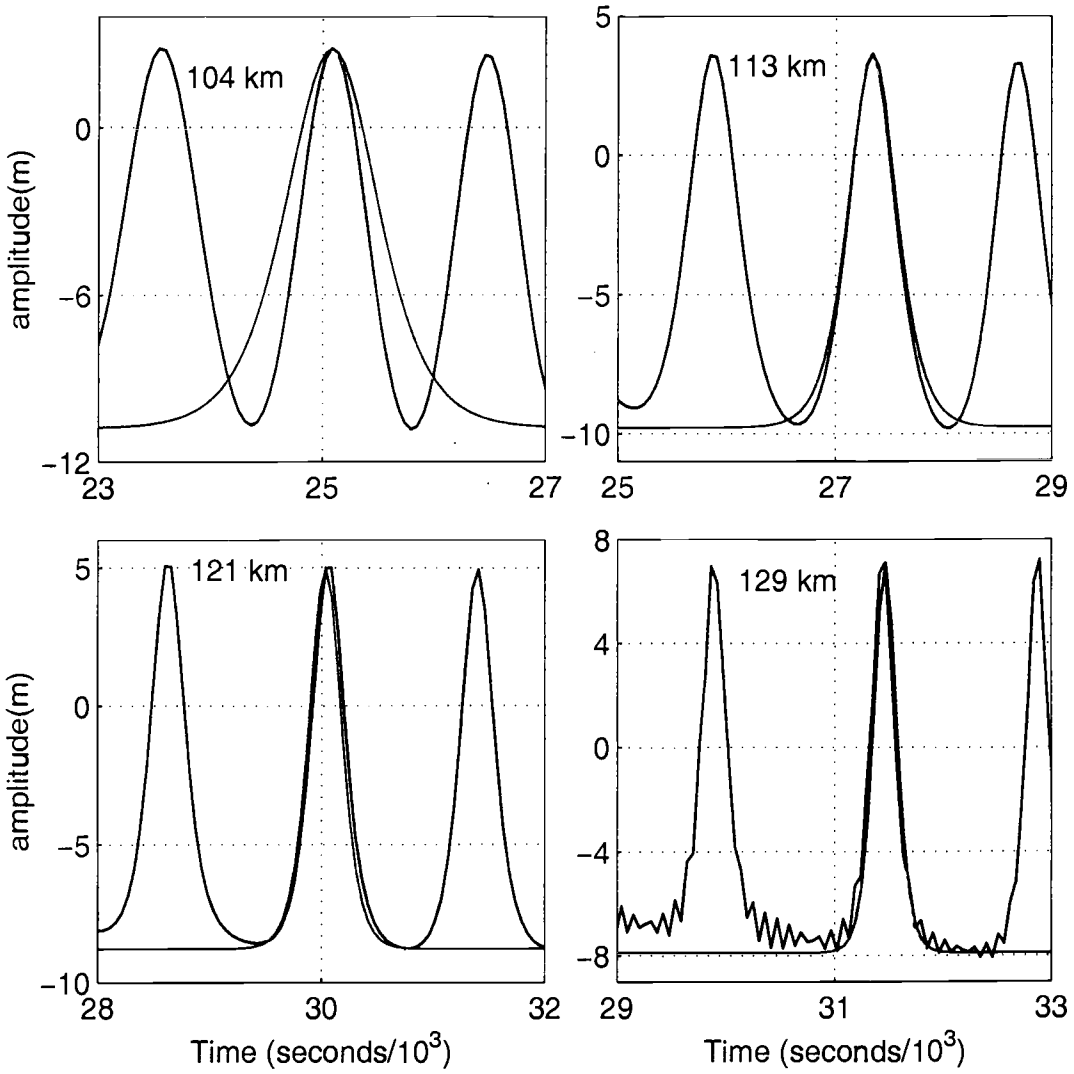

Figure 3.22. Case A (constant sloping bottom with flat interface, h_1 = 50 m). Leading waves of elevation (black line) at various distances greater than 100 km from the boundary plotted with individual sech^2 waves (blue lines) within KdV model framework.

into rank ordered solitary waves by 65 km. Figure 3.25 shows that most of the solitary waves eventually travel at a phase speed greater than c.

Figure 3.26 is a plot of χ for Case B. The waves are more nonlinear than dispersive and the increasing value of the nonlinear parameter combined with the diminishing value of the dispersive parameter leads to the model becoming numerically unstable.

3.1.3 Realistic topography and stratification

We next proceed to the transformation of the internal tide for the case of realistic topography. The KdV model was run for two separate cases. Realistic topography was constructed from observations made during the Coastal Mixing and Optics (CMO) and the Littoral Optics Experiment (LOE) field experiments.

The first case we investigate is at the CMO site in the Mid Atlantic Bight. CTD profiles were made across the continental shelf from shallow water to beyond the continental slope. T. Boyd (personal communication) has analyzed these data and the time series collected from the central mooring of the experiment located in 69 m of water. Boyd & Levine (1999) have concluded that the internal tide is primarily a first mode internal wave, further justifying our choice of a two layermodel. An upper layer thickness of 25 m is a representative average value for the duration of the experiment (July and August 1996). The line 'CMO' in Figures 3.1 - 3.4 shows the values that the KdV parameters take as the internal tide

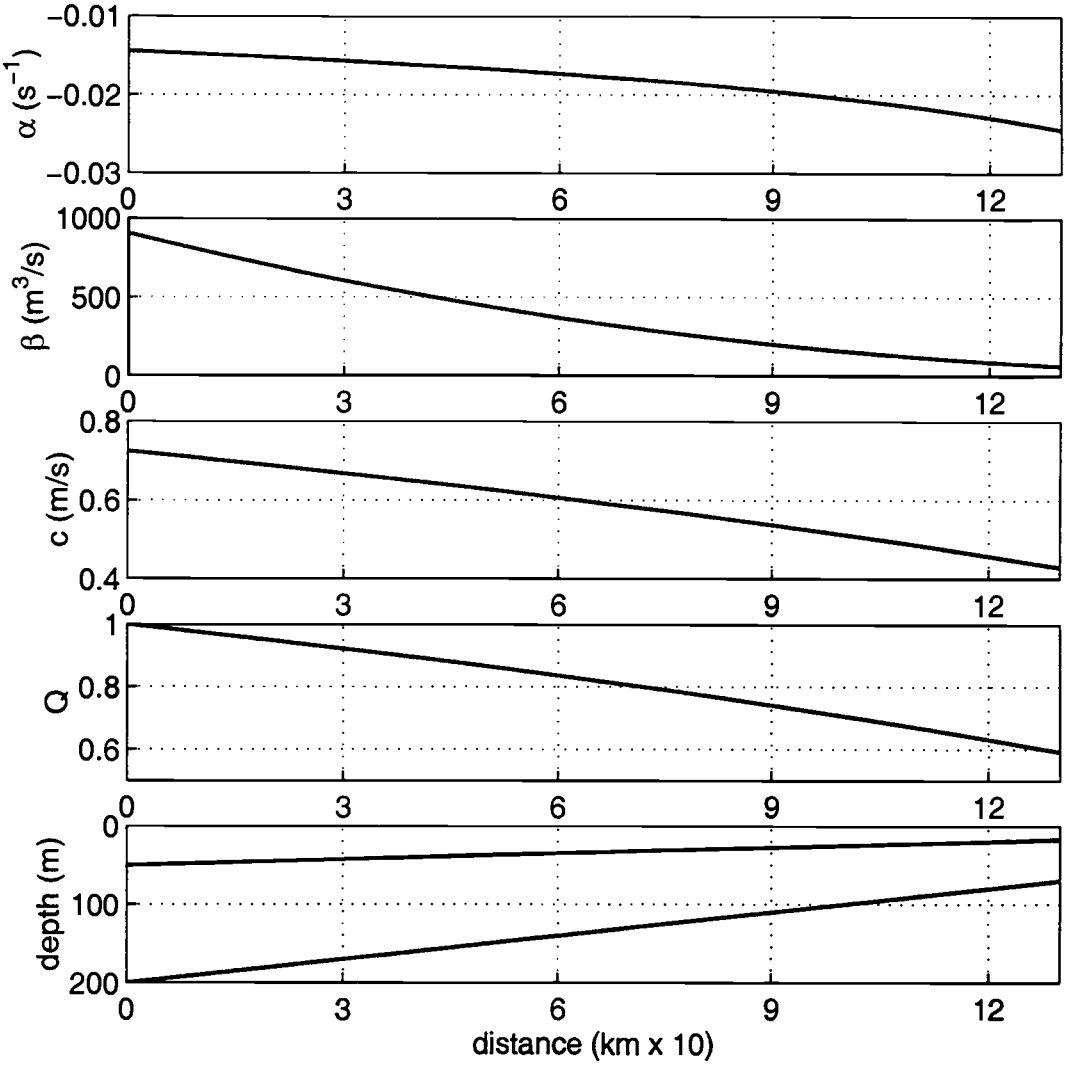

Figure 3.23. Case B (constant sloping bottom with sloping interface) KdV parameter values for quadratic nonlinear parameter, α, dispersion parameter, β, linear phase speed, c, horizontal variability factor, Q, and depth.

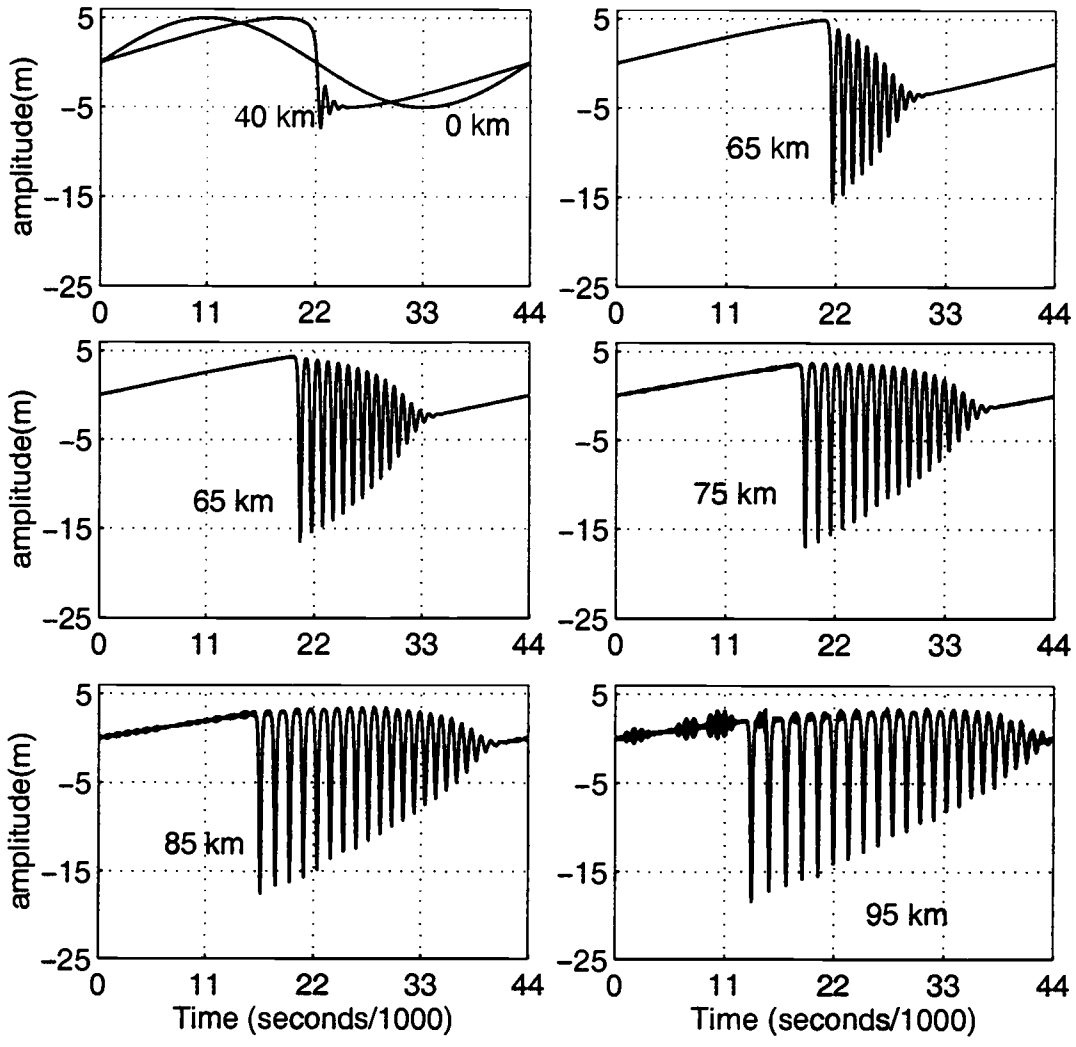

Figure 3.24. Case B (constant sloping bottom with sloping interface) amplitude of the internal mode for two layer fluid at various distances from the boundary within KdV model framework.

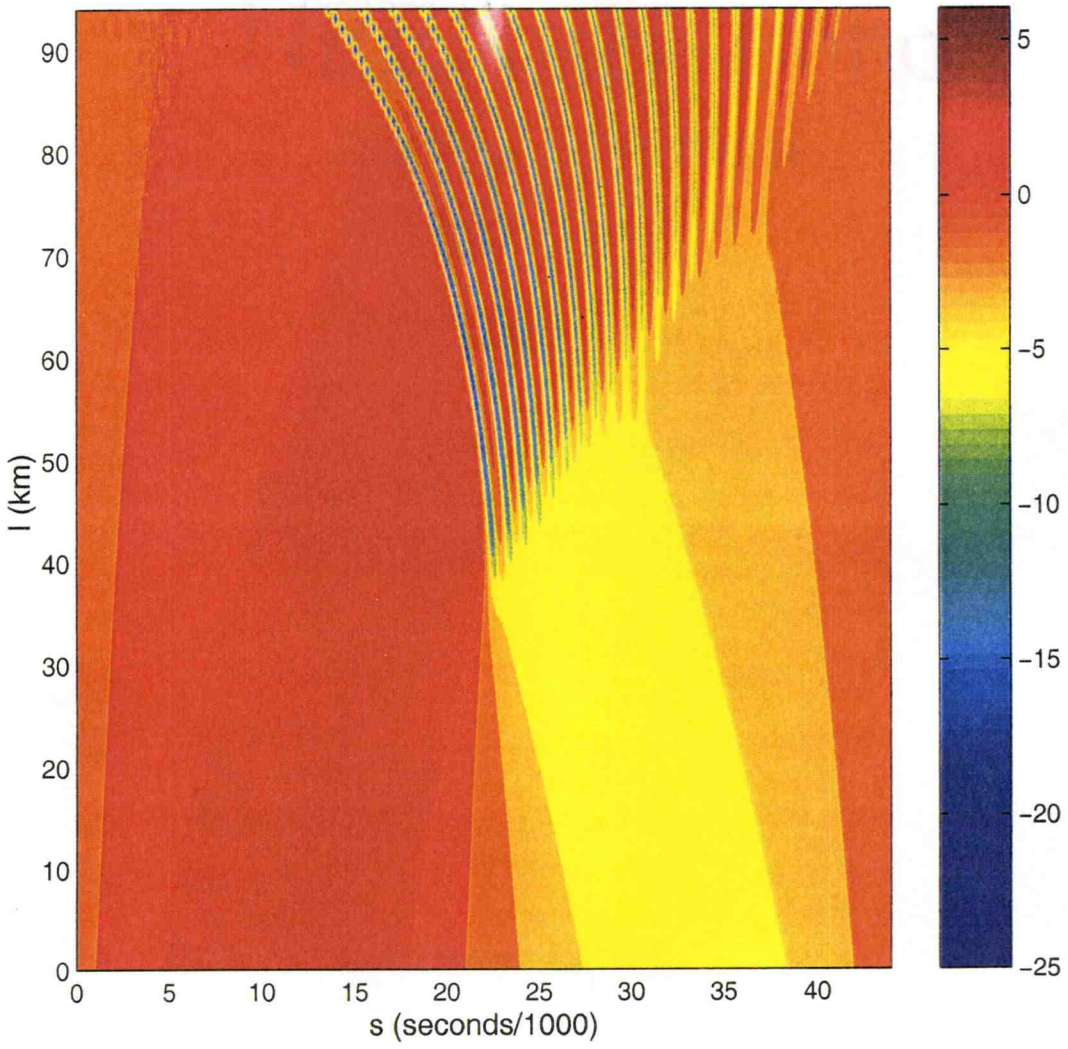

Figure 3.25. Case B (constant sloping bottom with sloping interface) amplitude of the internal mode for two layer fluid as a function of distance l and time s within KdV model framework. The panel on the right corresponds to the amplitude of the waves in meters.

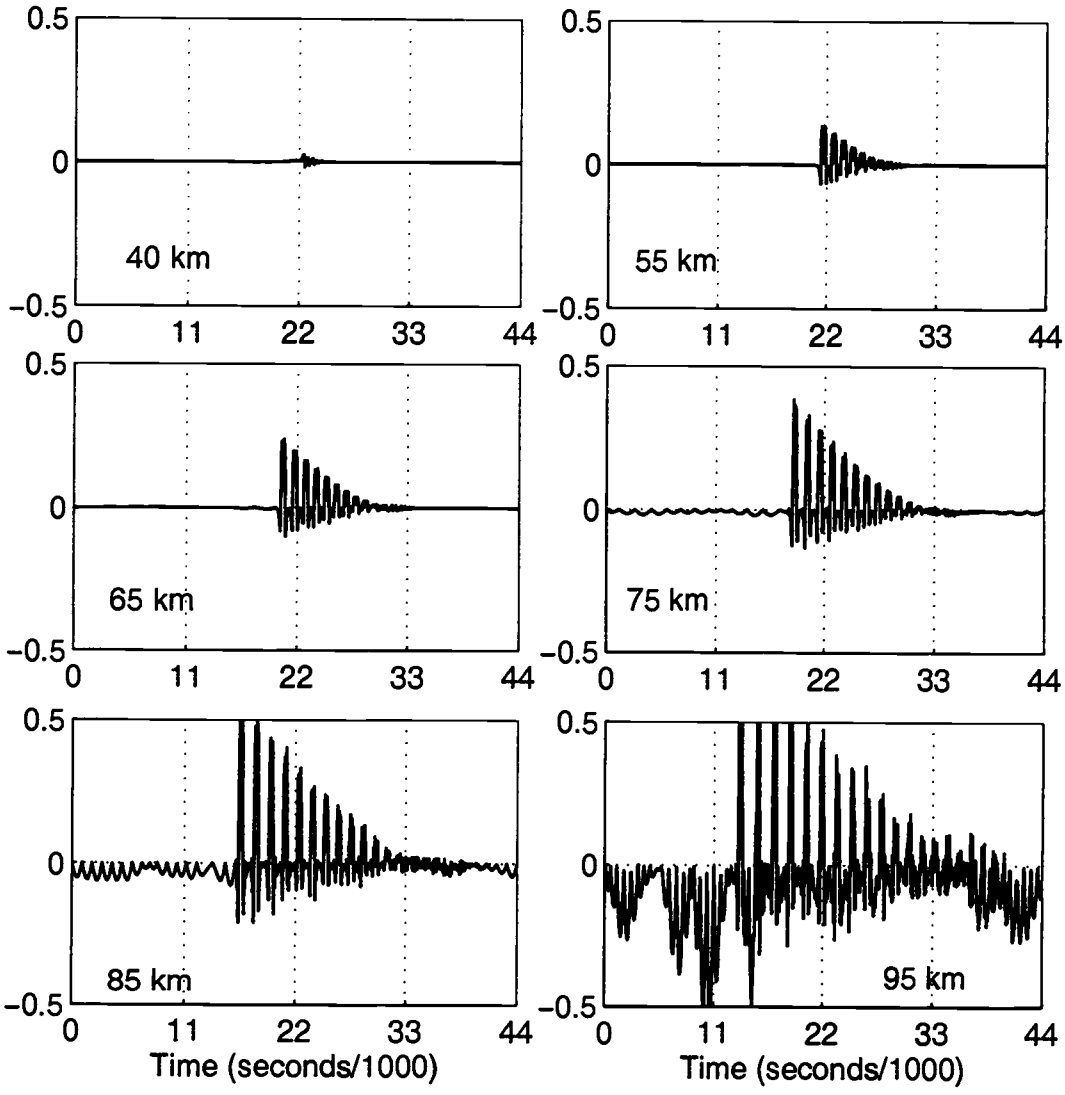

Figure 3.26. Case B (constant sloping bottom with sloping interface) difference between the magnitudes of the nonlinear and dispersive terms, χ (non-dimensional), at various distances from the boundary within KdV model framework.

propagates across the continental shelf. Since the upper layer, h_1, is constant, the 'CMO' line will be straight, but since the total depth does not vary linearly in l, the value of h_2 does not change linearly along this line. Figure 3.27 shows the values of the KdV parameters as a function of l. Though undulating, the bottom topography is similar to the constant sloping bottom cases. Recall that we chose an upper layer depth of 50 m for Case A (Figure 3.19), whereas here we have chosen h_1 = 25 m. The nonlinear coefficient, α, starts out negative with relatively large magnitude. The magnitude decreases, similar to Case A, changing sign after l = 100 km before rapidly increasing in value. The value of the dispersion coefficient, β, decreases similar to Case A and is near to zero at 100 km. The linear wave speed, c, and the horizontal variability parameter, Q, are similar to Case A.

The model results are shown in Figures 3.28 and 3.29 for a tidal forcing of amplitude 2 m at 180 m water depth. The internal tide evolves similarly to Case A (Figures 3.19 and 3.20). A shock-like front has formed on the back-face of the internal tide at l = 40 km. Several nonlinear waves have formed by l = 60 km (mooring location) with the leading 4 - 5 waves appearing like solitary waves of depression and the trailing waves looking more like a dispersive packet. Several more waves have formed by 80 km but the number of solitary-like waves seems to have been reduced to the leading two waves. All of the trailing waves do appear as a dispersive packet since the magnitude of α has decreased. More waves continue to form but by 100 km the packet is nearly non-polarized, not unlike Case A. Beyond l = 125 km the value of α becomes large, and the waves reverse polarity

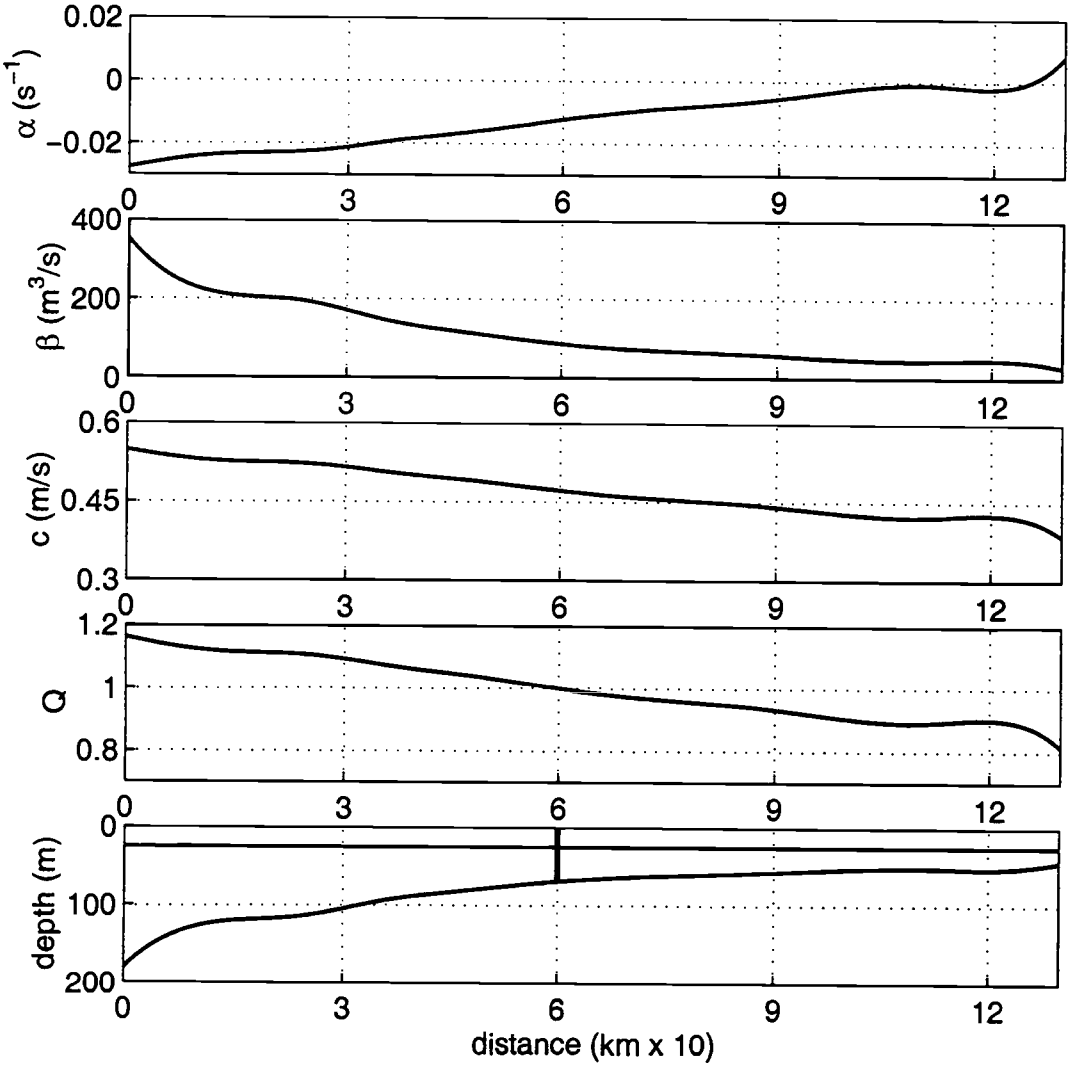

Figure 3.27. CMO experiment site (with flat interface, h_1 = 25 m) KdV parameter values for quadratic nonlinear parameter, α, dispersion parameter, β, linear phase speed, c, horizontal variability factor, Q, and depth. The CMO mooring location is shown by the black vertical line at 60 km in the depth diagram.

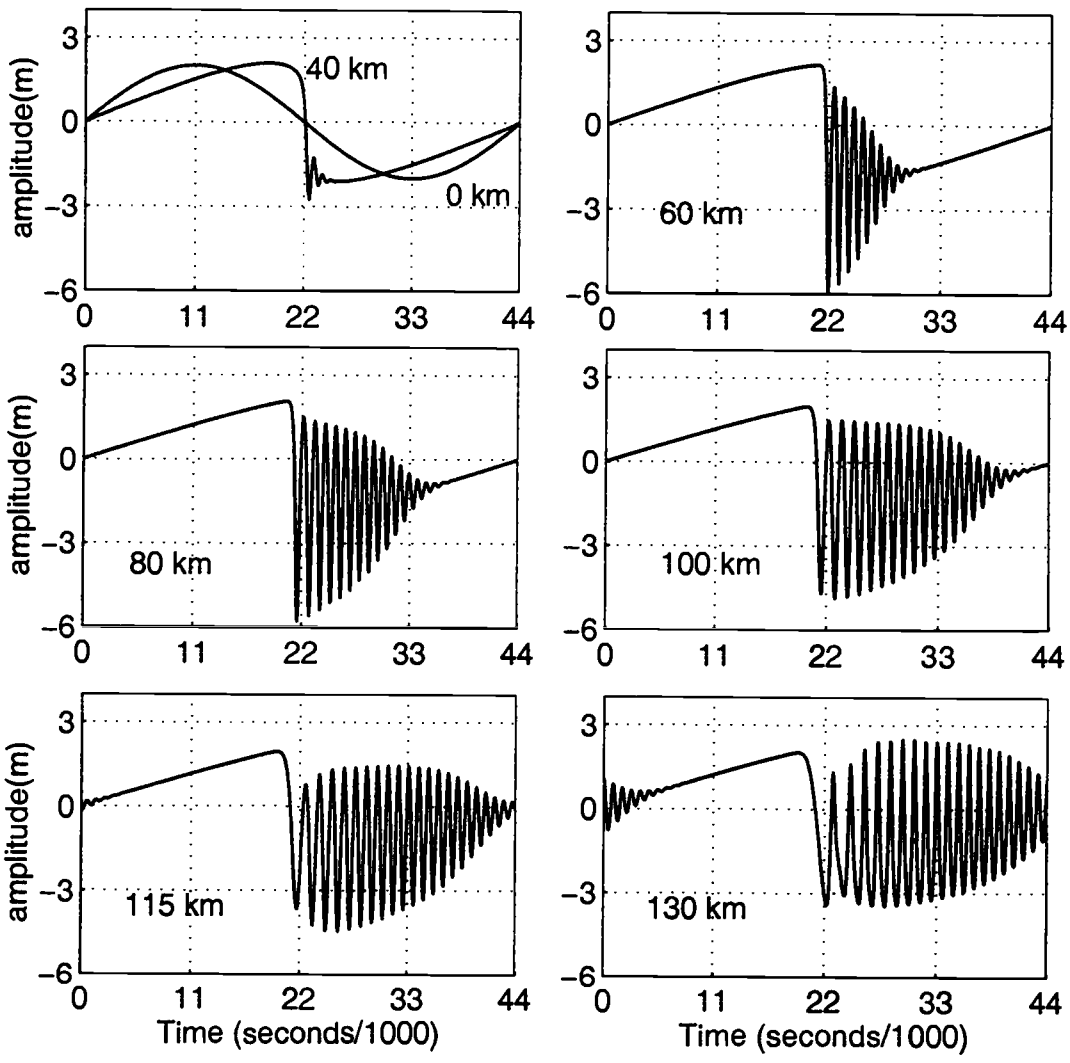

Figure 3.28. CMO experiment site (with flat interface, h_1 = 25 m) amplitude of the internal mode for two layer fluid at various distances from the boundary within KdV model framework.

and rapidly develop into mature solitary waves of elevation. The results show that the CMO case and Case A are similar, though more solitary waves have formed for the CMO case. This is due to the fact that at the CMO site the value of α is initially twice that of Case A. The internal tide becomes unstable beyond l = 130 km. This is a result of the increasing value of the nonlinearity parameter combined with the vanishing dispersion parameter. Figure 3.29 is a plot of the evolution of the internal tide as it propagates over the continental shelf, increasing in l. The leading solitary-like waves initially travel with speed very slightly greater than c, as in Case A (Figure 3.20). The waves slow down to travel at speed c where $l \approx 90$ km and α is very small. The speed of the waves then becomes slightly slower than c but more complicated than Case A, due to the undulating topography.

Figure 3.30 is a plot of the difference between the magnitudes of the nonlinear and dispersive terms, χ, for the CMO case. The leading 2 to 3 three waves are initially more nonlinear than dispersive but the diminishing magnitude of α leads to the waves becoming more dispersive-like and the waves begin to slow down. The negligible value of α between l = 100 km and l = 115 km results in the waves behaving very much like a dispersive packet and they travel with wave speed slightly less than c. The increasing value of α after it passes through zero, leads to the nonlinear term becoming almost the same order of magnitude as the dispersive term before the model becomes numerically unstable shortly beyond l = 130 km.

Next, we solve the KdV equation using the topography and stratification as observed at Oceanside, California in October 1995 during the Littoral Optics

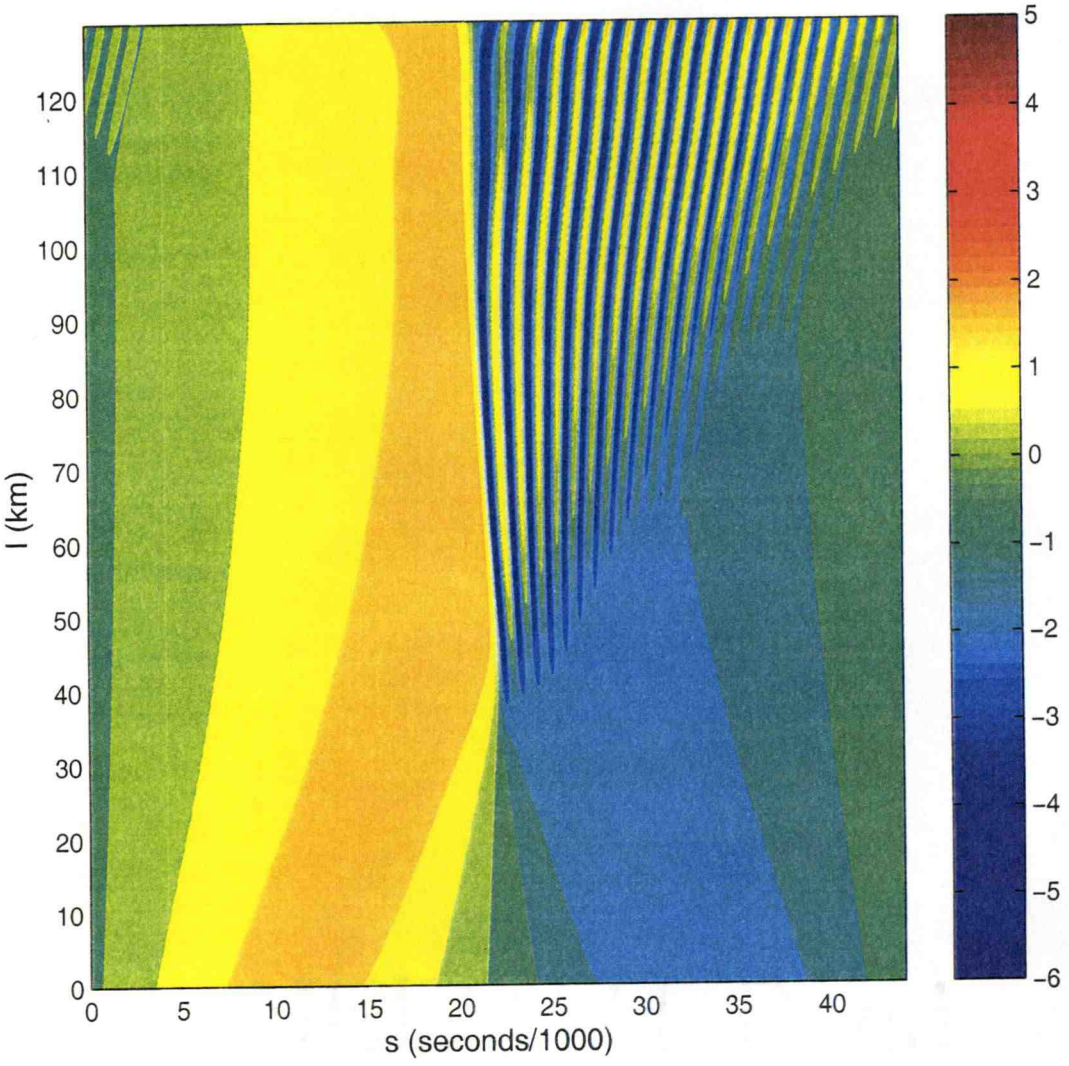

Figure 3.29. CMO experiment site (with flat interface, h_1 = 25 m) amplitude of the internal mode for two layer fluid as a function of distance l and time s within KdV model framework. The panel on the right corresponds to the amplitude of the waves in meters.

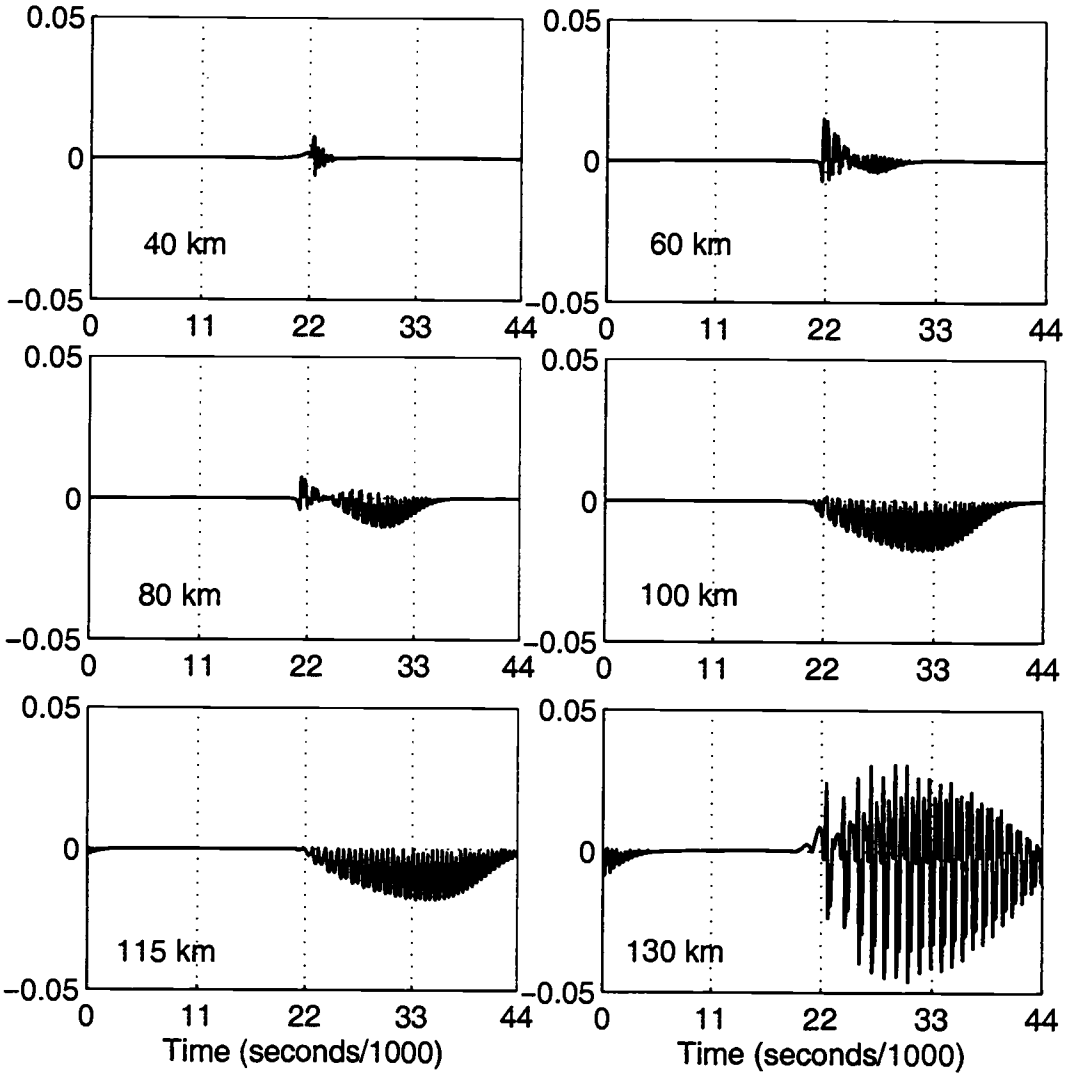

Figure 3.30. CMO experiment site (with flat interface, h_1 = 25 m) difference between the magnitudes of the nonlinear and dispersive terms, χ (non-dimensional), at various distances from the boundary within KdV model framework.

Experiment (LOE) (Figure 3.31). The depth varies from 130 to 20 m over a distance of ~ 5 km, yielding a slope of 1/100, about 10 times greater than the slope at the CMO site. Seaward of the steep slope region the depth remains approximately constant before arriving at the Gulf of Santa Catalina when the water depth rapidly increases to several hundreds of meters. The water depth again shoals at the open ocean end of the Gulf where it reaches the Outer Santa Barbara Passage before the open ocean is encountered. Current meter records made during the LOE experiment show that a large amount of tidal energy at Oceanside is contained at the tidal harmonics, particularly the 4^{th}, which may be a result of the complex topography introduced above. We run this case with sinusoidal boundary condition and period three hours, representative of the 4^{th} harmonic of the semi-diurnal tide. The internal tide is propagated inshore from 131 m water. Note that a lot of energy is contained in the tidal harmonics and is comparable to the fundamental period, particularly during the spring tide period.

The KdV parameters do not change much in the flat region (Figures 3.1 – 3.4, 3.31). The value of α is large in this flat region due mainly to the facts that $h_1 << h_2$, and that h_1 is small; here we have chosen $h_1 = 8$ m a reasonable choice based on CTD casts. It is also noteworthy that β and c are small here. Nonetheless, we do expect the internal tide to become very nonlinear off the slope since the magnitude of α is very large there. Figure 3.32 (a) is a plot of the 4^{th} harmonic of the internal tide as it propagates onto the shelf from the Gulf of Santa Catalina. A close up of these results is shown in Figure 3.32 (b). The 4^{th} harmonic steepens rapidly on the

back face as it propagates in along the relatively flat bottom. A shock-type wave of depression followed by nonlinear undulations is formed within the transforming internal tide between $l \approx 9.5$ and 11.5 km. A packet of solitary waves begins to develop shortly after. Figure 3.32 (b) shows that the leading waves are waves of depression but they rapidly change polarization to waves of elevation since the nonlinear parameter, α, changes sign at $l \approx 12$ km. The evolving waves are formed very closely together, an indication of relatively strong nonlinearity.

Upon comparing results of the CMO and LOE cases, the most striking difference is that the internal tide steepens much sooner for the LOE case. Although the ratio of upper to lower layer depth, h_1/h_2, is initially small for both cases it is a factor of two less for the LOE case. This factor directly results in the magnitude of α for the LOE case being twice that for the CMO case over the leading 10 km of propagation and is the reason for the emission of nonlinear waves much sooner in l for the LOE case.

3.2 The extended Korteweg - de Vries (eKdV) model

All of the model runs in section 3.1 were also made using the extended Korteweg-de Vries (eKdV) equation which includes the cubic nonlinearity term. The ratio of the nonlinear parameters α/α_1 for all cases is shown in Figure 3.5 (this ratio is also the theoretical maximum for the solitary wave solution to the eKdV solution). The ratio of the quadratic to cubic nonlinear terms

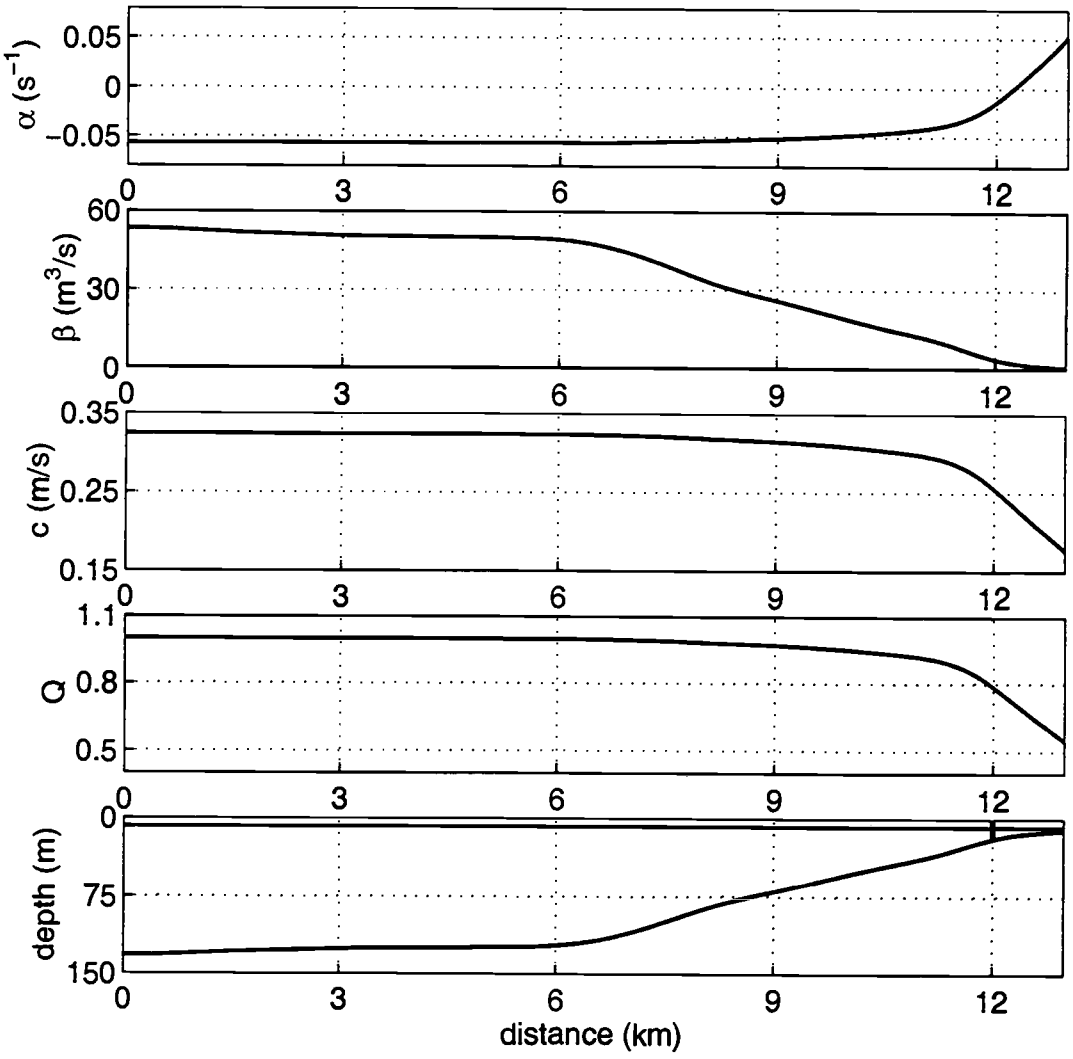

Figure 3.31. LOE experiment site (with flat interface, h_1 = 8 m) KdV parameter values for quadratic nonlinear parameter, α, dispersion parameter, β, linear phase speed, c, horizontal variability factor, Q, and depth. The vertical line at 12 km is the site of the current meter data used in Chapter 4.

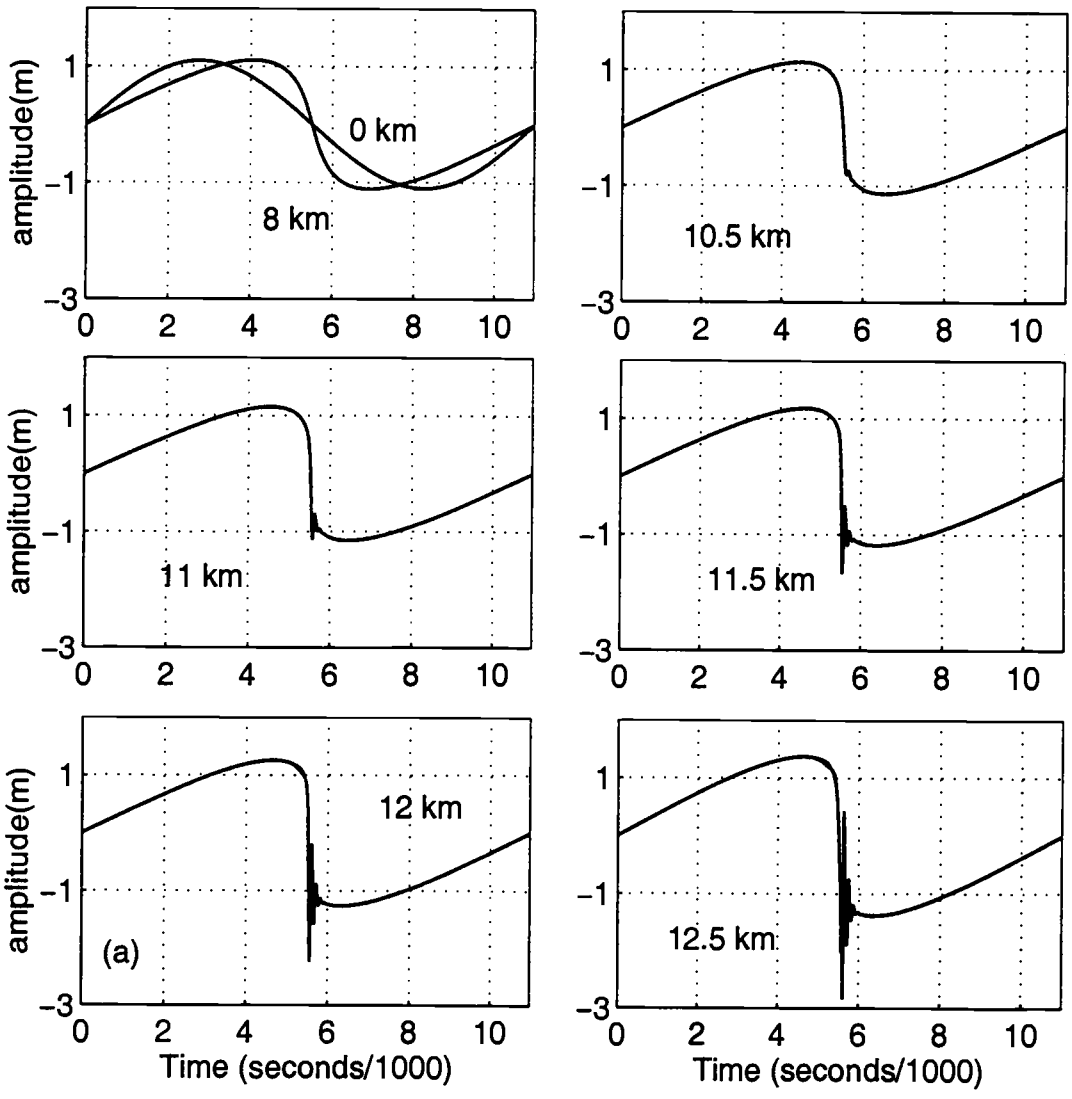

Figure 3.32 (a). LOE experiment site (with flat interface, h_1 = 8 m) amplitude of the internal mode for two layer fluid at various distances from the boundary within KdV model framework (a) over the period of the 4th harmonic of the semi-diurnal tide (continued).

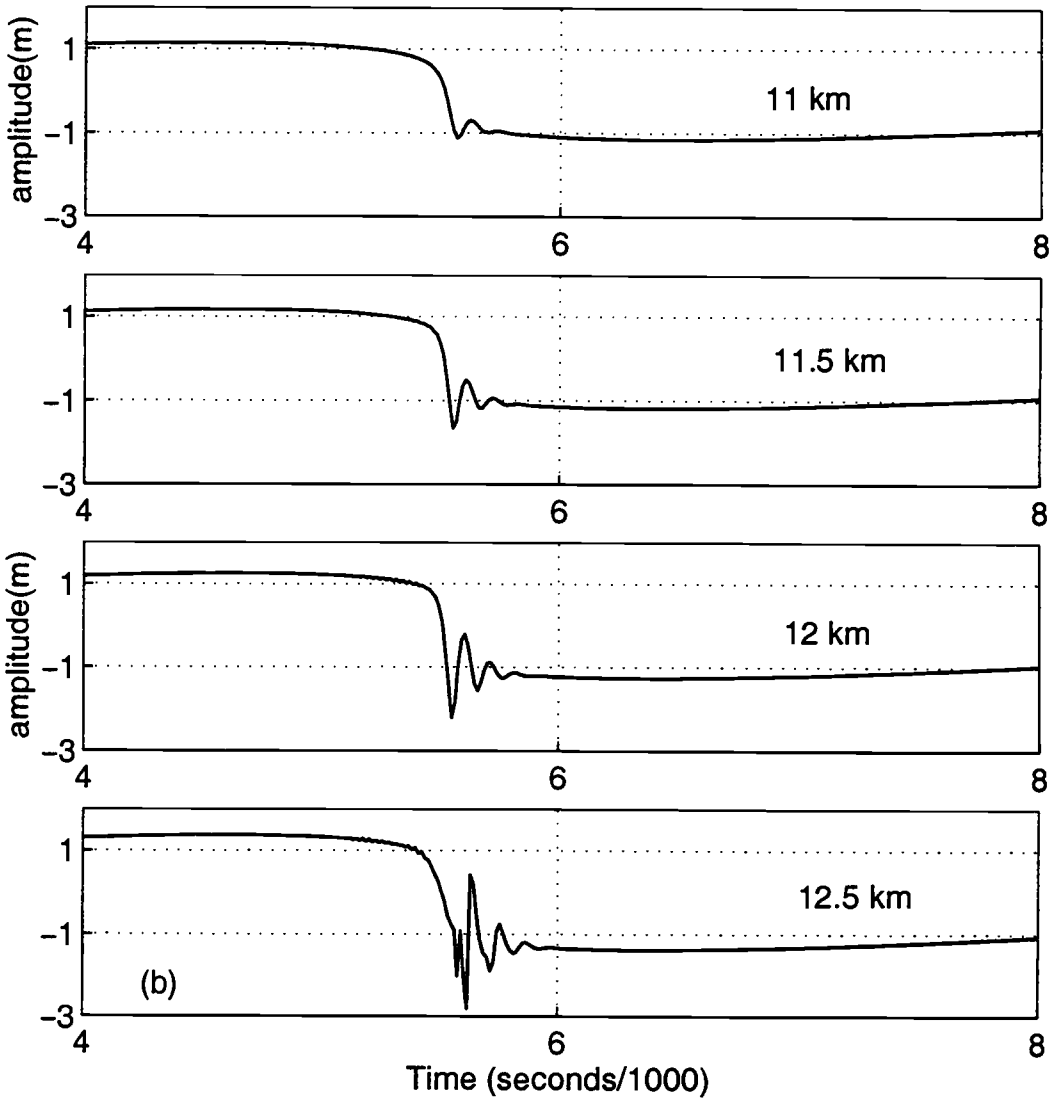

Figure 3.32 (b). Close up of (a) between 11 and 12.5 km.

in the eKdV equation depends upon the displacement height, η and is given by $\alpha/(\alpha_1 \eta)$. For flat bottom Cases 1, 2 and 4, the maximum amplitude η_0 is ~ 18 m for the KdV numerical solution. Figure 3.5 shows that $\alpha/\alpha_1 > 40$ for Case 1, and therefore the nonlinearities result predominantly from the quadratic nonlinear term. For Cases 2 and 4 the magnitude of α/α_1 is just over 20 m, and both the quadratic and cubic nonlinear terms will be important.

For the case of sloping bottom with horizontal interface, Case A, the ratio α/α_1 goes through zero, the value when $h_1 = h_2$, and we expect the cubic nonlinear term to be important. The results of this model run are shown in Figure 3.33. The internal tide evolves in a similar way to the KdV case (Figure 3.19). A shock-type wave is followed by several nonlinear oscillations on the back face of the internal tide at l = 50 km. The internal tide in both frameworks look similar at 70 km with several nonlinear waves of depression having formed. The KdV solitary-like waves flip polarity at 100 km due solely to the fact that α changes sign there.

For the CMO case, comparison of KdV and eKdV models shows a more significant difference than for Case A. Figure 3.34 shows the KdV and eKdV model results for a 4 m internal tide having propagated 60 km to a water depth of 69 m. The leading KdV model solitary wave arrives at the CMO central mooring ~ .1 tidal period ahead of the leading eKdV model solitary wave. The reason the KdV and eKdV models are so different at the CMO site when compared to Case A is due to the fact that the magnitude of α_1 is greater at the CMO site. Though the

magnitude of α is less in Case A, the fact that the magnitude of α_1 is so small when compared to α means the addition of the cubic nonlinear term does little to change the KdV results. This is not true at the CMO site where the greater magnitude of α_1 is the reason for the difference between the KdV and eKdV frameworks, particularly as the internal tide propagates into shallower water and the magnitude of the ratio α/α_1 is much greater for case A (see Figure 3.5). Comparing the leading waves from the eKdV and KdV solutions reveals a fundamental difference in wave form; the KdV waves are taller and thinner (Figure 3.34 (c)). Solitary type solutions to the KdV (sech^2) and to the eKdV (tanh) are fitted to the leading waves (Figure 3.35). The leading wave in the KdV model is very well approximated by a sech^2 wave. The lead wave in the eKdV model is neither well approximated by sech^2 nor tanh, but appears to be a hybrid of the two. Fits of sech^2 and tanh waves were made by subjectively choosing values of η_0 and υ, respectively, while using the value of KdV and eKdV parameters for 69 m water depth. Note that the amplitude of the tanh wave is limited at α/α_1. Increasing υ only serves to make the waves wider ('thicker') once the value of υ is close to one (Figure 2.2). The amplitude and width of the leading waves of the packet are also compared in Figure 3.36. The width is defined as the time it takes the wave to pass a fixed point, as measured at 42% of the amplitude. Results from a range of different tidal amplitudes are also shown. For reference the dotted lines represent sech^2 and tanh for the local values of parameters h_1, h_2, and $g\Delta\rho/\rho$. For KdV the leading wave of

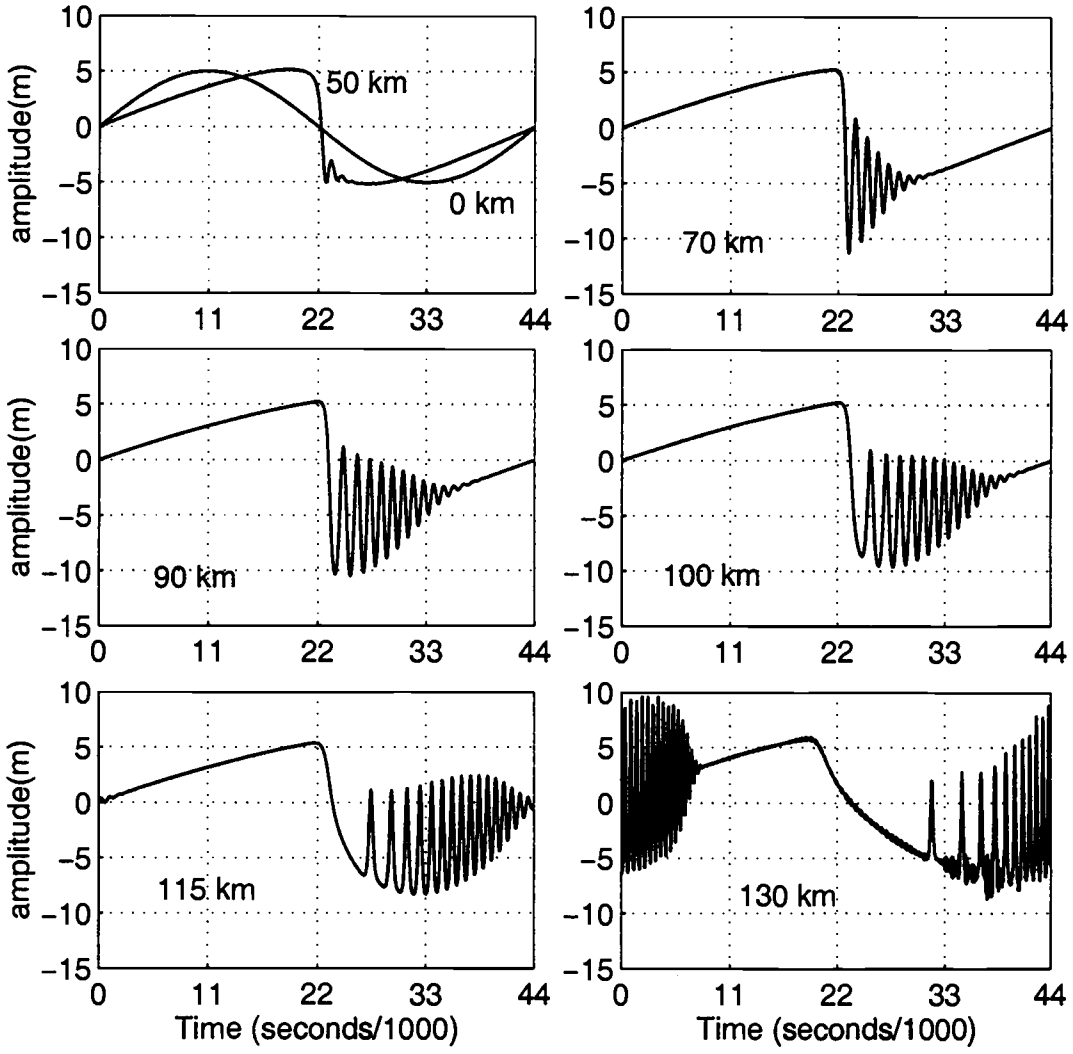

Figure 3.33. Case A (constant sloping bottom with flat interface, h_1 = 50 m) amplitude of the internal mode for two layer fluid at various distances from the boundary within eKdV model framework.

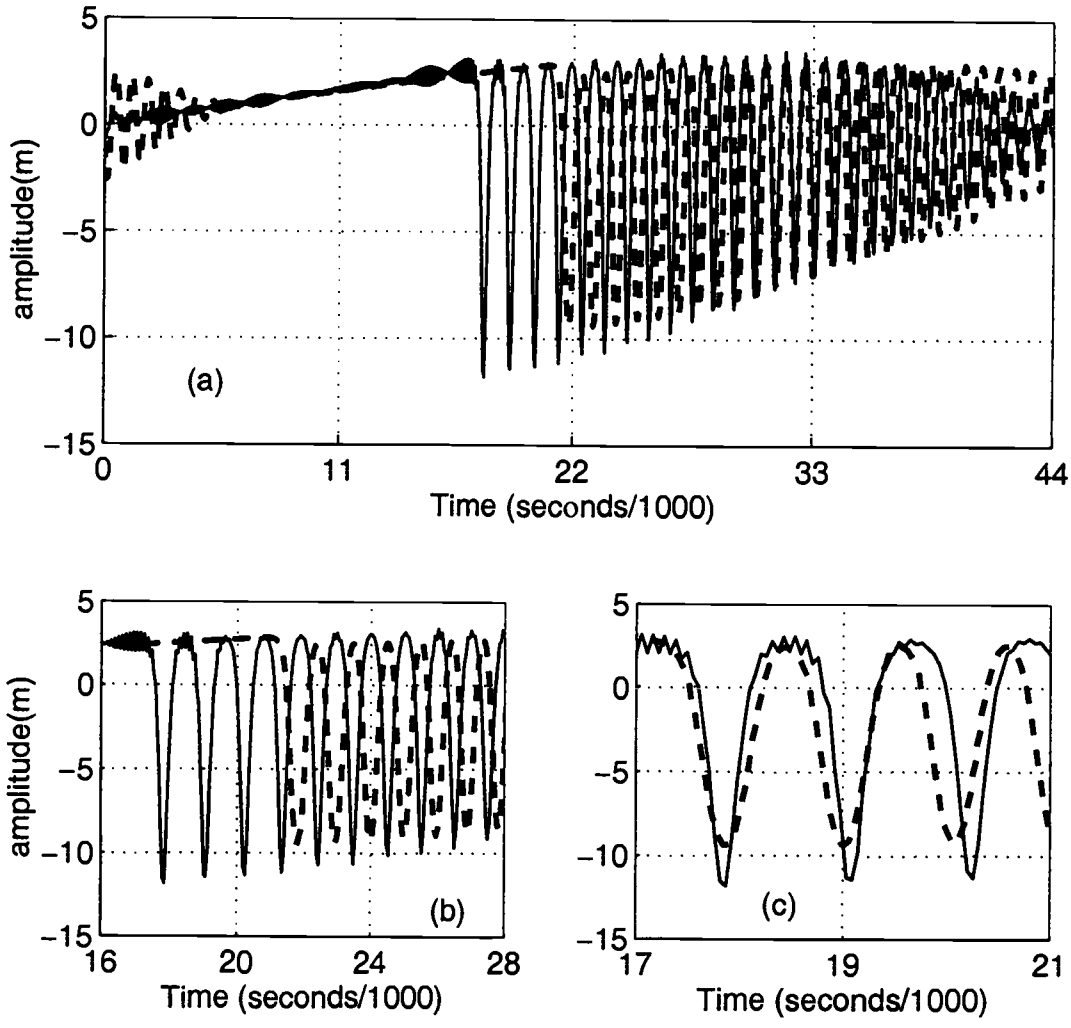

Figure 3.34. CMO experiment site (realistic topography with level interface, h_1 = 25 m) amplitude of the internal mode for two layer fluid at 60 km in 69 m depth water (CMO mooring site). a) Comparison of KdV (solid line) and eKdV (broken line) solutions. b) Close up of (a). c) Leading KdV model waves (solid line) with superimposed eKdV model waves (broken line) shifted forward in time (s) so that the leading waves coincide.

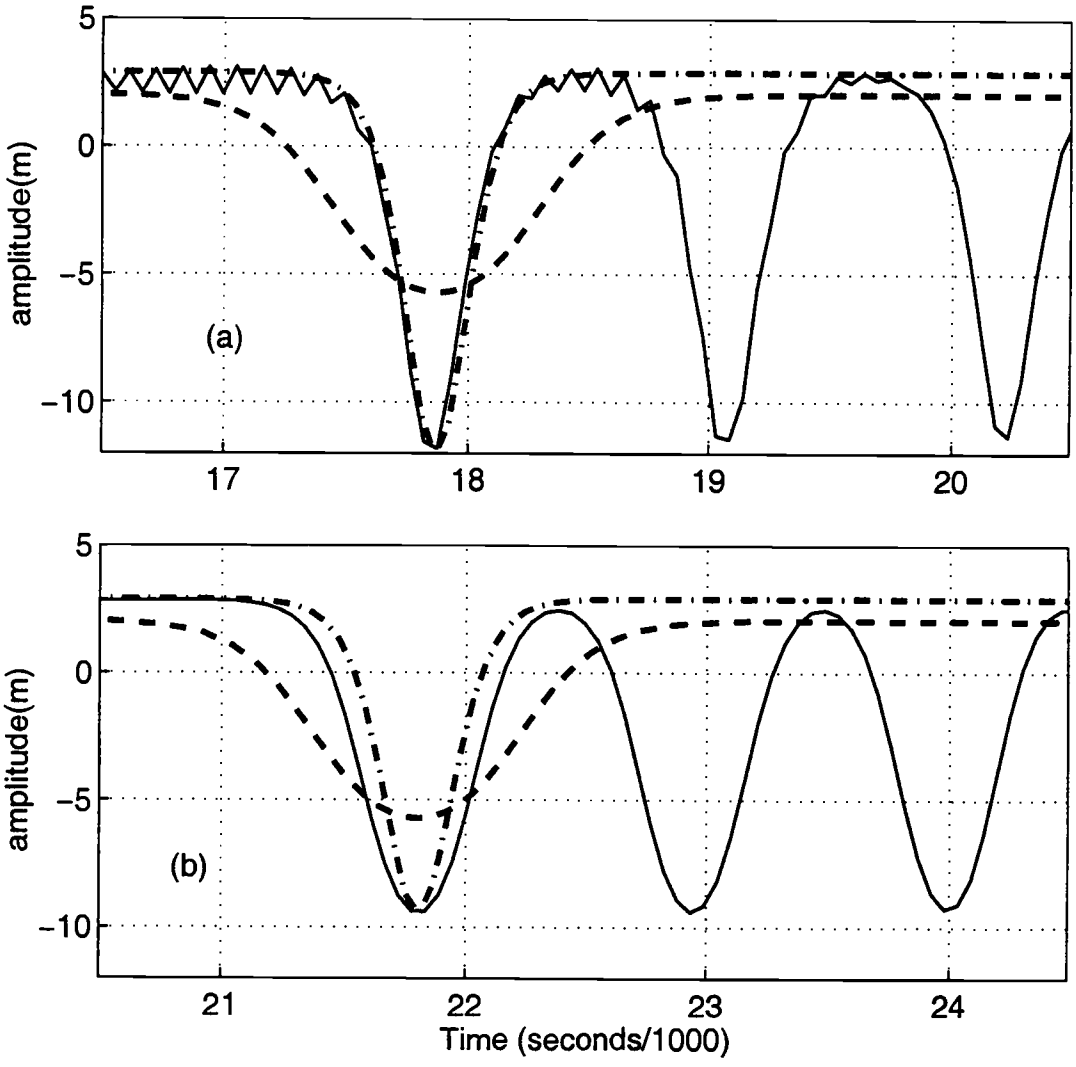

Figure 3.35. CMO experiment site (realistic topography with flat interface, h_1 = 25 m) amplitude of the internal mode for two layer fluid at 60 km in 69 m depth water (CMO mooring site). The leading wave of depression (solid line) plotted with an individual $sech^2$ wave (dot-dash line) and with an individual tanh wave (dashed line) for KdV model (a), and eKdV model (b).

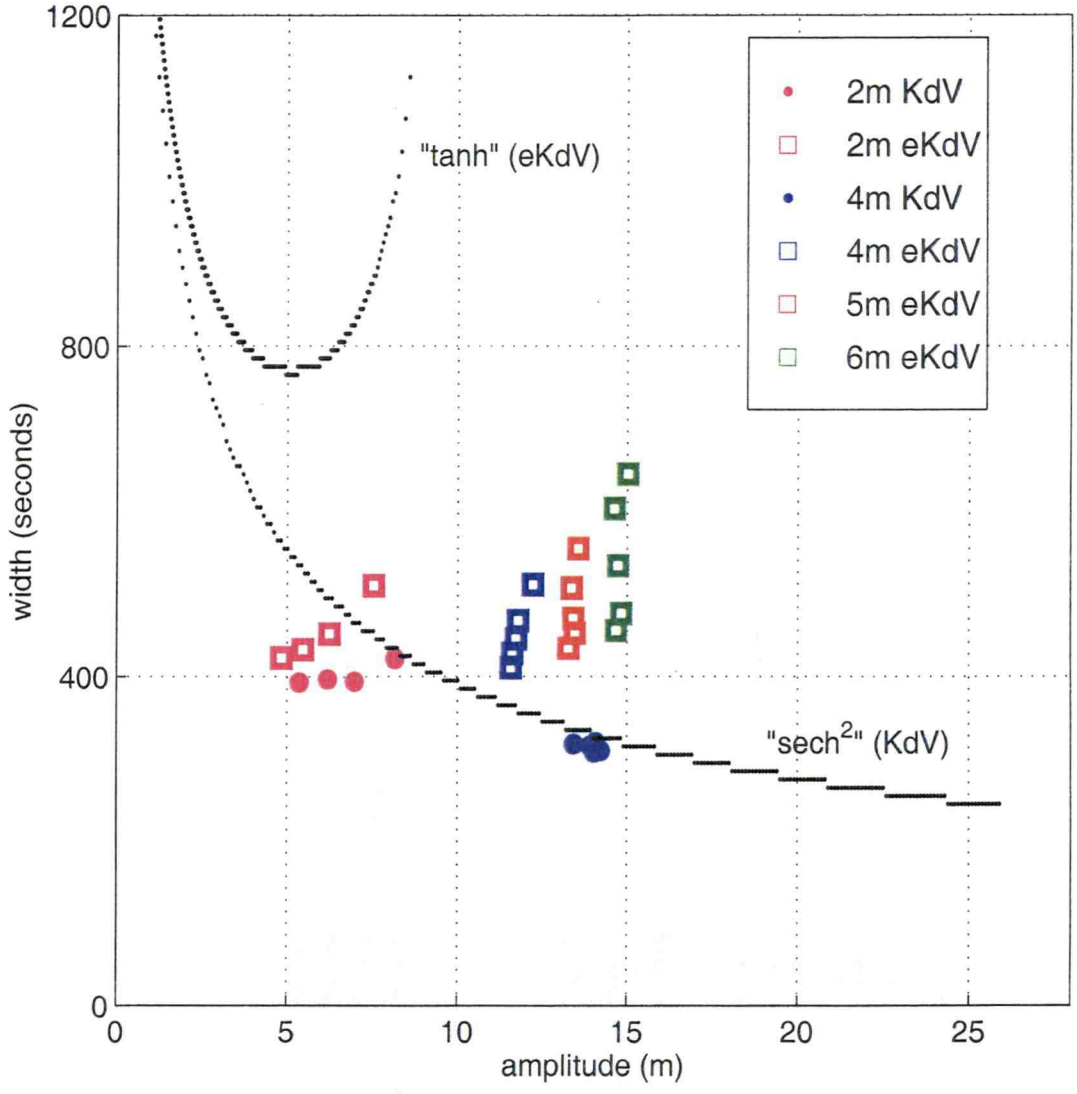

Figure 3.36. The width vs. amplitude of the leading waves of the KdV and eKdV solutions at the CMO mooring site (h_1 = 25 m, h_2 = 44m) at 60 km from the boundary in 69 m depth water. Results for initial tidal amplitudes of 2, 4, 5, and 6 m are shown. The theoretical values for sech^2 and tanh waves using local parameters are also shown (solid lines). The width is calculated at 42% of the total amplitude.

thicker than the trailing ones which are all approximately equal in width. For eKdV the leading wave has larger amplitude and is thicker than the trailing waves. For the KdV model with 4 m amplitude all the waves fall on the same spot on the $sech^2$ curve. For the eKdV model with 4 m amplitude, the waves appear on the 'thick' side of the $sech^2$ curve with the lead wave the most removed from the KdV theoretical curve. The same is true for amplitudes of 5 m and 6 m. The eKdV model waves appear to be evolving toward the theoretical eKdV 'tanh' curve. Note the 2 m tide has amplitude greater than the second wave, and the amplitudes of subsequent waves decrease in a rank ordered fashion. The leading wave is slightly that the amplitude of many of these waves exceeds maximum *tanh* wave amplitude of 9 m as determined by the local parameters at the CMO site.

To learn more about the evolution of a sine wave to waves with $sech^2$ and tanh form, we ran the model with constant parameters (flat bottom) using values at the mooring site. The runs were made with initial tidal amplitudes of 1, 2 and 4 m in both KdV and eKdV frameworks and the width vs. amplitude for the first and second wave in each packet is plotted at various increments of l (see Figure 3.37). The KdV waves grow in amplitude with approximately constant width before turning to hug the theoretical KdV line. They then decrease in amplitude but increase slightly in thickness. Though the KdV model waves continue to evolve, most of them can be well approximated as being '$sech^2$' waves after ~ 100 km (as has previously been shown for Case 1 and case 4). For the eKdV case, the waves are initially close to the theoretical $sech^2$ KdV curve. The waves move slowly

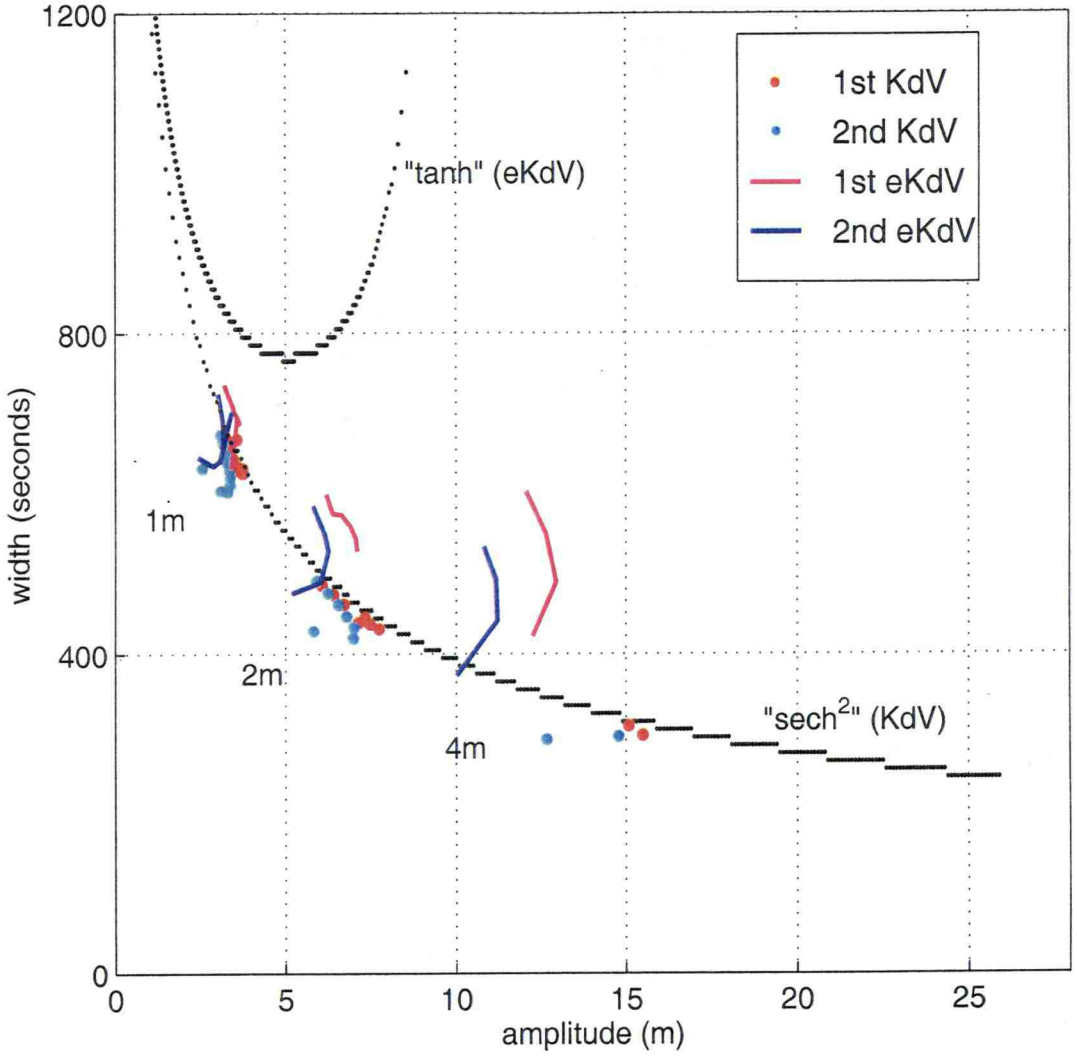

Figure 3.37. Evolution of the width vs. amplitude of the two leading waves of the KdV and eKdV solutions for flat bottom (h_1 = 25 m, h_2 = 44 m) with same parameters as at the CMO site. Results for initial tidal amplitudes of 1, 2, and 4 m are shown. A value is plotted every 10 km for the 1 m tide beginning at 160 km and the lines run from 160 km to 260 km. A value is plotted every 20 km for the 2 m tide beginning at 80 km and the lines run from 80 km to 200 km. A value is plotted every 20 km for the 4 m tide beginning at 40 km and the lines run from 40 km to 100 km. The theoretical width vs. amplitude for sech^2 and tanh waves is also shown (dotted lines). The width is calculated at 42% of the total amplitude.

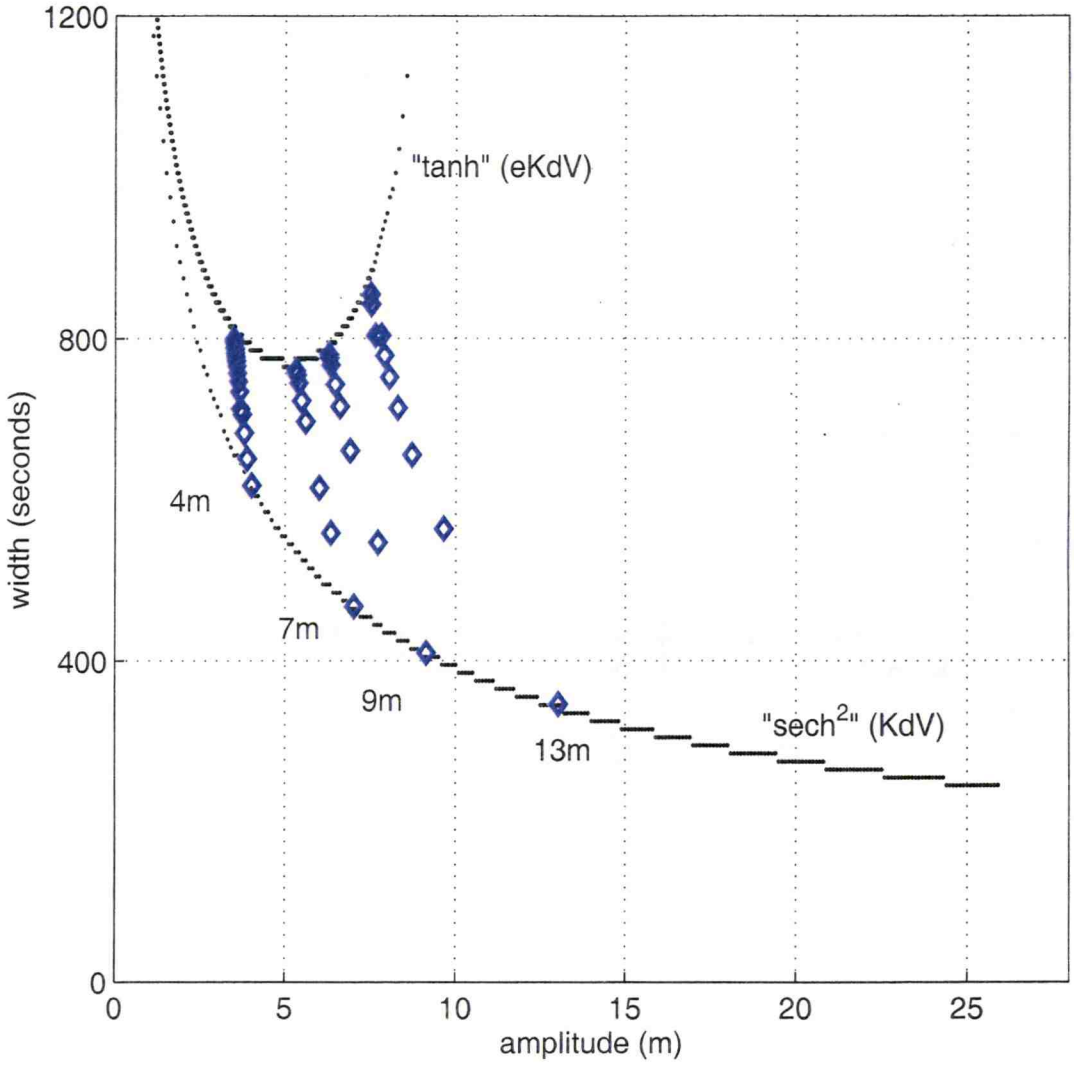

Figure 3.38. Evolution of the width vs. amplitude of four sech^2 waves of the eKdV solutions for flat bottom (h_1 = 25 m, h_2 = 44 m) with same parameters as at the CMO site. Results are shown for sech^2 amplitudes of 4, 7, 9 and 13 m. A value is plotted every 1 km up to a maximum distance of 15 km. The theoretical width vs. amplitude for sech^2 and tanh waves is also shown (dotted lines). The width is calculated at 42% of the total amplitude.

towards the theoretical eKdV tanh curve, ultimately decreasing in amplitude and increasing in thickness. The last points have been plotted after the internal tide has propagated ~ 240km. It appears that these waves are evolving toward tanh form, but take a long time to mature. Also, the amplitudes of the waves are greater than the theoretical eKdV maximum but their magnitudes decrease as the tide evolves.

Another investigation to explore the evolution in the eKdV model (constant parameters) was made using an initial condition of a $sech^2$ wave, the solitary wave solution to the KdV equation. $Sech^2$ amplitudes of 4 m, 7 m, 9 m, and 13 m (Figure 3.38) were chosen. The $sech^2$ waves are rapidly transformed to tanh waves, e.g. the 4 examples plotted reach the theoretical eKdV curve after the wave has propagated of order 10 km. A $sech^2$ wave evolves much more rapidly to the tanh form, when it is all alone (Figure 3.38) than when it is part of a packet of waves (Figure 3.37). The reason for this has not been thoroughly investigated, but provides caution for treating a packet as a group of non-interacting waves.

4. Observations of Nonlinear Internal Waves

The data to be presented and discussed were collected during two field experiments: the Coastal Mixing and Optics experiment, on which we shall mainly focus, and the Littoral Optics Experiment. The locations of the two field experiments are shown in Figure 4.1.

The CMO experimental field program was conducted to increase our understanding of the role of vertical mixing processes in determining the mid-shelf vertical structure of hydrographic and optical properties. The field program was conducted on a wide shelf so as to reduce the influences of shelf break and nearshore processes. The data we discuss was collected from the CMO Central Mooring in July and August 1996, a time when a strong thermocline is present as a result of large-scale surface heating. The data is available in the data report by Boyd et al., (1997).

The goals of the LOE experiment were to understand which regions in the nearshore environment have the highest optical variability and which forcing mechanisms are responsible for this variability. The objectives of the study were to determine: the vertical variability in optical properties over time scales of a few to 10 days; the effect of the total water depth on the optical variability; and the portion of the optical variance associated with internal waves, tides, surface waves and mixing. The data we discuss was collected at the LOE Optical Mooring in October

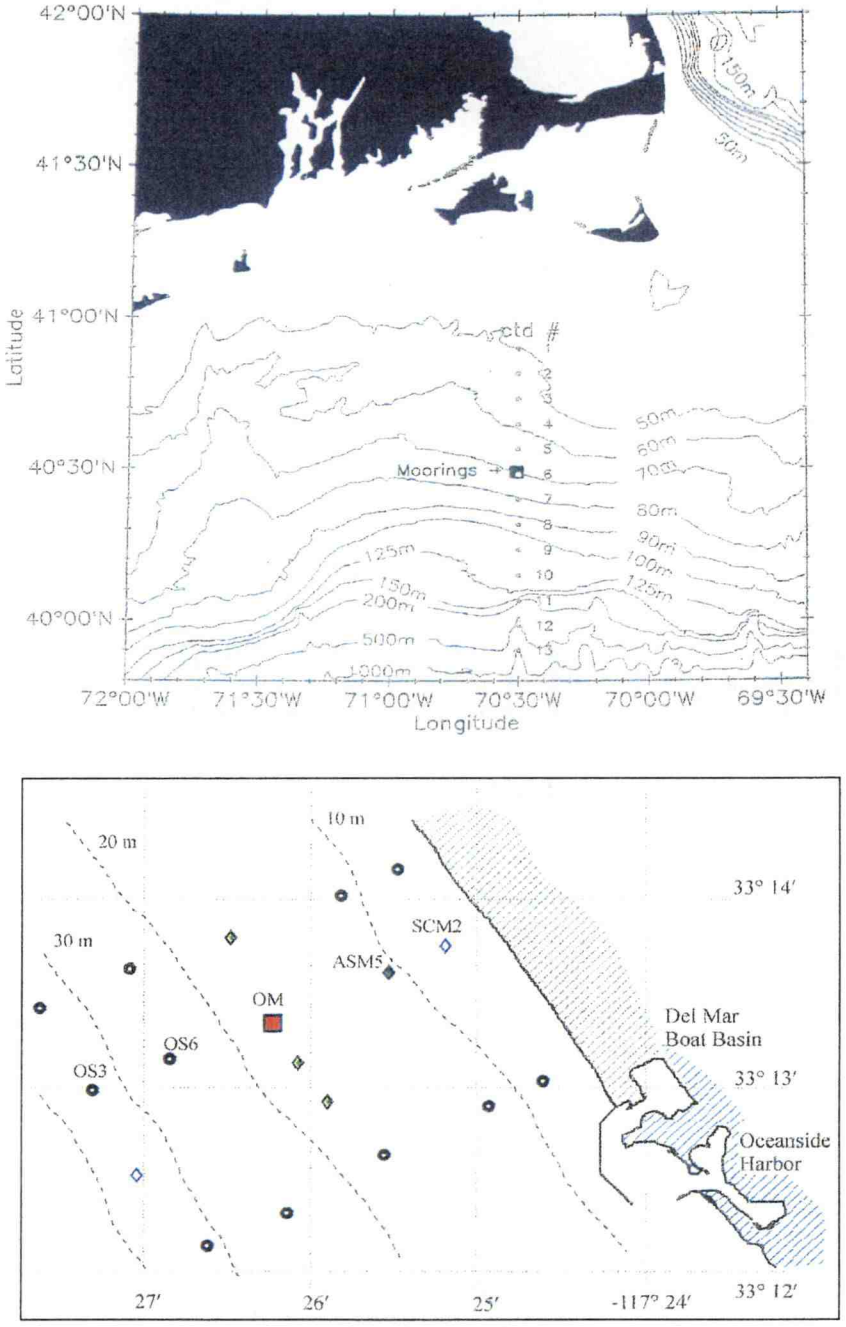

Figure 4.1. Site of the Coastal Mixing & Optics experiment (top) located in the Mid Atlantic Bight to the south of Massachusetts. The data we discuss was collected at the mooring marked 'CTD #6'. Site of the Littoral Optics Experiment (bottom) located close to shore at Oceanside, California. The data we discuss was collected at the mooring marked 'OM'.

1995, a time when the water column can be approximated by a two-layer fluid. Details and results of the experiment are available in the report by Zaneveld & Pegau (1997).

4.1 Observations during the Coastal Mixing and Optics Experiment

The Central Mooring of the CMO experiment was located at 40° 29.50' N 70°30.46' W in water depth of 69 m. A total of 24 temperature recorders and 5 conductivity sensors were distributed along the mooring. Currents were measured at 14 depths from an ADCP placed a few meters above the bottom.

Boyd & Levine (1999) have calculated the first mode internal wave amplitude from the velocity time series from the 29 July to the 31 August (year day 210 - 245, Figure 4.2). The dominant barotropic tidal signal in the Mid Atlantic Bight is semi-diurnal, (Figure 4.3 (a)), and is strongest over the period day 241 - 245 (Figure 4.4) during spring tide. A semi-diurnal signal is apparent in the first mode record, particularly during the spring tide period.

A spectrum of the first mode amplitude (Figure 4.5) shows a peak of energy at the lower tidal frequencies and also at high frequencies. Much of the high frequency energy is due to bursts or pulses of high frequency nonlinear internal waves that occur for a short period during the semi-diurnal tidal cycle. These nonlinear internal waves propagate towards shore (to the north) across the continental shelf to the south of Martha's Vineyard. The energy at high frequency

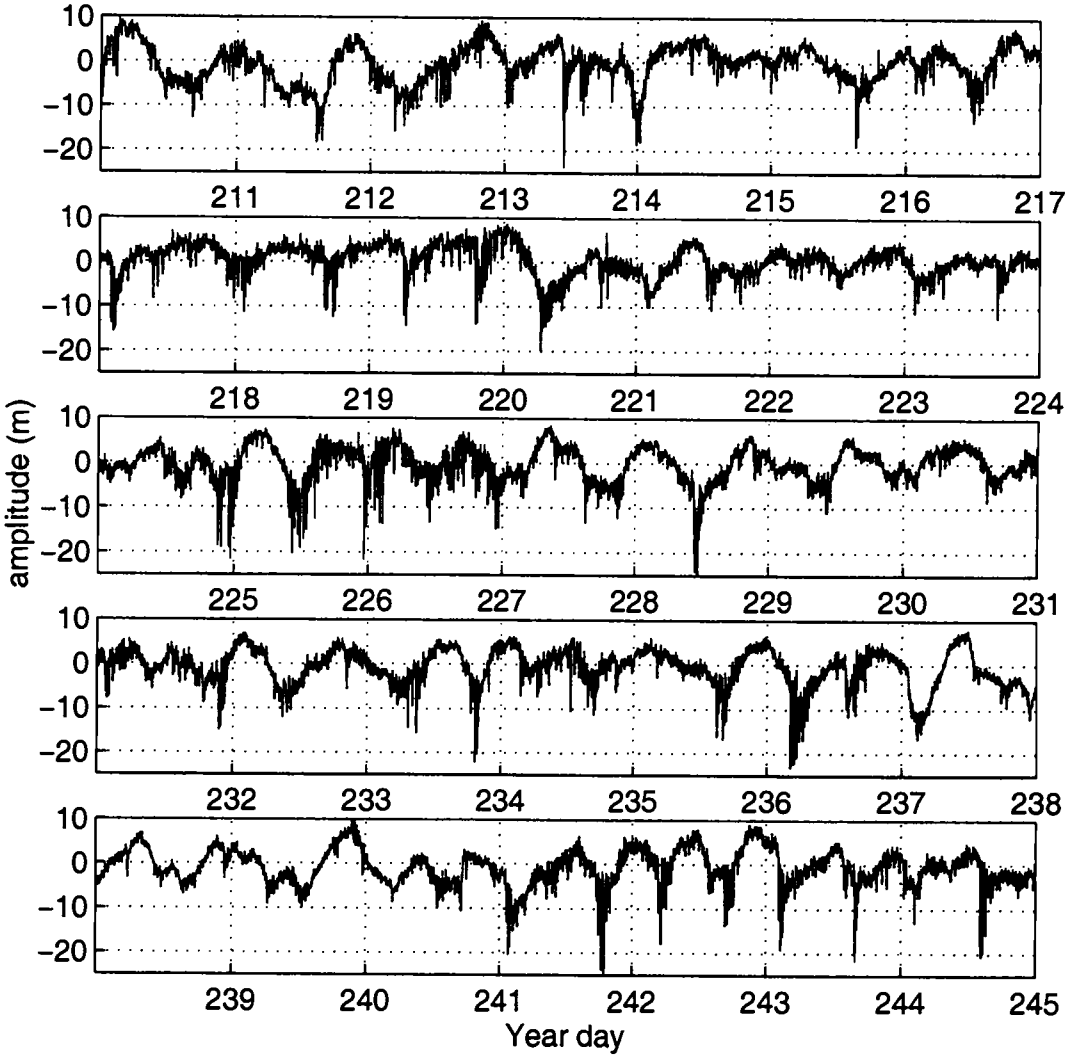

Figure 4.2. Amplitude of the first internal mode calculated from the current meter record at the CMO mooring site over the period day 210 – 245.

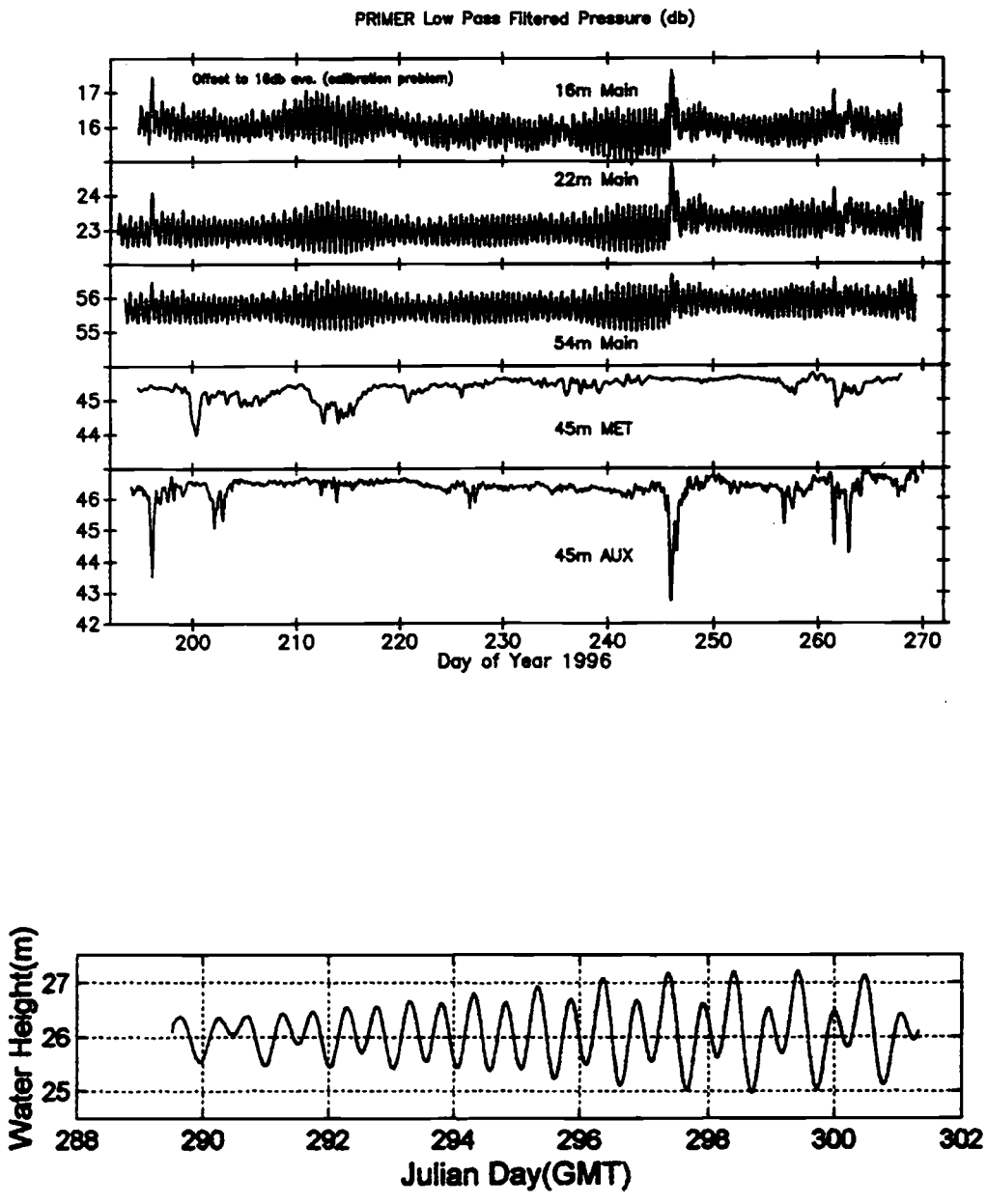

Figure 4.3. Pressure (tidal) record at the CMO mooring site (top) over the period day 210 – 245, and at the LOE experiment site (bottom) for the duration of the LOE experiment.

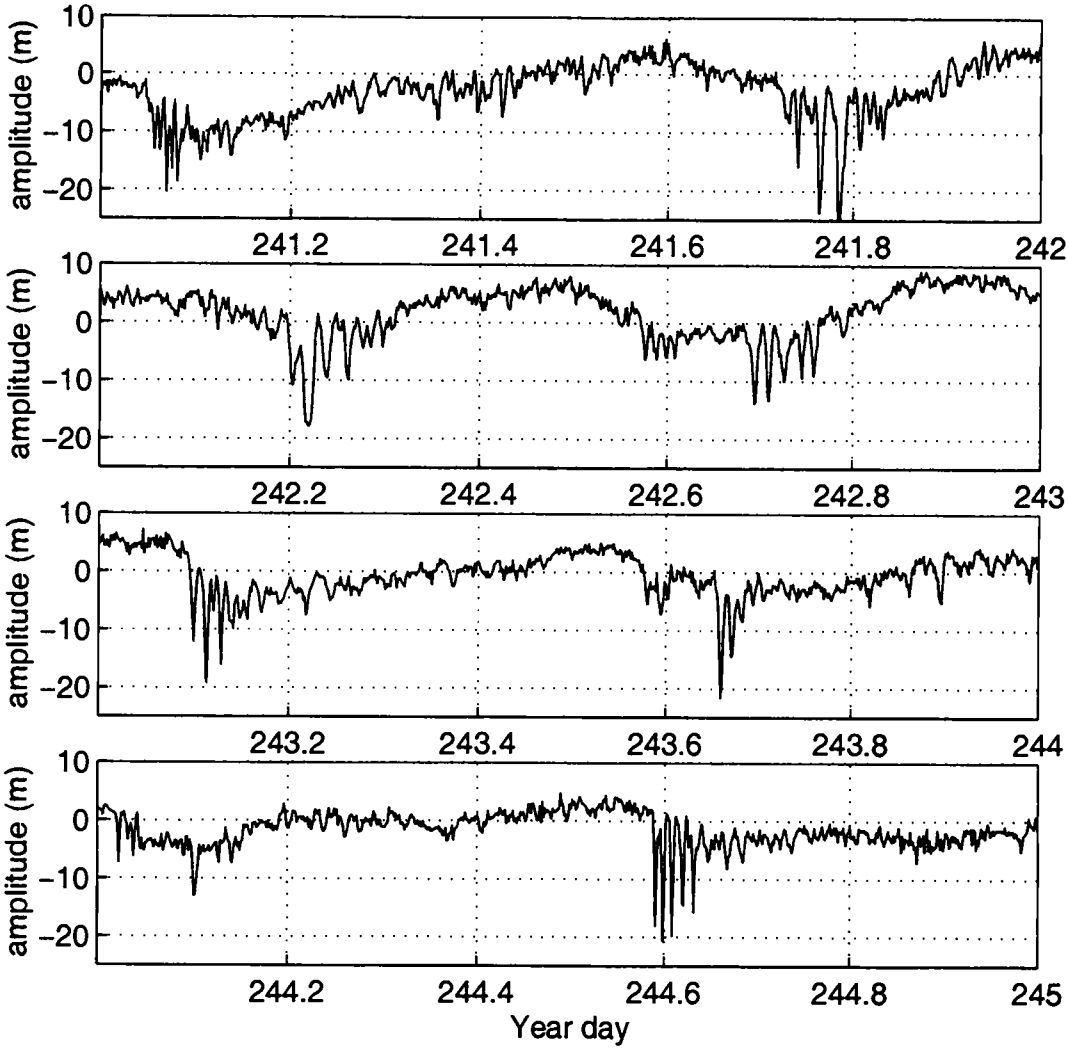

Figure 4.4 Same as Figure 4.2 except for the period day 241 – 245.

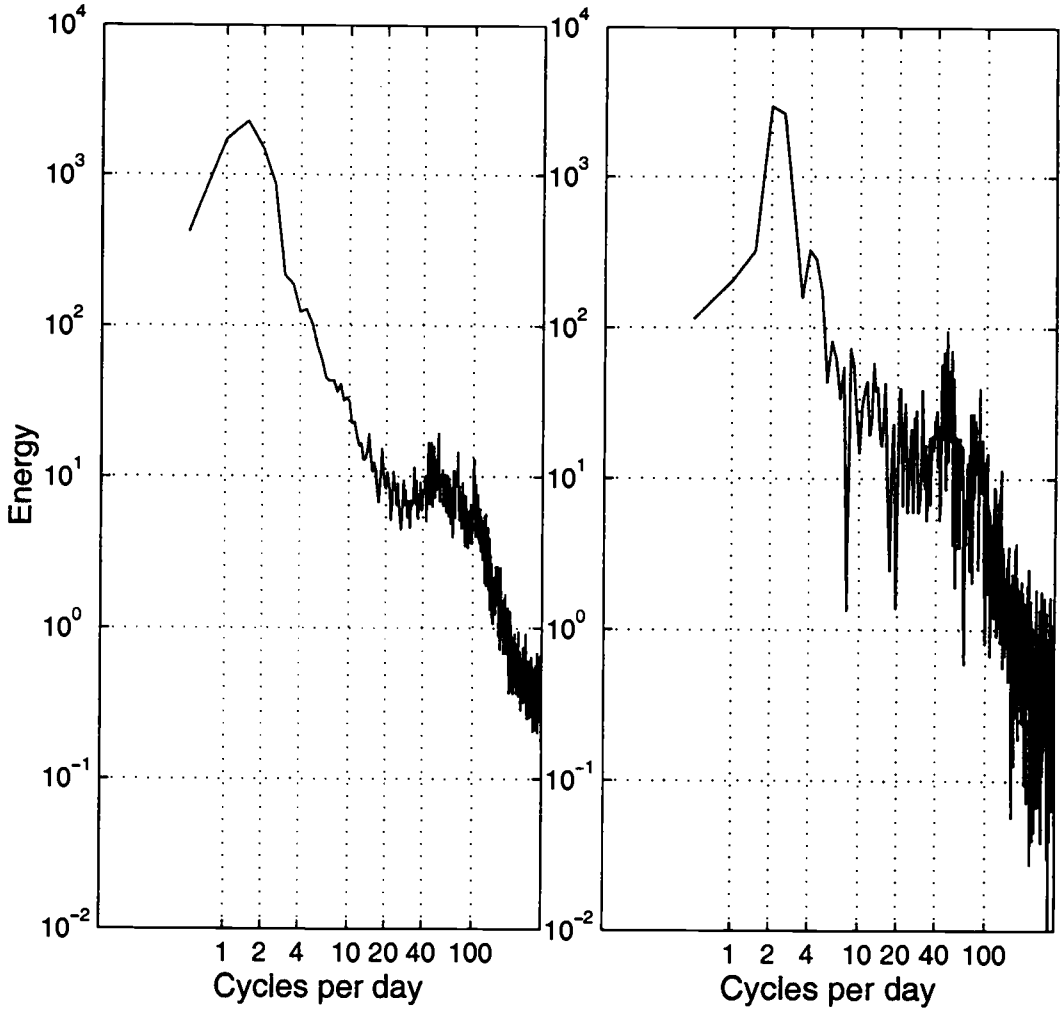

Figure 4.5. Energy spectra of the first internal mode at the CMO mooring for the period day 210 – 245 (left), and the period 241 – 245 (right).

is greater over the period day 241 - 245 during spring tide (Figure 4.5 (b)). There is a clear maximum in energy at 2 cpd over this period, and a significant amount of energy is also contained at 4 cpd. The energy rapidly drops for frequencies greater than 4 cpd but there is a significant increase in energy at ~ 50 cpd and at ~ 90 cpd.

To help interpret these observations, we compare them with the two-layer eKdV model using the CMO parameters. Since we do not know where the internal tide is generated or its amplitude, the model was run assuming a sinusoidal internal tide at distances of 24 km, 48 km and 60 km seaward of the mooring site. Three initial amplitudes of 2 m, 4 m and 6 m were used at each distance. Figure 4.6 shows the internal tide as it appears at the CMO mooring site for these nine cases. In all cases, the leading face of the periodic sinusoidal wave slackens (or flattens) as the internal tide propagates shoreward. This is followed by a steepening of the back face which develops into a shock-like front. The shock-like front is followed by oscillations which subsequently evolve into a packet of solitary-like waves.

This same pattern can often be seen in the observed time series of the first internal mode. Figures 4.7, 4.8 and 4.9 show several individual jumps at the CMO mooring. Figure 4.7 shows first modes which best match the model results of Figure 4.6. Some features of the observations compare well with the model. The slackened leading face of the tide is always followed by a steep – almost shock like – front followed by several highly nonlinear short period waves. Although not rank ordered, the largest amplitude wave in the observed packet is always at or near the jump. The model results (Figure 4.6) show that the amplitude of the jump is greater

for larger initial condition, and that the amplitude of the jump decreases with distance from the point of generation. Although nonlinear waves continue to evolve, their amplitudes decrease as they propagate shoreward from their generation point, and they become 'thicker', i.e. they become more tanh like. Though the observed waves have amplitudes greater than the tanh limit for local eKdV parameters, they nonetheless fit the shape of several model waves at the CMO site (since several of the model waves also have amplitude greater than the theoretical eKdV limit).

There are also many features of the observations that are not found in the model. Figures 4.7 (f) and (g) differ in that the packet that follows the shock-like front, persists until the end of the tidal period, and the waves are spread apart from each other. Figure 4.7 (c) shows two packets of solitary-like waves which pass the mooring site over a tidal period. The leading slackened face is followed by a shock-like front and a packet of solitary waves. The trailing face then slackens to assume a slope similar to the leading face but a second shock-like front, followed by a packet of solitary waves, passes before the end of the tidal period.

Another common observation that is not found in the model results is a 'drop' in amplitude before the jump that occurs at the beginning of the wave packet. Figure 4.7 (h) shows that the first internal mode drops between 243.5 and 243.6 but the slackening slope is restored before the arrival of the jump and packet of solitary waves. Similar drops also occur in Figures 4.7 (b) and (e), Figure 4.8 (a) and (i). Another phenomenon observed is that the slope of the leading face of the

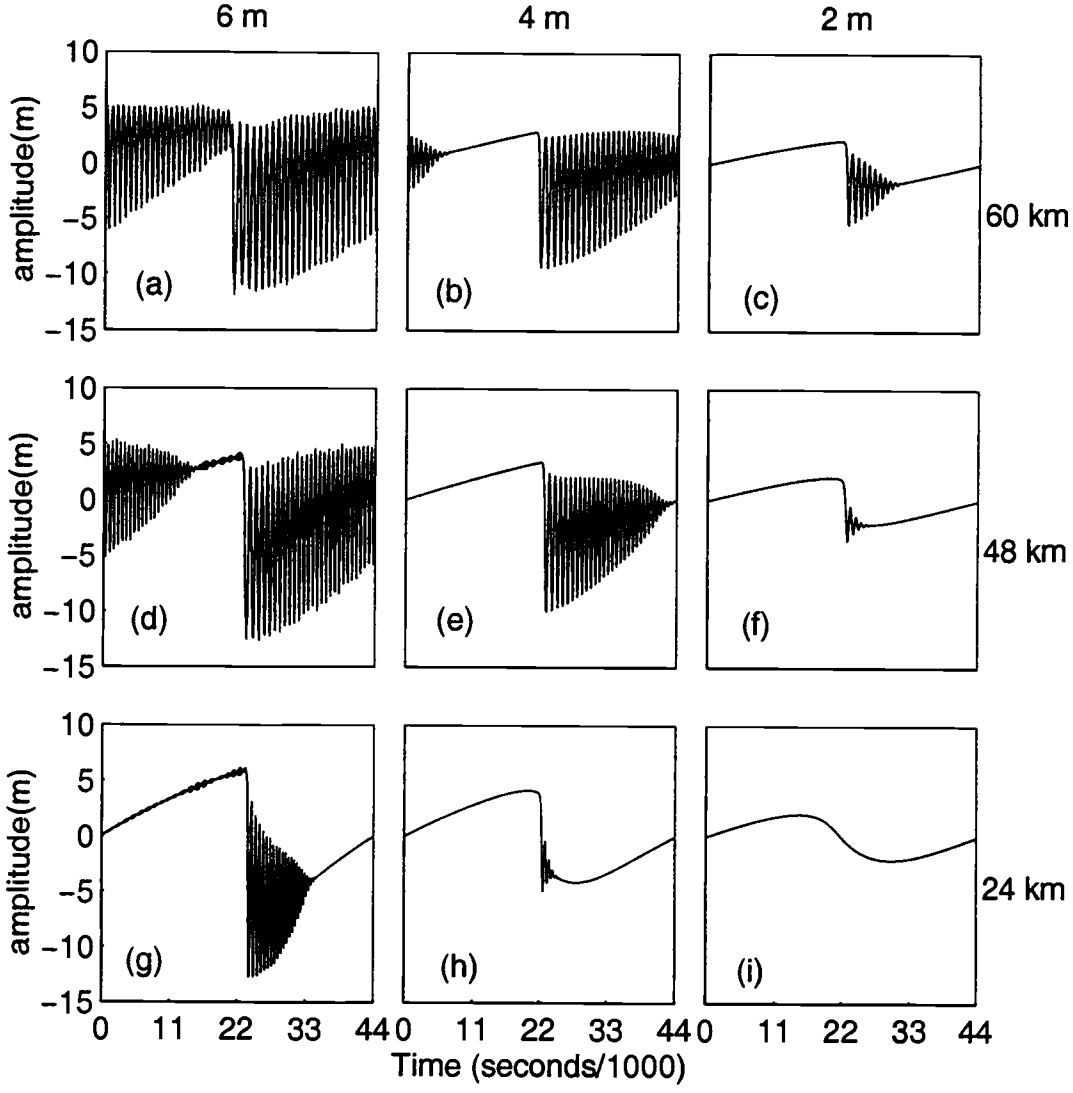

Figure 4.6. Three sinusoids of amplitude 2 m, 4 m and 6 m, respectively, and with tidal period, as they appear at the CMO mooring site in the eKdV framework. The sinusoids have propagated shoreward from boundaries at 60 km, 48 km and 24 km offshore, respectively.

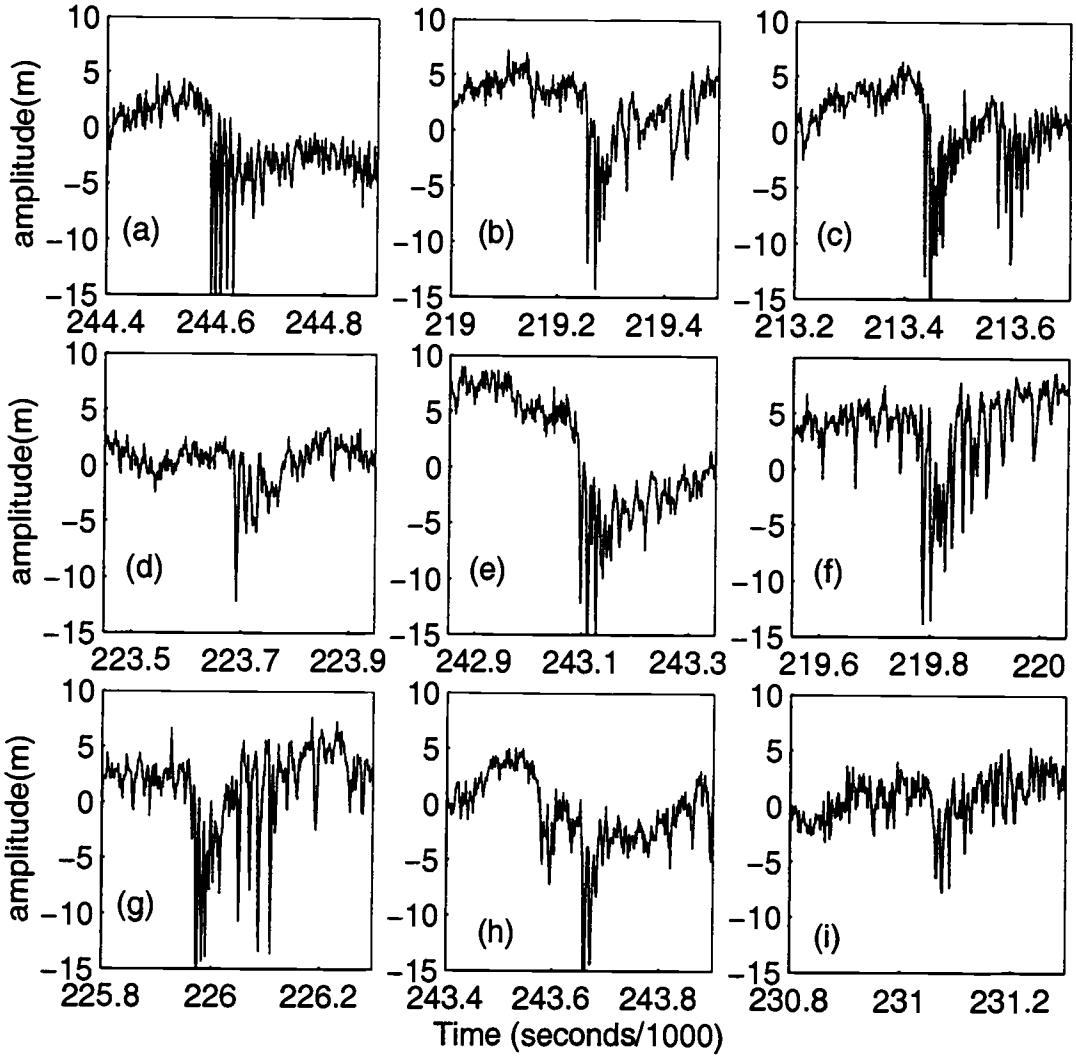

Figure 4.7. Observations at the CMO Mooring site over a semi-diurnal period. These sections of the record were chosen since they are similar to events observed over a tidal period in the model runs of Figure 4.6.

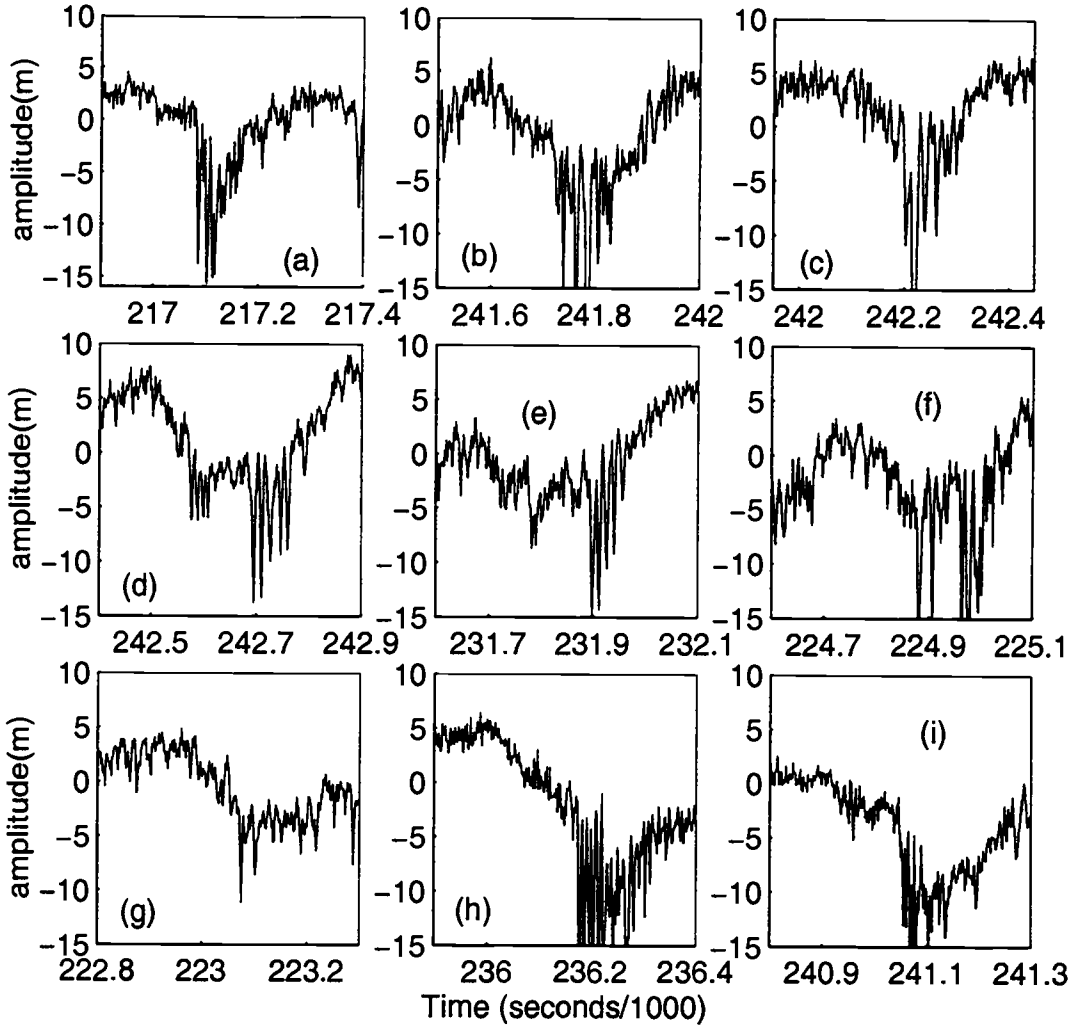

Figure 4.8. Same as for Figure 4.7 except the record is a little bit more complicated over a tidal period.

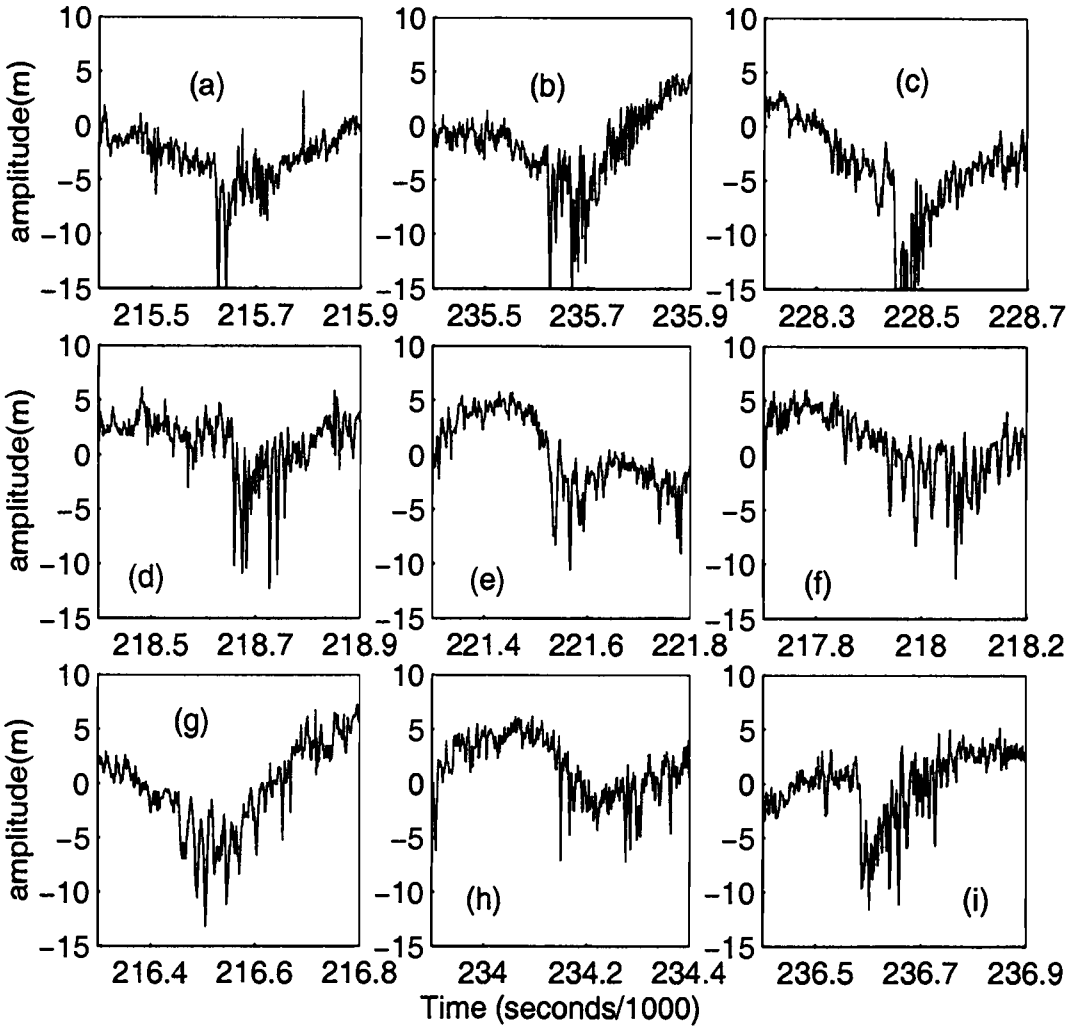

Figure 4.9. Same as for Figure 4.7 and Figure 4.8 except the record is a little bit more complicated over a tidal period.

tide changes sign before the packet in several of the examples in Figure 4.8. In Figure 4.8 (h) the low frequency slope changes sign at day 236. The solitary waves appear as usual ahead of the trailing, low frequency signal. The signal becomes even more complicated when both a 'drop' and low frequency slope change are present, e.g. Figure 4.8 (d). In this case, the slope of the leading slackening low frequency signal changes sign at day 242.5 and is followed by a packet of four solitary waves. The low frequency signal is restored before the passage of a jump followed by a packet of five large solitary waves. The trailing face retains the slope of the low frequency signal. Figure 4.9 shows a series of jumps which are more complex than those in Figures 4.7 and 4.8, though they retain the basic structure of the model results over the tidal period.

To examine the details of the wave packets themselves, the width vs. amplitude was estimated for each wave from all events during the period day 210 - 245 (Figure 4.10). These waves are plotted along with the leading two waves from six of the nine model runs shown in Figure 4.6. Also shown are the theoretical relations for solitary waves for the eKdV and KdV equations using CMO site parameters. The observed nonlinear waves vary greatly in amplitude and width, generally having amplitudes of between 5 and 25 meters, and widths of between 200 and 600 seconds. Larger amplitude observed waves are well approximated by model runs with large initial amplitude, particularly the 4 m model. The 6 m model run from 24 km seaward of the CMO site is also a very good match for several of the observed waves. A large fraction of observed waves with amplitude less than

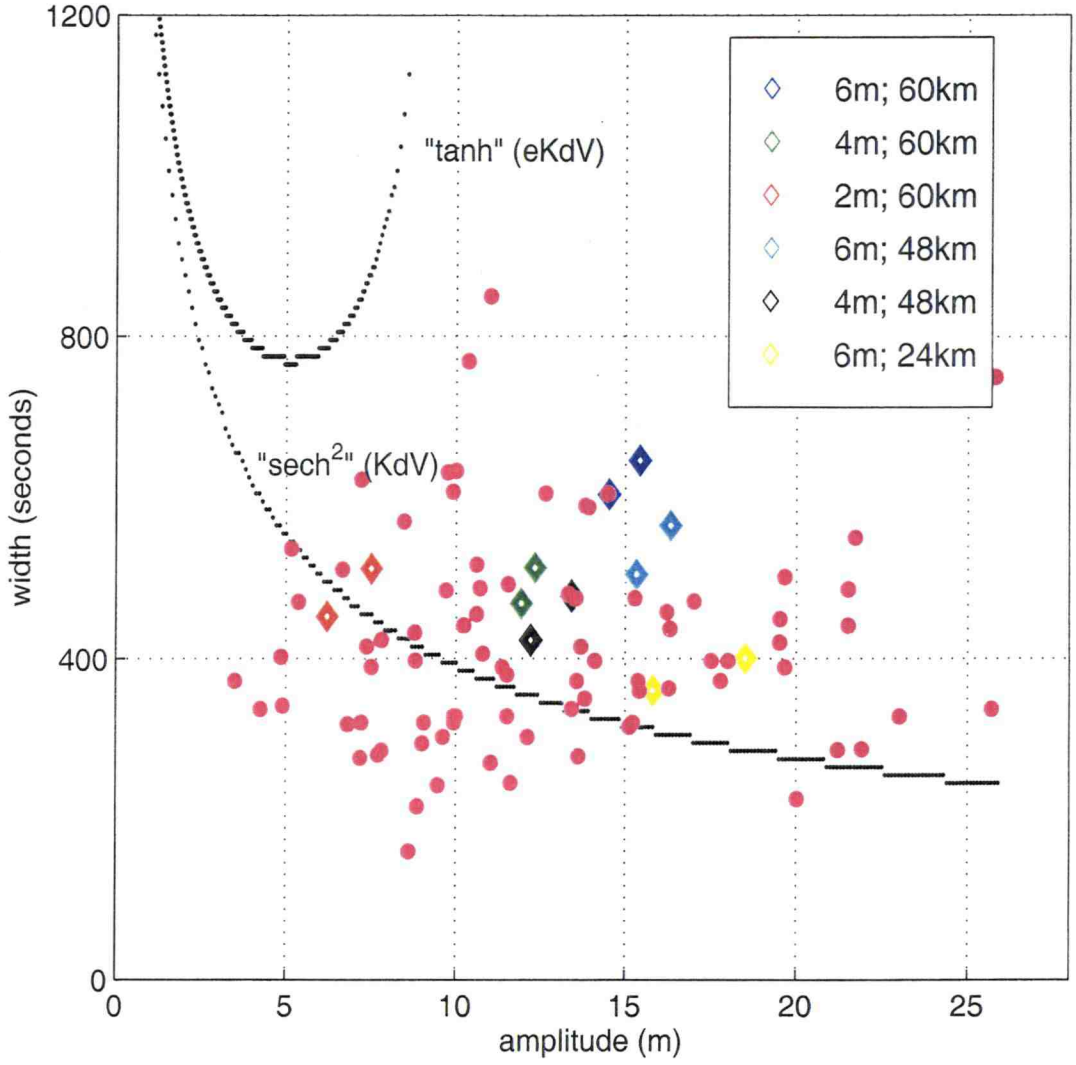

Figure 4.10. Wave amplitude vs. wave width at the CMO mooring for waves from all events during the period day 210 - 245. Also plotted are the two leading waves from six of the nine model runs shown in Figure 3.6 (diamonds).

15 m, and particularly less than 10 m, are much 'thinner' than model waves with similar amplitudes. However, it seems reasonable to say that the observed waves are a good fit to the model waves.

While some features of the observations are reproduced in the model, there are many differences. The eKdV model used here is highly idealized. There are many effects that have not been included. These include bottom and internal friction, earth's rotation and mean shear. Given these limitations, we conclude that the observations are reasonably well matched by the model.

4.2 Observations during the Littoral Optical Experiment

We have conducted a preliminary investigation into nonlinear signals in the time series record at the Littoral Optics Experiment site. The bottom onshore velocity record at the site, 1 m above bottom in 17 m water, for the duration of the experiment (13 days: day 288 - 301) is shown in Figure 4.11 and a shorter period (3 days: day 298 – 301) is shown in Figure 4.12). Figure 4.13 shows the cross-shelf section of the density field for a particular day and is typical of the midday stratification at the site for this time of year. Note the velocity record of Figure 4.11 was made 1 m above bottom at the site marked 'OM' in Figure 4.13. The cross section shows that the stratification is well approximated by a two-layer fluid; an upper mixed layer separated from a weakly stratified bottom layer by a thin thermocline. The period day 298 – 301 corresponds to spring tide in the semi-

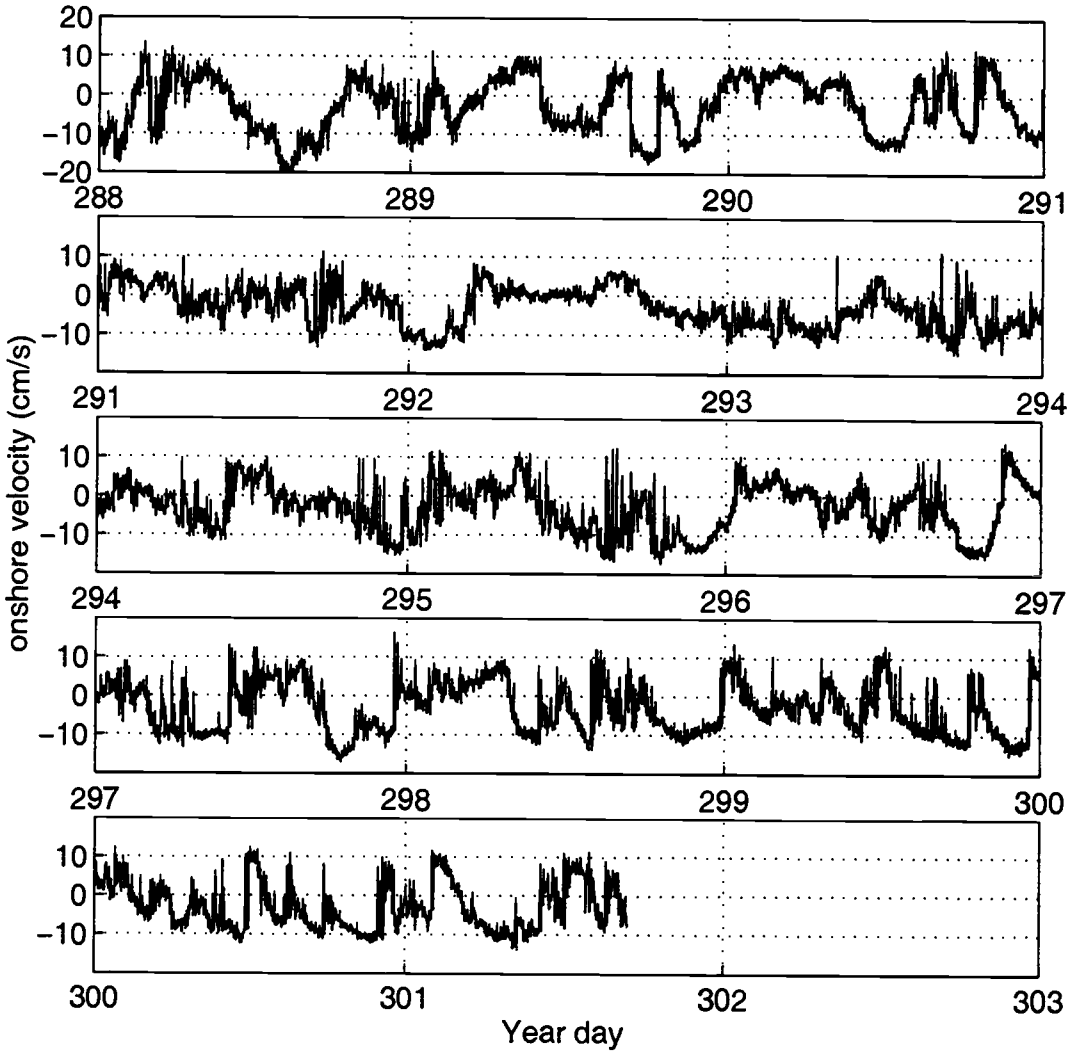

Figure 4.11. Bottom current meter record at the Littoral Optics Experiment experiment over the period year day 288 –301, 1995. The measurements were made in 17 m water 1 m above bottom.

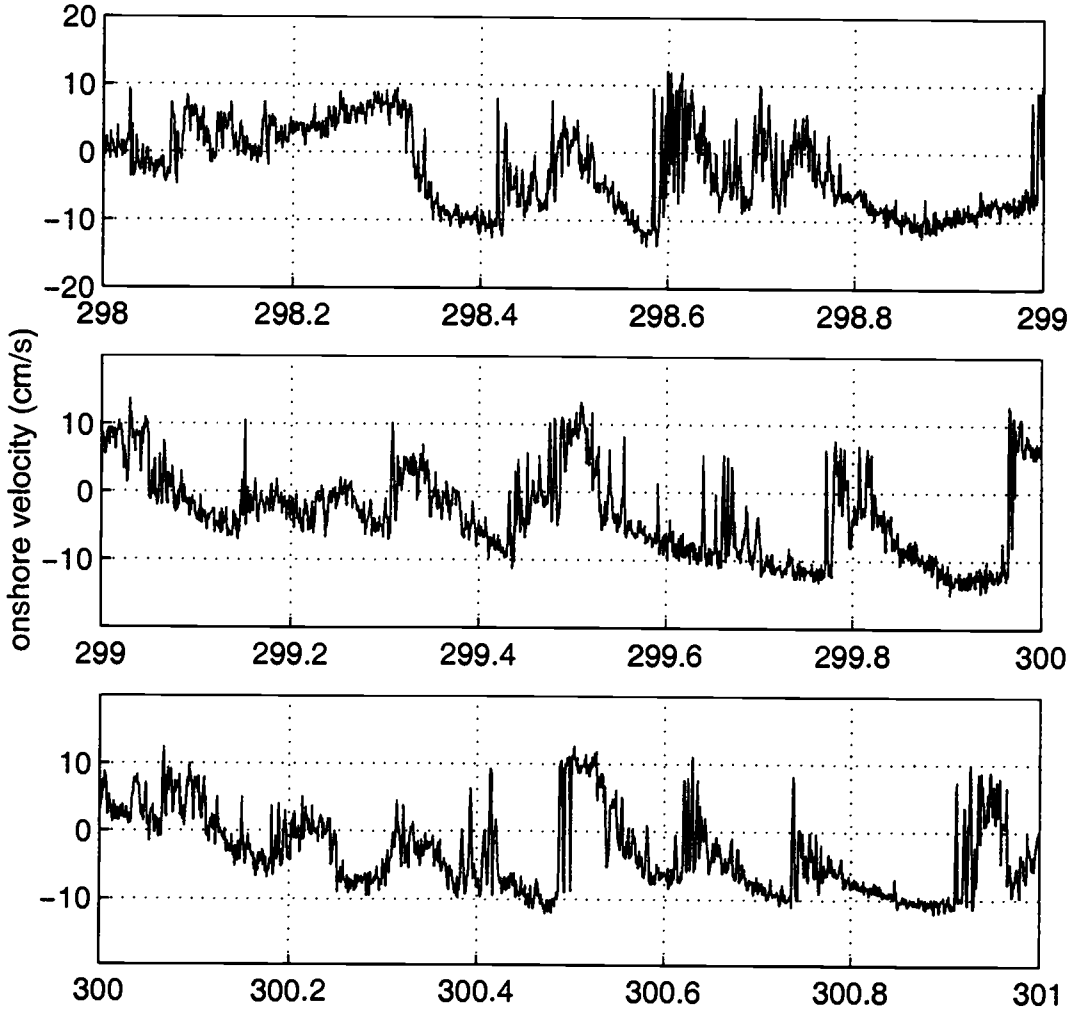

Figure 4.12. Same as Figure 4.11 but over the period year day 298 – 301, 1995.

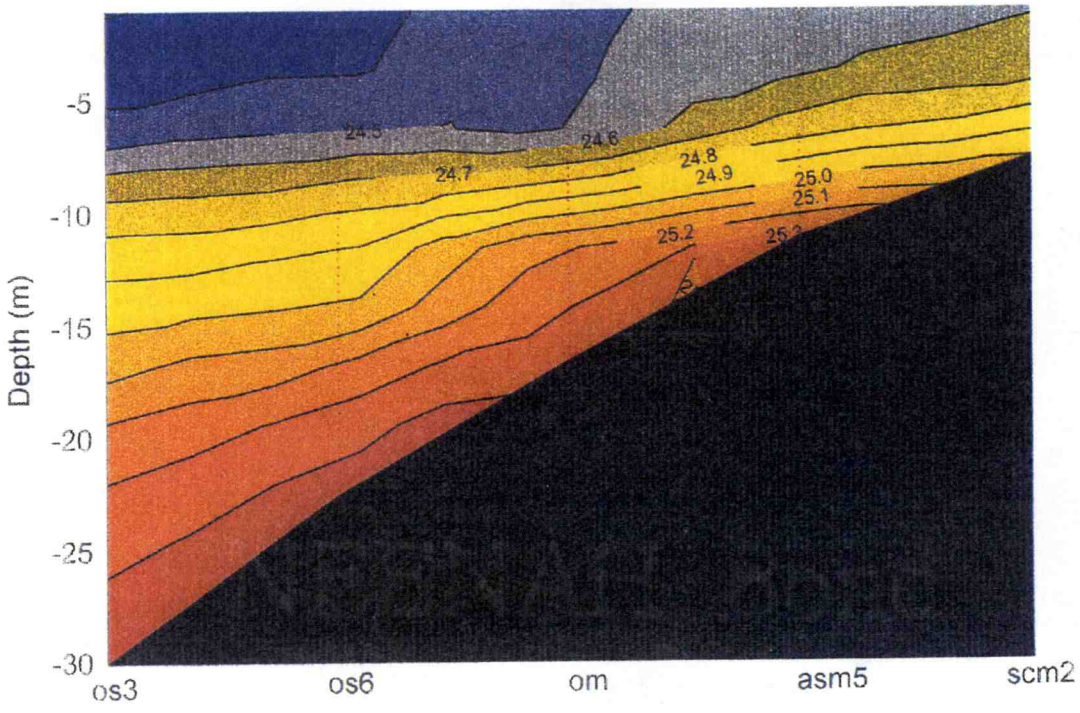

Figure 4.13. Typical midday cross-shelf structure of the density stratification for the duration of the Littoral Optics Experiment over the period year day 288 – 301, 1995.

diurnal tide and we note there is a diurnal inequality in the two semi-diurnal signals. There is a lot of activity in the bottom current meter record during this period, for example there are four jump-like features during the half-day period day 300.5 – 301. This is in contrast to other periods, for example day 293 – 295 when there are few, if any, jumps. A simple first mode analysis was made to relate the current meter time series to oscillations of the interface. It is easily shown that positive jumps in the bottom current meter time series correspond either to onshore propagation of solitary waves of elevation, or offshore propagation of solitary waves of depression. Nonlinear internal waves have been remotely sensed at this location and are well known to propagate onshore (Pegau, personal communication). We conclude that the positive jumps in velocity correspond to internal solitary waves of elevation which propagate toward shore. The wave fronts are very steep and are followed by very nonlinear oscillations and are spaced very closely together. The fourth in the series of jumps during the period day 300.5 – 301 is followed by a reverse jump which can occur when the nonlinear parameter of the KdV equation changes sign, that is when the layer depths are approximately equal. This feature is a fairly prominent occurrence over the duration of the experiment.

The use of the 4^{th} harmonic of the semi-diurnal internal tide in the model runs allows for a good comparison to be made between model results and observations during the spring tide period. The four internal jumps during the period day 300.5 – 301 appear at approximately three-hour intervals and usually

generate two to three large and very high frequency oscillations. The model generates a similar number of waves which switch polarization at the site corresponding to current meter location. The reverse hydraulic jump at day 301 shows the KdV parameters at the 'OM" site may be well matched by model parameters. There are also other periods of activity when the model results are a reasonable fit to the observations.

5. Conclusions

Observations of highly nonlinear internal waves contained in the first mode time series on the mid-continental shelf and in current meter records in shallow water have led us to investigate the transformation of the shoaling internal tide. Observations were made in the mid-continental shelf at the site of the Coastal Mixing and Optics Experiment (CMO), and in very shallow water, at the site of the Littoral Optics Experiment (LOE). An existing model based on generalized KdV and eKdV equations has been simplified for use in a two layer ocean, which is representative of realistic stratification. The model accounts for weakly nonlinear and dispersive properties of the internal tide. Earth's rotation, internal dissipation, bottom friction, and internal shear are not included. The internal tide was forced with a periodic sinusoidal boundary condition and allowed to propagate shoreward.

The model was first run within a KdV framework with realistic continental shelf parameters. The internal tide steepens on its back face as it propagates shoreward. Nonlinear waves evolve from the internal tide after the back face forms a shock-like front. The waves appear as a rank ordered packet with the leading waves traveling fastest, since they are the most nonlinear. The leading waves usually travel faster than the linear wave speed, c; the trailing waves usually travel slower than c. The lead waves nearly fit solitary wave form for local KdV parameters ("sech^2"). The trailing waves tend to be thinner than the local sech^2 waves and are relatively more dispersive than the leading waves.

The transformation of the internal tide is dependent upon the ratio of the nonlinear to linear terms, $\alpha\eta/c$, in the KdV equation: for greater values of this ratio the internal tide steepens sooner and nonlinear waves are emitted sooner. The amplitude of the jump and subsequent waves is dependent upon the initial tidal amplitude: larger tidal amplitudes imply larger jump and nonlinear wave amplitudes. For a fixed nonlinear parameter, α, the internal tide becomes nonlinear sooner upon decreasing the value of the dispersive parameter, β.

The nonlinear waves are waves of depression when the nonlinear parameter, α, is negative, and waves of elevation when it is positive. If a packet of waves of depression propagates into a region where $\alpha > 0$, then the minima, or troughs, of the waves of depression become maxima, or peaks, of the waves of elevation.

All of the model runs made within the KdV framework were also made within the eKdV framework which includes a cubic nonlinearity term scaled by α_1. The results may or may not be similar, depending upon the ratio of the two nonlinear terms, $\alpha/\alpha_1\eta$. If this ratio is large (greater than one) the cubic nonlinear term is not important and the KdV and eKdV results are similar. If the ratio is of order one or less the eKdV may evolve differently from the KdV. For most of the model runs made the model results were similar in both frameworks. However, there are some significant differences to the waves that cross the shelf using CMO parameters. The modeled leading waves at the CMO mooring site were much 'thicker' than sech^2 waves with local KdV parameters, but they had not quite developed into solitary wave solutions of the eKdV equation ("tanh").

To understand better the evolution of waves toward tanh form in an eKdV framework, without the complications of varying parameters, model runs were made using constant eKdV parameters representative of the CMO site. Upon formation, the leading waves of the packet are similar to $sech^2$ waves. The waves become "thicker" and tend toward the tanh form upon further propagation, but never reach the theoretical tanh curve in our limited domain. To try to understand why the evolution of waves from being close to $sech^2$ waves to being close to tanh waves was so slow, the internal tide was forced with a $sech^2$. The evolving $sech^2$ rapidly moves to the theoretical tanh curve for all amplitudes. We conclude that the interaction between the solitary like-waves in a packet slows them from evolving into exact solitary "$sech^2$" or "tanh" waves.

Model runs with varying initial amplitudes and generation regions were made to help interpret the observations made at the CMO site. Some features of the observations compare well with the model. The leading face of the internal tide steepens to form a shock like front. Nonlinear high frequency waves evolve shortly after the appearance of the jump. Although not rank ordered, the wave of maximum amplitude is always close to the jump. Some features of the observations are not found in the model. Nonlinear waves can be very widely spaced and persist over a tidal period. The amplitude of the observed waves often 'drops' before the arrival of the jump. The leading face may change slope before the arrival of the jump.

Individual observed waves were examined and the details compared to model waves. The observed nonlinear waves vary greatly in amplitude and width, generally having amplitudes of between 5 and 25 meters, and widths of between 200 and 600 seconds. Larger amplitude waves are well approximated by waves evolving from large amplitude model waves. A large fraction of smaller amplitude, particularly less than 10 m, observed waves are thinner than model waves of similar amplitude. We conclude that the observed waves are a good match to modeled waves given the highly idealized eKdV model used, and the fact that we have neglected friction, rotation and mean shear.

A preliminary analysis was made using data collected during the LOE experiment. Highly nonlinear oscillations were recorded in the bottom current time series. A simple first mode analysis showed that the observed jumps corresponded to nonlinear waves of elevation which propagate on shore. The activity observed varied greatly between spring and neap tide with observations of at least four nonlinear jumps followed by packets of closely spaced nonlinear oscillatory being recorded within a tidal period at spring tide. For this reason, the internal tide was modeled using the 4th harmonic as forcing. The internal tide steepened rapidly, as a result of the large amplitude of the nonlinear parameter, and nonlinear waves of depression evolved after the harmonic propagated between 10 and 12 km. The nonlinear parameter changed sign at this value of l and the waves switched polarity very rapidly. The model waves of elevation are similar to the observed waves. The

observed waves of elevation are often followed by reverse hydraulic jumps, an indication that the layer depths are similar, such as is the case where the model waves of elevation become nonlinear.

Bibliography

Apel, J.R., 1987. *Principles of ocean physics,* International Geophysics Series, Volume 38, Academic Press, pp. 634.

Apel, J.R. & F.I. Gonzalez, 1983. Nonlinear features of internal waves off Baja California as observed from the SEASAT imaging radar, *J. Geophys. Res.*, **88,** 4459-4466.

Apel, J.R. & R.-Q. Lin, 1991. Multiple interactions of oceanic internal solitons, *Proc. 8th Ann. Conf. Atmos. And Oceanic Waves and Instabilities, Bull. Am. Meteor. Soc.* **72,** 1094.

Benney, D.J., 1966: Long nonlinear waves in fluid flows. *J. Math. Phys.,* **45,** 52 - 63.

Berezin Yu.A., 1987. *Modeling Nonlinear Wave Processes.* VNU Science Press, pp. 182.

Boussinesq, M.J., 1872. Theorie des ondes et des remous qui se propagent le long d'un canal rectangulaire horizontal, en communiquant au liquide contenu dans ce canal des vitesses sensiblement pareilles de la surface au fond. *J. Math. Pures Appl.* (2) 17:55-108; transl. A.C.J. Vastano, J.C.H. Mungall, Texas A&M Univ., Ref. 76-2-T (March 1976).

Boyd, T., & M.D. Levine, 1999. Moored observations of nonlinear internal waves during the Coastal Mixing and Optics Experiment, *J. Geophys. Res.*, to be submitted.

Boyd, T., M.D. Levine, & S.R. Gard, 1997. Mooring observations from the Mid-Atlantic Bight, *Oregon State University,* Data Report 97-2, pp. 226.

Cacchione, D.A. & D.A. Drake, 1986. Nepheloid layers and internal waves over continental shelves and slopes, *Geo-Marine Lett.,* **6,** 147-152.

Defant, A., 1960. *Volume II of Physical Oceanography,* Pergamon Press, pp.598.

Drazin, P.G. & R.S. Johnson, 1989. *Solitons: an introduction*, Cambridge texts in applied mathematics, Cambridge University Press, pp. 226.

Ekman, V.W., 1904. On dead water. *Sci. Results Norw. North Polar Expedi. 1893-96,* **5** (15).

Farmer, D.M. & L. Armi, 1988. The flow of Atlantic water through the Strait of Gibraltar, *Prog. Oceanogr.*, **88,** 1-

Fu, L.-L., & B. Holt, 1984. Internal waves in the Gulf of California: Observation from a space-borne radar, *J. Geophys. Res.*, **89,** 2053-2060.

Garrett, C. & W. Munk, 1979. Internal waves in the ocean, *Ann. Rev. Fluid Mech.*, **11,** 339-369.

Gasparovic, R.F., J.R. Apel, & E.S. Kasischke, 1988. An overview of the SAR internal wave signature experiment, *J. Geophys. Res.*, **93,** 12,304 - 12,316.

Gill, A.E., 1982. *Atmosphere-Ocean Dynamics*, Academic Press, Inc., pp.662.

Grimshaw, R., 1979. Slowly varying solitary waves. I. Korteweg - de Vries equation. *Proc. R. Soc., Lond., Ser. A,* **368,** 359-375.

Halpern, D., 1971, Observations on short-period internal waves in Massachusetts Bay, *J. Mar. Res.*, **29,** 116-132.

Haury, L.R., M.G. Briscoe & M.H. Orr, 1979. Tidally generated wave packets in Massachusetts Bay, *Nature,* **278,** 312-317.

Holloway, P.E., 1983. Internal tides on the Australian North-West Shelf: a preliminary investigation, *J. Phys. Oc.*, **13,** 1357-1370.

Holloway, P.E., 1984. On the semidiurnal internal tide at a shelf-break region on the Australian North-West Shelf, *J. Phys. Oc.*, **14,** 1787-1799.

Holloway, P.E., 1985. A comparison of semidiurnal tides from different bathymetric locations on the Australian North-West Shelf, *J. Phys. Oc.*, **15,** 240-251.

Holloway, P.E., 1987. Internal hydraulic jumps and solitons at a shelf break region on the Australian North West Shelf, *J. Geophys. Res.*, **92,** 5405-5416.

Holloway, P.E., 1987. On the dissipation of internal tides, in *Tidal Hydrodynamics*, B.B. Parker editor, Wiley, 449-468.

Holloway, P.E., S.E. Humphries, M. Atkinson & J. Imberger, 1985. Mechanisms for nitrogen supply to the Australian North-West Shelf. *Aust. J. Mar. Freshw. Res.*, **36,** 753-764.

Holloway, P.E., E. Pelinovsky, T. Talipova & B. Barnes, 1997. A nonlinear model of internal tide transformation on the Australian North West Shelf. *J. Phys. Oc.*, **27,** 871-896.

Ivanov, V.A. & K.V. Konyaev, 1976. Bore on a thermocline, *Izv. Akad. Nauk. SSSR Fiz. Atmos. Okeana,* **12,** 416-423. (*Izv. Acad. Sci. USSR Atmos. Oceanic Phys.*, Engl. Transl., **12,** 1976.)

Kelvin, Lord (Sir W. Thomson), 1887. On the waves produced by a single impulse in water of any depth, or in a dispersive medium, *Proc. Roy. Soc. A.*, **42,** 80-85.

Korteweg, D.J. & G. de Vries, 1895. On the change of form of long waves advancing in a rectangular canal, and on a new type of long stationary waves, *Phil. Mag. (5),* **39,** 422-443.

Lamb, K.G. & L. Yan, 1996. The evolution of internal wave undular bores: Comparisons of a fully nonlinear numerical model with weakly-nonlinear theory, *J. Phys. Oc.*, **26,** 2712 - 2734.

Lapidus, L. & G.F. Pinder, 1982. *Numerical solution of partial differential equations in science and engineering,* John Wiley & Sons, Inc., pp. 677.

Lee, C. & R.C. Beardsley, 1974. The generation of long nonlinear internal waves in a weakly stratified shear flow, *J. Geophys. Res.*, **79,** 453-462.

Lighthill, J., 1978. *Waves in fluids,* Cambridge University Press, pp. 504.

Munk, W.H., 1981. Internal waves and small-scale processes. *Evolution of Physical Oceanography* (B.A. Warren & C. Wunsch, eds.), Chapter 9. MIT press, Cambridge Massachusetts.

Osborne, A.R. & T.L. Burch, 1980. Internal solitons in the Andaman Sea, *Science,* **208,** 451-460.

Osborne, A.R., T.L. Burch & R.I. Scarlet, 1978. The influence of internal waves on deep-water drilling. *J. Pet. Technol.*, **30,** 1497.

Ostrovsky, L. A. & Yu. A. Stepanyants, 1989. Do internal solitons exist in the ocean ? *Rev. Geophys.*, **27,** 293 310.

Pelinovsky, E. & S. Shavratsky, 1976. Propagation of nonlinear internal waves in the inhomogeneous ocean, *Izv. Atmos. Oceanic. Phys.*, **12,** 41 - 44.

Pelinovsky, E., S. Shavratsky & M.A. Raevsky, 1977. The Korteweg de Vries equation for nonstationary internal waves in an inhomogeneous ocean, *Izv. Atmos. Oceanic. Phys.*, **13,** 373 - 276.

Pelinovsky, E., Yu.A. Stepenyants, & T.G. Talipova, 1994. Simulation of nonlinear internal wave propagation in horizontally inhomogeneous ocean, *Phys. Atm. Oc.*, **30,** 77 - 83.

Pinkel, R, 1979. Observations of strongly nonlinear internal motions in the open sea using a range-gated Doppler sonar, *J. Phys. Oceanogr.*, **9,** 675-686.

Rayleigh, Lord (J.W. Strutt), 1876. On waves. *Phil. Mag. (5),* **1,** 257-279.

Russell, J.S., 1844. Report on Waves, *Rep. 14th Meet. Brit. Assoc. Adv. Sci., York,* 311-390. John Murray, London.

Sandstrom, H. & J.A. Elliott, 1984. Internal tide and solitons on the Scotian shelf: a nutrient pump at work., *J. Geophys. Res.*, **89,** 6415-6426.

Shea, R.E., & W.W. Broenkow, 1988. The role of internal tides in the nutrient enrichment of Monterey Bay, California, *Estuarine, Coastal and Shelf Sci.*, **15,** 57-.

Stanton, T. P. & L. A. Ostrovsky, 1998. Observations of highly nonlinear internal solitons over the Continental Shelf, *Geophys. Res. Letts.*, **25,** 2695-2698.

Ufford, C.W., 1947a. Internal waves in the ocean, *Transactions, American Geophysical Union,* **28,** 79-86.

Ufford, C.W., 1947b. Internal waves measured at three stations, *Transactions, American Geophysical Union,* **28,** 87-95.

Ufford, C.W., 1947c. The theory of internal waves, *Transactions, American Geophysical Union,* **28,** 96-105.

Willmott, A. & P.D. Edwards, 1987. A numerical model for the generation of tidally forced nonlinear internal waves over topography, *Continental Shelf Res.*, **7,** 457-.

Winant, C. D., 1974. Internal Surges in Coastal Waters, *J. Geophys. Res.*, **89,** 4523-4526.

Zabusky, N.J. & M.D. Kruskal, 1965. Interactions of 'solitons' in a collisionless plasma and the recurrence of initial states. *Phys. Rev. Lett.*, **15,** 240-243.

Zaneveld, J.R.V, & W.S. Pegau, 1997. Variability of optical properties within the littoral environment, *Annual Report to the Office of Naval Research,* No. N000149710383.

Zhou, X. & R. Grimshaw, 1989. The effects of variable currents on internal solitary waves, *Dyn. Atm. Oc.*, **14,** 17-39.